Technische Universität Braunschweig

Metabolic adaptation processes of the marine bacterium *Dinoroseobacter shibae* DFL12^{T} to changing environmental conditions

Von der Fakultät für Lebenswissenschaften

der Technischen Universität Carolo-Wilhelmina zu Braunschweig

zur Erlangung des Grades

einer Doktorin der Naturwissenschaften

(Dr. rer. nat.)

genehmigte

D i s s e r t a t i o n

von Sarah Kleist
aus Fritzlar

1. Referent: Professor Dr. Dietmar Schomburg
2. Referent: Professor Dr. Irene Wagner-Döbler
eingereicht am: 14.03.2016
mündliche Prüfung (Disputation) am: 07.07.2016

Druckjahr 2016

Vorveröffentlichungen der Dissertation

Teilergebnisse aus dieser Arbeit wurden mit Genehmigung der Fakultät für Lebenswissenschaften, vertreten durch den Mentor der Arbeit, in folgenden Beiträgen vorab veröffentlicht:

Publikationen

Laass, S.*, Kleist, S.*, Bill, N., Drüppel, K., Kossmehl, S., Wöhlbrand, L., Rabus, R., Klein, J., Rohde, M., Bartsch, A., Wittmann, C., Schmidt-Hohagen, K., Tielen, P., Jahn, D., Schomburg, D., (2014). Gene regulatory and metabolic adaptation processes of *Dinoroseobacter shibae* DFL12^T during oxygen depletion. J. Biol. Chem. 289, 13219–13231 (*equally contributed)

Kleist, S., Ulbrich, M., Bill, N., Schmidt-Hohagen, K., Geffers, R., and Schomburg, D. (2016) Dealing with salinity extremes and nitrogen limitation – an unexpected strategy of the marine bacterium *Dinoroseobacter shibae*. *Environ. Microbiol.* doi:10.1111/1462-2920.13266

Tagungsbeiträge

Kleist, S. (2015). Newly identified osmoprotectants in *Dinoroseobacter shibae*. Statusseminar des SFB TRR 51, 07.05.2015, Oldenburg

Posterbeiträge

Kleist, S., Laaß, S., Schomburg, D. (2014). Metabolic and gene regulatory adaptation processes of *Dinoroseobacter shibae* during oxygen depletion. Trends in Metabolomics – Analytics and Application. 0.3 – 05.06.2014, Frankfurt am Main.

Table of Contents

Abbreviations

Abbreviation	Explanation
AAnP	Aerobic anoxygenic phototrophic
ADP	Adenosine diphosphate
ANOVA	Analysis of variance
APCI	Atmospheric pressure chemical ionisation
ATP	Adenosine triphosphate
BLAST	Basic local alignment search tool
BSTFA	N,O-bis(trimethylsilyl)trifluoro-acetamide
CDW	Cell dry weight
cfu	Colony forming units
CoA	Coenzyme A ester
C/N ratio	Carbon/nitrogen ratio
2D-DIGE	2 Dimension-Difference gel electrophoresis
EI	Electron ionisation
eV	Electronvolt
GC	Gas chromatography
GG	α-Glucosylglycerol
GgpP	Glucosylglycerol-phosphate phosphatase
GgpPS	Enzyme combines GgpS and GgpP
GgpS	Glucosylglycerol-phosphate synthase
GpgP	Glucosyl-3-phosphoglycerate phosphatase
GpgS	Glucosylglycerate-3-phosphate synthase
GS-GOGAT	Glutamate synthase-glutamine oxoglutarate aminotransferase
HCA	Hierarchical cluster analysis
HCl	Hydrochloric acid
HEPES	4-(2-Hydroxethyl)-1-piperazineethanesulfonic acid
HPLC	High performance liquid chromatography
IBVT	Institute for Biochemical Engineering (Technische Universität Braunschweig, Germany)
ICBM	Institute for Chemistry and Biology of the Marine Environment (Carl von Ossietzky Universität Oldenburg, Germany)
kbp	Kilo base pairs

Abbreviation	Explanation
LB medium	Luria & Bertani medium
L_n	Norm litre
$[M\text{-}CH_2]^+$	Molecule ion minus a CH_2-moiety
$[M\text{-}CH_4]^+$	Molecule ion minus a CH_4-moiety
$[M+C_3H_9Si]^+$	Molecule ion plus C_3H_9Si-moiety
$[M+H]^+$	Molecule ion plus H^+
MB medium	Marine bouillon medium
MeV4	MultiExperiment Viewer 4
MS	Mass spectrometer
MSTFA	N-methyl-N-(trimethylsilyl)trifluoro-acetamide
MSTFA-*d9*	N-methyl-N-(trimethylsilyl)trifluoro-acetamide, 9-times deuterated
NaOH	Sodium hydroxide
NCBI	National Center for Biotechnology Information
NMR	Nuclear magnetic resonance
OD_{max}	Maximal optical density
PHB	poly-(R)-3-Hydroxybutanoate
PMSF	Phenylmethanesulfonyl fluoride
ppt	Parts per thousand
PTV	Programmed temperature vaporising
RCA	Roseobacter-clade affiliated
RI	Retention index
TCA	Tricarboxylic acid
TMS	Trimethylsilyl
TOF	Time of flight
UDP	Uridine diphosphate
UTP	Uridine triphosphate

Furthermore, units were abbreviated according to the international unit system (SI, Systéme international d'unités), except for molar concentrations (mol/L), which were abbreviated with the capital letter M. Chemical elements were abbreviated by their symbols of the periodic table of elements.

Summary

Marine bacteria essentially contribute to the marine life and are thus globally of importance. However, bacteria have to deal with challenging conditions according to season or region such as the bacteria of the heterotrophic Roseobacter group.

In the present work, adaptation processes to changing environmental conditions of the marine bacterium *Dinoroseobacter shibae* DFL12^T were investigated. Collaborative systems biology studies were conducted with focus on the metabolome in this work.

Time-resolved analyses during the transition from oxygen to nitrate respiration showed an efficient and target-oriented adaptation of *D. shibae*. Observed changes in the proteome and transcriptome primarily concerned the establishment of the denitrification apparatus. Regeneration of ATP and NAD(P)$^+$ was strongly inhibited due to a temporary lack of an adequate electron acceptor. This led to a distinct metabolic crisis. Partially, the organism overcame this crisis by forming the storage compound poly-(R)-3-hydroxybutanoate. Its formation consumes excess NAD(P)H and thus enabled essential metabolic processes. With starting denitrification the metabolism relaxed again.

Within the scope of this thesis, two so far unknown metabolites of *D. shibae* were identified, namely α-glucosylglycerol and α-glucosylglycerate. The latter was detected here for the first time within the class of α-proteobacteria. The identified glycosides as well as glutamate and putrescine have been shown to act osmoprotective under certain conditions. Under hypo-osmotic conditions, putrescine is assumed to be a protector for macromolecules. Otherwise, predominantly glutamate is used for osmoregulative purposes, assisted by α-glucosylglycerol. A salt shock experiment revealed the essential role of the 153 kb chromid of *D. shibae* in adaptation to changing salinity. In general, conducted experiments showed growth of *D. shibae* in a salt concentration range of 0.3 to 5 %.

D. shibae exposed to nitrogen-limitation has been shown to replace glutamate by α-glucosylglycerate to maintain an adequate turgor. Furthermore, high quantities of poly-(R)-3-hydroxybutanoate were detected. Probably, poly-(R)-3-hydroxybutanoate is formed to store excess carbon.

Overall, the present work gives detailed insights in adaptation strategies of *D. shibae* to changing environmental conditions, which thus serves as model for further marine bacteria.

Zusammenfassung

Meeresbakterien sind global von Bedeutung, da sie wesentlich zum marinen Leben beitragen. Dabei müssen Bakterien wie auch die heterotrophe Roseobacter Gruppe, abhängig von Jahreszeit und Region, mit schwierigen Bedingungen umgehen.

In der vorliegenden Arbeit wurden umweltbedingte Adaptationsprozesse des marinen Bakteriums *Dinoroseobacter shibae* DFL12^T in kollaborativen Systembiologie-Studien untersucht. Der Fokus dieser Arbeit lag auf dem Metabolom.

Während der Umstellung von Sauerstoff- auf Nitratatmung zeigten zeitaufgelöste Analysen eine effiziente und zielorientierte Adaptation von *D. shibae*. Beobachtete Änderungen im Proteom und Transkriptom beschränkten sich vornehmlich auf die Etablierung des Denitrifikationsapparats. Durch das kurzzeitige Fehlen eines adäquaten Elektronenakzeptors war die Regeneration von ATP und NAD(P)$^+$ stark gehemmt. Dies führte zu einer ausgeprägten metabolischen Krise. Teilweise bewältigte der Organismus diese durch die Produktion des Speicherstoffes poly-(R)-3-Hydroxybutanoat, um überschüssiges NAD(P)H zu verbrauchen und somit essentielle metabolische Prozesse zu ermöglichen. Mit beginnender Denitrifikation klang die metabolische Krise ab.

Im Rahmen dieser Arbeit wurden zwei bisher in *D. shibae* unbekannte Metabolite identifiziert: α-Glucosylglycerol und α-Glucosylglycerat. Letzteres wurde hier zum ersten Mal in α-Proteobakterien nachgewiesen. Für die identifizierten Glycoside sowie Glutamat und Putrescin wurde gezeigt, dass sie unter bestimmten Bedingungen osmoprotektiv wirken. Unter hypoosmotischen Bedingungen wird angenommen, dass Putrescin Makromoleküle schützt. *D. shibae* verwendet vornehmlich Glutamat, unterstützt von α-Glucosylglycerol, für osmoregulative Zwecke. Ein Salzschock-Experiment offenbarte die essentielle Rolle des 153 kb Chromids von *D. shibae* bei der Adaptation an veränderte Salinität. Generell zeigten die durchgeführten Experimente, dass *D. shibae* in einem Salzkonzentrationsbereich von 0.3 bis 5 % wächst.

Unter Stickstofflimitierung zeigte sich, dass Glutamat durch α-Glucosylglycerat ersetzt wird, um einen adäquaten Turgor aufrecht zu erhalten. Außerdem wurden große Mengen poly-(R)-3-Hydroxybutanoat detektiert. Wahrscheinlich wird poly-(R)-3-Hydroxybutanoat gebildet, um überschüssigen Kohlenstoff zu lagern.

Allgemein bietet die vorliegende Arbeit detaillierte Einblicke in umweltbedingte Adaptationsstrategien des Meeresbakteriums *D. shibae*, das daher als Modell für weitere Meeresbakterien dient.

1 Introduction

1.1 The marine environment

The world's oceans comprise more than 70 % of the earth's surface, which accords an area of about 3.6 x 10^8 km^2 and a volume of 1.3 x 10^9 km^3 and are thus the most important ecosystems on earth (Charette and Smith, 2010). They supply habitats for numerous species. In sum about 225000 plants, heterokonts, protozoa and animals are known (Appeltans *et al.*, 2012). About 2000 species are classified as bacteria (WoRMS, 03/2016). Because of the size, the oceans have an enormous impact on the ecosystem earth and in particular on the earth's climate.

Marine habitats are characterised by several parameters: temperature, pressure, pH, salinity, dissolved gases, nutrient and light supply in connection with distance to shore regions, sea layer and latitude (Fuhrman *et al.*, 2008). Hence, ecological niches in the marine environment are extremely diverse. Most marine life is found in coastal regions and in the euphotic zone. The euphotic zone corresponds to the layer of sea water which receives sufficient light for photosynthesis, up to a depth of 200 m. Indeed, the light intensity fluctuates according to season and latitude (Sommer, 2005). Photosynthesis is the basis of the food chain and the phytoplankton of the oceans fixes nearly 50 % of the global carbon (Giovannoni and Stingl, 2005). In addition to light, phytoplankton requires nutrients supplied by degrading organism, in majority bacteria. This interaction indicates the essential role of bacteria in the marine environment.

Despite the partially challenging conditions described, bacterial species are found everywhere. However, the bacterial communities found, underlie regional and seasonal changes, often influenced by seasonal phytoplankton blooms (Riemann and Winding, 2001; Gilbert *et al.*, 2012; Ladau *et al.*, 2013; Sintes *et al.*, 2013). Generally, the microbial cell concentrations in the ocean surface layer are about 10^5/mL and the phylogenetic diversity is limited to less than 20 microbial clades as revealed by rRNA sequencing (Giovannoni and Stingl, 2005).

Since this study is about the marine bacterium *Dinoroseobacter shibae* DFL12^T, the introducing chapters concentrate on bacteria.

1.1.1 Oxygen supply and denitrification

The dissolved oxygen in the world's oceans differs due to various parameters. High temperatures and salinity lead to a lower oxygen concentration in the seawater and the concentration decreases with increased pressure (Murphy, 2007). A decreased oxygen supply can also be the result of a collapsed algal bloom. During the collapse, algae sink down to the sediment, are lysed and consequently massive nutrients are released. These are utilised by other organisms, mainly bacteria, which leads to oxygen depletion by the extremely increased respiratory activity. The described process is a natural one, but is anthropological increased. Because of excess fertiliser used for crops, the fertiliser can enter the coastal regions by rivers. The inflow of such growth promoting substances, triggers explosive algae growth to an unnatural extent. The thus strongly increased nutrient supply leads to so called *dead zones* in which growth of obligate aerobic organisms is reduced or even inhibited (Dybas, 2005). Figure 1 shows an overview of *dead zones* observed in the coastal regions. Numerous dead zones have been found at the east coast of North America and in the North and Baltic sea (Diaz and Rosenberg, 2008). In times of

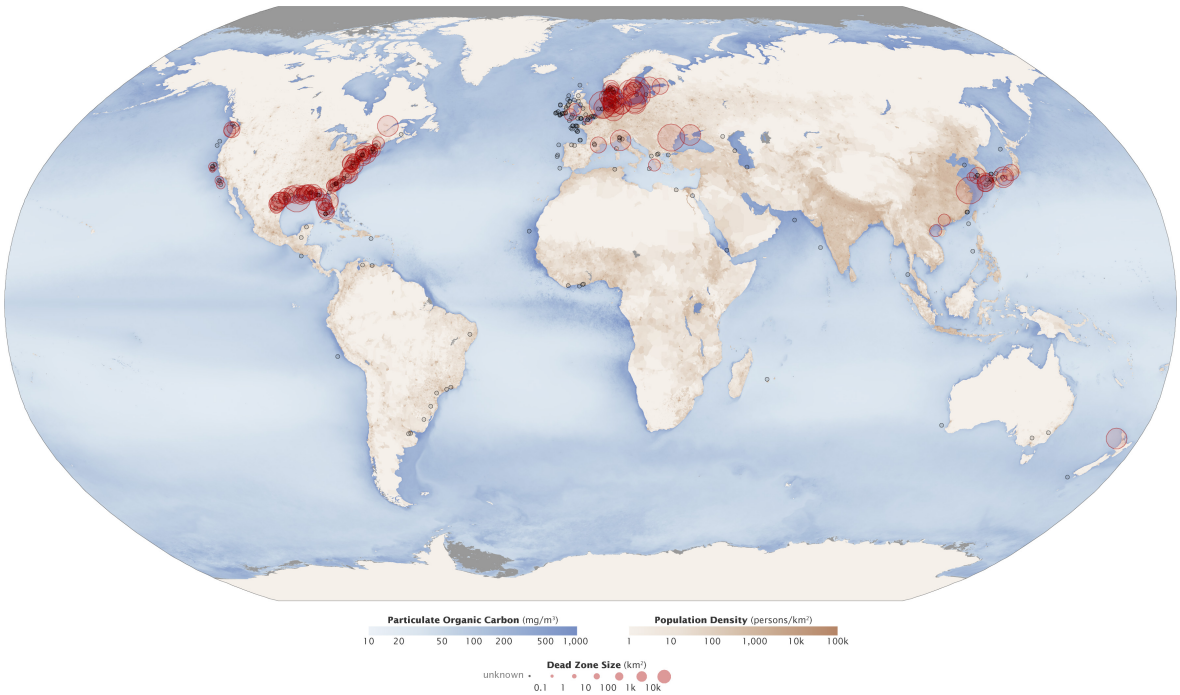

Figure 1: Occurrence of *dead zones*, low-oxygen zones, in the world oceans, due to anthropological eutrophication. Red circles indicate the location and size of many dead zones. Black dots show where dead zones have been observed, but their size is unknown. Map by Robert Simmon and Jesse Allen; based on data from Diaz and Rosenberg (2008). http://earthobservatory.nasa.gov/IOTD/view.php?id=44677

oxygen depletion, facultative anaerobic organisms may use nitrate as an alternative electron acceptor instead of oxygen (Grasshoff *et al.*, 1983).

Denitrification is the only biological process which transfers bounded nitrogen to elementary nitrogen. By a dissimilatory redox process, nitrate is stepwise reduced via the intermediates nitrite, nitric oxide and nitrogen dioxide to elementary nitrogen. Similar to the respiratory chain, a proton-motive force is generated by the transfer of protons out of the cytoplasm. This force is used for the synthesis of ATP by ATPase (Zumft, 1997). Denitrification takes place under anoxic conditions, for example, in the described *dead zones* and in rich organic sediments such as those of many marine coastal areas (Sørensen, 1978). The majority of denitrifying bacteria are facultative anaerobic and belong to the phylum proteobacteria.

However, nitrate is not unlimited. Amongst others, the nitrate concentration changes with the seasons and is in autumn and winter higher than in spring and summer. Again, this is related to oxygen depletion as consequence of increased microbial remineralisation processes, so that nitrate is used as alternative electron acceptor. Maximal nitrate concentrations are 32 µmol/L in the Atlantic ocean, 40 µmol/l in the Pacific ocean and 45 µmol/L in the Indian ocean (Grasshoff *et al.*, 1983). Alternatively to nitrate, dimethyl sulfoxid can be used as electron acceptor by several organisms such as phototrophic bacteria (Zeyer *et al.*, 1987; Visscher and Gemerden, 1991). Dimethyl sulfoxid is a by-product of the dimethylsulphoniopropionate (DMSP) degradation (Librando *et al.*, 2004; Curson *et al.*, 2011). Algae use DMSP as an osmolyte (Sunda *et al.*, 2002). By the collapse of an algae bloom, massive amounts of DMSP might be released and can be utilised as electron acceptor.

1.1.2 Salinity and compatible solutes

The marine environment comprises a number of special challenges. One of them is the high salinity with an average of 3.5 % in the world oceans (Pawlowicz, 2013). Salinity is defined as the total dissolved salt content and is varying with region, depth and seasons in seawater (Reul *et al.*, 2014). The reference salt composition of the major salts of seawater is shown in Table 1. Salt concentrations in seawater of higher or lower salinities can be

found approximately by scaling all values up or down by the same factor (Pawlowicz, 2013).

Table 1: Salt composition of major salts of seawater. (Sommer, 2005). Concentrations are per kilogram of seawater.

Cations	Conc. [g/kg]	Anions	Conc. [g/kg]
Sodium	10.556	Chloride	18.980
Magnesium	1.272	Sulphate	2.649
Calcium	0.400	Bicarbonate	0.140
Potassium	0.380	Bromine	0.065
Strontium	0.013	Borate	0.026
		Fluoride	0.001

Figure 2 shows the annual salinity of the world oceans 2009 with a minimum value of 0.5 % and a maximum value of 4.0 %. The salinity of the North sea is 3.4 % and of the German Wadden Sea 3.0 %. In the Wadden Sea, the salinity can be strongly increased due to wind, solar irradiation, a dry period or increased formation of ice. Furthermore, the salinity is influenced by the inflow of freshwater (precipitation and rivers) according to the

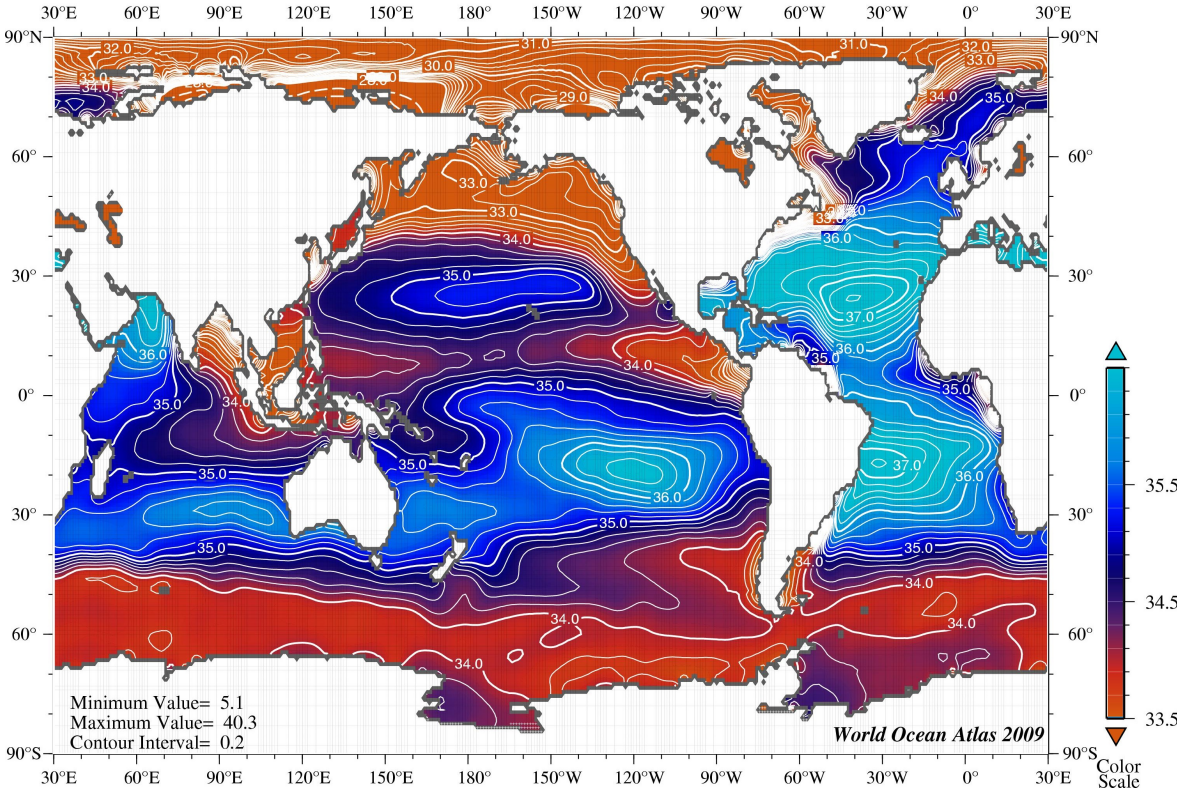

Figure 2: Annual salinity (ppt) at the surface of the world oceans 2009. modified (NOAA National Centers for Environmental Information, 2009)

season. The salinity of the Wadden Sea ranges between 2.5 and 3.2 % in dependence of the season (Becker, 1998).

Biochemical functions depend on specific inorganic ions. However, when a certain concentration is exceeded or underrun, these functions can disrupt as salts affect the catalytic rate and the Michaelis constant of enzymes (Yancey *et al.*, 1982). This concentration threshold is very individual for every organism and indeed is influenced by the particular ecological niche in which the organism is found. By exceeding or underrunning the specific optimal salt range, biochemical processes and thus replication are strongly affected.

To confront salinity and changing salinity, organisms have developed several strategies. One of them is the accumulation of organic compounds, the so-called compatible solutes. They are low-molecular mass organic compounds, which can be accumulated intracellularly in high concentrations without interfering with cellular metabolism (Brown, 1976). The intracellular accumulation of these compatible solutes leads to an exclusion of excess of salt (Roeßler and Müller, 2001; Hagemann, 2011). Other organisms, such as extremely halophilic Archaea of the family *Halobacteriaceae* and halophilic bacteria of the order *Haloanaerobiales*, can accumulate enormous quantities of inorganic ions as they have developed proteins and other macromolecules that cope with high intracellular salt concentrations (Costa *et al.*, 1998).

During a change to hyper- or hypoosmotic conditions bacteria have to deal with a rapid water efflux respective influx. The first response to these life-threatening changes, is the osmoregulation with potassium ions. In a second step, cells accumulate compatible solutes by de-novo synthesis or import them from their environment (Csonka, 1989). Compatible solutes are carbohydrates and their derivatives, polyols, amino acids and their derivatives, ectoines and betaines such as glycine-betaine. Table 2 shows an overview of predominant compatible solutes in various groups of microorganisms. Negatively charged molecules such as glutamate act mostly as counter-ion for cations.

For cyanobacteria it has been shown, that the chemical class of the compatible solute correlates with the salt-tolerance and habitat of the strain. Thus, freshwater strains accumulated saccharides, marine strains accumulated the heteroside glucosylglycerol, and hypersaline strains accumulated saccharides together with glycine-betaine or glutamate-betaine (Mackay *et al.*, 1984). Accordingly, in the marine environment carbohydrate

derivatives like galactosylglycerol in red algae and glucosylglycerol in *e.g.* cyanobacteria and marine pseudomonads are common representatives (Karsten *et al.*, 1993; Mikkat *et al.*, 2000; Hagemann, 2011).

Table 2: Predominant compatible solutes accumulated by eukaryotic micro-algae, bacteria and Archaea (Welsh, 2000).

Group	Solutes accumulated
Micro-algae	Sucrose
	Glycerol
	Mannitol
	Proline
	Glycine-betaine
	Dimethylsulfoniopropionate
Cyanobacteria	Sucrose/trehalose
	Glucosylglycerol
	Glycine-betaine
Photoheterotrophic bacteria	Sucrose/trehalose
	Glycine-betaine
	Ectoine/hydroxyectoine
	N-Acetylglutaminylglutamine amide
Sulphate reducing bacteria	Trehalose
	Glycine-betaine
Heterotrophic bacteria	Glutamate
	Proline
	N-Acetylglutaminylglutamine amide
	Glycine-betaine
	Ectoine/hydroxyectoine
	Trehalose
Archaebacteria	Glycine-betaine
	β-Glutamate

1.2 The Roseobacter group and Dinoroseobacter shibae

1.2.1 The Roseobacter group

Only a few bacterial clades dominate the world oceans. These are two Archaea clades that are associated with coastal ocean ecosystems, cyanobacteria that are ubiquitous but limited to the euphotic zone and globally distributed clades of Actinobacteria, Bacteriodetes, γ-proteobacteria including the abundant clade SAR86 and α-proteobacteria with the highly abundant clade SAR11 and the Roseobacter group (Giovannoni and Stingl, 2005). Figure 3 shows the relative abundance of bacterial clades of bacterioplankton in the oceans. In the underlying study, it has been clearly shown that the α-proteobacteria including the SAR11 clade and the Roseobacter group are the most abundant one in the marine bacterioplankton (Wietz *et al.*, 2010). Unfortunately, most of the microbial groups mentioned remain uncultured, unlike members of the Roseobacter group. This ubiquitous group has been shown to represent up to 20 % of the total bacterial communities (Buchan

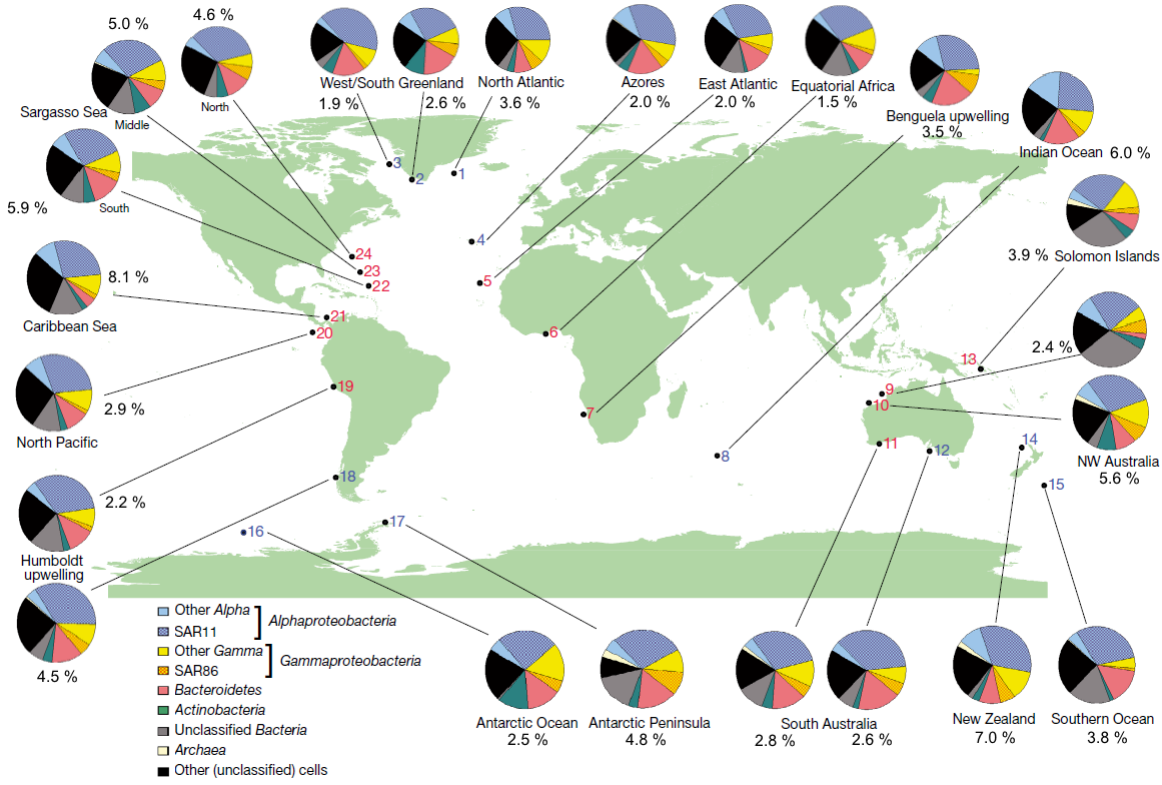

Figure 3: Relative abundance of higher phylogenetic bacterioplankton groups (in % 4',6-diamidin-2-phenylindole-stained cells) at 24 stations worldwide. Blue numbers designate stations at higher (>35°), red numbers designate station at lower (0 to 35°) latitudes (Wietz *et al.*, 2010). x % corresponds to the relative abundance of members of the Roseobacter group (computed on the basis of Table 1 (Wietz *et al.*, 2010)).

et al., 2005). Because of their global distribution, their high diversity and of cultivable members, the Roseobacter group emerged as important model organisms for marine microbial ecology (Newton *et al.*, 2010). The Roseobacter group belongs to the family *Rhodobacteraceae* and the first members, namely *Roseobacter denitrificans* and *Roseobacter litoralis*, were described by Shiba (1991). The genus name *Roseobacter* and group name originate from the pink colour of the first isolates, arising from bacteriochlorophyll *a* and the abundant carotinoid spheroidenone in these organisms (Shiba, 1991).

Roseobacters are heterotrophic and predominantly mesophilic bacteria that are ecological generalist, showing very versatile morphological, physiological and metabolic features (Moran *et al.*, 2004, 2007; Brinkhoff *et al.*, 2008; Newton *et al.*, 2010). This versatility within the Roseobacter group, is partly based on the numerous extrachromosomal elements that most of the Roseobacters exhibit. Twelve plasmids has been found in *Marinovum algicola* (Pradella *et al.*, 2009), however, the pelagic organism *Planktomarina temperata* is free of extrachromosomal elements and possesses one of the smallest genomes within the Roseobacters (Giebel *et al.*, 2013). In several studies, the essential role of the plasmids have been shown, as they carry, for example, genes for the motility of cells, denitrification or the formation of important secondary metabolites (Petersen *et al.*, 2013). Some members of the Roseobacter group are capable to denitrify and several species are anoxygenic aerobic phototrophs (AAnP) such as *R. denitrificans* and *Dinoroseobacter shibae* (Shiba, 1991; Biebl *et al.*, 2005; Piekarski *et al.*, 2009; Wagner-Döbler *et al.*, 2010). AAnPs are photoheterotrophic bacteria that are able of transforming light energy into a proton gradient, resulting in a proton-motive force which is utilised to generate ATP. Thereby, no oxygen is formed (Yurkov and Beatty, 1998). Furthermore, several species form rosettes and biofilms such as *Phaeobacter inhibens* (Labrenz *et al.*, 1998; Pukall *et al.*, 1999; Bruhn *et al.*, 2007; Drüppel *et al.*, 2013). Many metabolic features of the Roseobacter group are assumed to play important roles for marine communities or even for the global carbon and sulphur cycles. As most Roseobacter are capable of forming cobalamin (vitamin B_{12}) and thiamine (vitamin B_1), they are important vitamin provider for algae that are auxotrophic for these vitamins (Newton *et al.*, 2010; Wagner-Döbler *et al.*, 2010). Therefore, Roseobacters are essential in promoting algae blooms and are often found to be associated with such (González *et al.*,

2000; Alavi, 2003). Besides, some Roseobacters, such as *Phaeobacter* spp. and *Silicibacter* spp., have been shown to form antibiotics which are assumed to protect, for example, an algal host against other bacteria (Bruhn *et al.*, 2007). In return, hosts are assumed to provide nutrients, thus a symbiotic interaction results. Otherwise, in some cases this symbiosis has been shown to be followed by a pathogenic phase due to the production of secondary metabolites (Seyedsayamdost *et al.*, 2011; Wang *et al.*, 2015; D'Alvise *et al.*, 2016). Furthermore, many bacteria of the Roseobacter group are capable of degrading dimethylsulfoniopropionate (DMSP) (González *et al.*, 2003; Dickschat *et al.*, 2010), whose volatile degradation product dimethyl sulphide is an important intermediate for the global sulphur cycle (Lovelock *et al.*, 1972). Further metabolic characteristics of the Roseobacter group, are the formation of quorum sensing molecules (Patzelt *et al.*, 2013; Zan *et al.*, 2014), the storage compound poly-(R)-3-hydroxybutanoate (Cho and Giovannoni, 2004; Vandecandelaere *et al.*, 2008; Cai *et al.*, 2012) and the usage of the ethylmalonyl-CoA pathway instead of the glyoxylate shunt for utilising C_2-carbon sources such as acetate or glyoxylate (Newton *et al.*, 2010). Non of the described traits is representative of the entire group, underlining the versatility of the Roseobacter group.

This extremely diverse group of bacteria is, as previously mentioned, ubiquitous and thus found in a large variety of habitats (Figure 3), including coastal regions, open oceans, marine snow, variety of micro- and macroalgae, microbial mats, sediments, polar sea ice and marine invertebrates (Buchan *et al.*, 2005; Wagner-Döbler and Biebl, 2006). The largest fraction of the Roseobacter group is the pelagic Roseobacter-clade affiliated (RCA) cluster that comprises mainly uncultured phylotypes (Selje *et al.*, 2004; Brinkhoff *et al.*, 2008; Voget *et al.*, 2015), except few representatives such as *P. temperata* type strains (Giebel *et al.*, 2013).

1.2.2 The strain *Dinoroseobacter shibae* DFL12^T

The type strain *Dinoroseobacter shibae* DFL12^T was first described and isolated from the benthic dinoflagellate *Prorocentrum lima* in the North Sea around the island Helgoland (Allgaier *et al.*, 2003; Biebl *et al.*, 2005). The genus name *Dinoroseobacter* consists of *dinos,* as the organism was isolated from a Dinophyceae, and *Roseobacter*, as it is a *Roseobacter*-like organism. The species *D. shibae* is named after Prof. Tsuneo Shiba. The

organism is chemoheterotrophic, forms variable-sized ovoid rods but also long filaments, is motile by means of a polar flagellum, the optimal pH for growth ranges from 6.5 to 9.0 and the optimal temperature is 33 °C (Biebl *et al.*, 2005; Patzelt *et al.*, 2013).

The genome of *D. shibae* consists of a 3790 kilo base pairs (kbp) chromosome and five extrachromosomal elements: three plasmids with 191, 126 and 86 kbp and two chromids with 153 and 72 kbp (Wagner-Döbler *et al.*, 2010; Soora *et al.*, 2015). Chromids carry some core genes, and their nucleotide composition and codon usage are similar to those of chromosomes (Harrison *et al.*, 2010). The 86 and 191 kb plasmids have been shown to be crucial for anaerobic growth (Ebert *et al.*, 2013) and only recently, the 72 kb chromid has been shown to play an essential role during starvation while applying a light/dark cycle (Soora *et al.*, 2015) and curing of the 191 kb plasmid led to the loss of the ability to kill the algal host (Wang *et al.*, 2015).

Meanwhile, *D. shibae* was investigated in several studies. In this context, the previously described strict aerobic organism has been shown to be capable of denitrification (Figure 4). Instead of using a Nar type nitrate reductase, which is limited to anaerobic respective microaerophilic conditions, *D. shibae* uses a Nap type reductase, which is also active under aerobic conditions (Piekarski *et al.*, 2009; Wagner-Döbler *et al.*, 2010). Besides, *D. shibae* is able to form vitamin B_1 and B_{12}. These are essential vitamins for many dinoflagellates. In co-culture experiments, it has been shown that these vitamins are provided to algal hosts

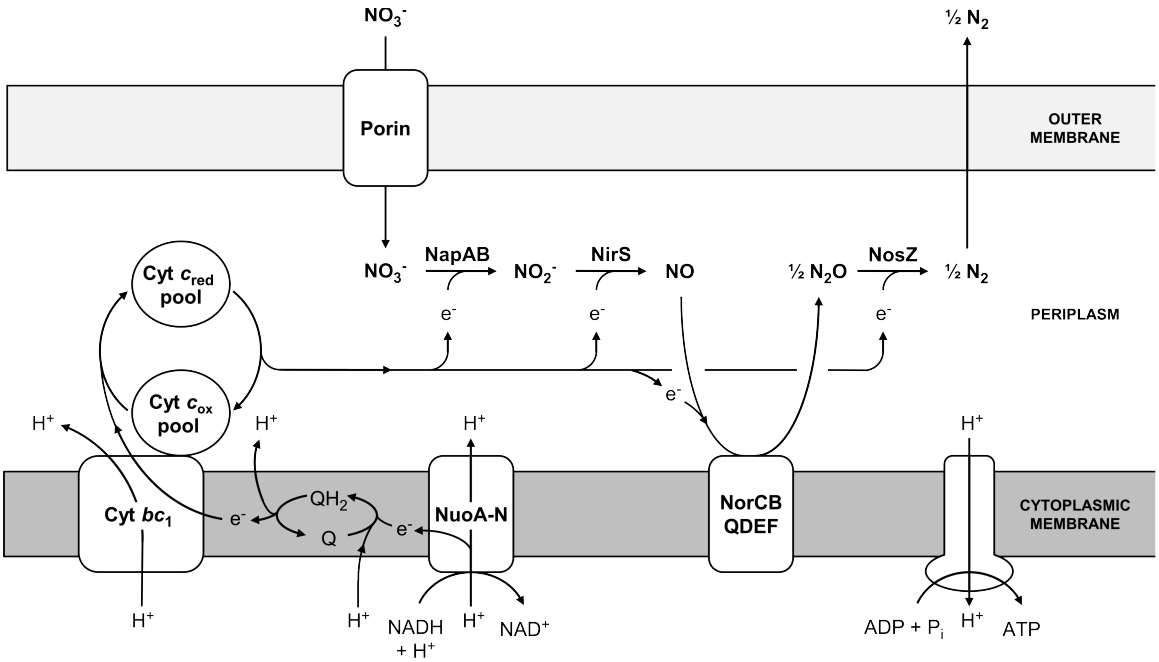

Figure 4: Schematic representation of the denitrification apparatus of *D. shibae* (Laass, Kleist *et al.*, 2014).

and a mutualistic interaction was observed (Wagner-Döbler *et al.*, 2010; Paul *et al.*, 2013). However, the mutualistic phase was reported to be followed by a pathogenic phase, as it has been reported for other members of the Roseobacter group (Seyedsayamdost *et al.*, 2011; Wang *et al.*, 2015). According to the eponymous characteristic of Roseobacter, *D. shibae* is pink, due to the formation of the carotinoid spheroidenone and the coloured bacteriochlorophyll *a*. Amongst others, these substances enable *D. shibae* to gain energy from light by aerobic anoxygenic photosynthesis (Biebl and Wagner-Döbler, 2006; Wagner-Döbler *et al.*, 2010; Tomasch *et al.*, 2011).

Some Roseobacter and also *D. shibae* produces *N*-acyl homoserine lactones (AHL), molecules, which are used for cell-to-cell-communication. *D. shibae* forms three AHLs which control cell heterogeneity, flagellation and the expression of a type IV secretion system. Furthermore, *D. shibae* reacts to foreign AHLs which probably enable interspecies communication (Patzelt *et al.*, 2013).

A first metabolic study of *D. shibae* revealed that the organism degrades glucose via the phosphorylative Entner-Doudoroff pathway because of a not active phosphofructokinase, which would enable degradation via glycolysis (Fürch *et al.*, 2009).

Overall, *D. shibae* employs a narrow spectrum of substrates compared with for example *Phaeobacter inhibens* (Martens *et al.*, 2006; Rex *et al.*, 2013), but has several strategies to confront most diverse environmental challenges.

1.3 Systems biology

Systems biology is the attempt to understand an entire biological system, for example a cell, in its composition, structure and dynamic. This attempt requires an inter-disciplinary approach of several so called “Omic” fields, namely: genomics, transcriptomics, proteomics and metabolomics. Figure 5 shows the “Omics” cascade including the analysis of the genome, transcriptome, proteome and metabolome. The integrative analysis of a biological system's response to a perturbation on these levels lead to a better understanding of the biochemical and biological mechanisms in complex systems (Dettmer *et al.*, 2007).

The genome offers the information what possibilities or restrictions an organism underlies. Thus, it is the essential basis for the interpretation of the following omic approaches.

The transcriptome is the set of all gene transcripts present in the investigated system at a defined time point. Consequently, it provides the information, which possibilities of the genome are accessed. The most common analytical approaches for genome wide transcriptome analyses are DNA microarrays and RNA sequencing (Wang *et al.*, 2009; Tachibana, 2015).

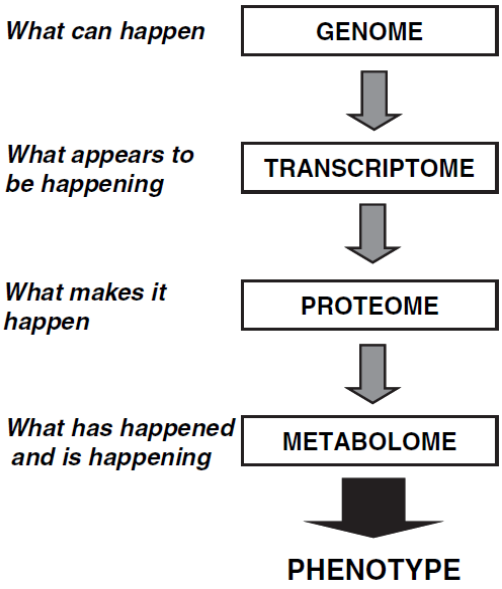

Figure 5: The "Omics" cascade comprises complex datasets that as an entity comprehensively describe the response of biological systems to disease, genetic, and environmental perturbations (Dettmer *et al.*, 2007).

The proteome comprises all proteins present at a certain time under particular conditions. Since proteins are the main tools of every biological system, proteome analysis offers distinct information about the current state and activities of the system. The major approaches of proteome analyses are 2D-difference gel electrophoresis (2D-DIGE) which is only applicable for soluble proteins and liquid chromatography coupled with a matrix-assisted laser desorption/ionisation mass spectrometer (Cox and Mann, 2011).

The metabolome includes all metabolites and is the most complex omic approach, in regard to the chemical and physical characteristics, the concentration ranges and its immense dynamic. However, the metabolome is the most predictive of phenotype and therefore contributes in an important way to systems biology studies (Dettmer *et al.*, 2007).

1.4 Metabolome analyses

1.4.1 Metabolomics

Metabolomics seeks an analytical description of complex biological samples, and aims to characterise and quantify all the small molecules in such a sample at a certain time in response to a biological stimuli or genetic manipulation (Nicholson and Lindon, 2008).

Contrarily to other omic approaches, the metabolome cannot be handled with one single-instrument platform, because of the high physico-chemical variances and the wide range of abundances (Kell, 2004; Dettmer *et al.*, 2007). Thus, "true" metabolomics is not possible yet and several approaches are needed to cover a majority of the present metabolites. Metabolome studies conducted so far, performed metabolite profiling or fingerprinting. Metabolite profiling is the analysis of selected metabolites with accordingly adapted sample preparation in regard to their chemical properties. These metabolites may belong to a certain class of compounds or a particular pathway (Fiehn, 2002). Metabolic fingerprinting is a metabolic pattern analysis of partly unidentified metabolites that intends to define different patterns in dependence on disease, toxin exposure, environmental or genetic alterations (Dettmer *et al.*, 2007). However, in many cases the identity of particular metabolites is essential and high-resolution instruments such as mass spectrometer, nuclear magnetic resonance (NMR) spectrometer or Fourier transform infrared spectrometer are required for their identification.

In the present study small, polar, soluble metabolites of *D. shibae* were analysed in untargeted approaches.

1.4.2 Sample preparation for metabolomics in bacteria

In respect to the extreme dynamic of the metabolism, the first and most challenging step for metabolome sample preparation is always the attempt of rapidly stopping the enzyme activity to minimise further metabolic transformations. Contrarily to, for example, plant tissues or cell cultures, the sample preparation of bacterial cell suspensions is more difficult, because cells cannot freeze clamped with liquid nitrogen without a previous separation of the growth medium (Fiehn, 2002; Dettmer *et al.*, 2007; Spura *et al.*, 2009).

This separation step is done by filtration (Bolten *et al.*, 2007) or centrifugation (Spura *et al.*, 2009). Afterwards, the cells have to be washed to guarantee the removal of extracellular metabolites. Washing have to be conducted with a solution with suitable ionic strength to prevent cell leakage and thus loss of metabolites. Alternative methods, without removal of the growth medium, are so called quenching methods. Here, usually temperature adjusted organic solutes are used that enter the cells without disturbing the cell integrity and lead to denaturation of proteins. Such quenching methods have to be carefully adapted to the investigated organism to minimise cell leakage (Bolten *et al.*, 2007; Spura *et al.*, 2009).

After the separation of cells, extraction methods according to the target metabolite class are performed. Usually, this is done by liquid-liquid extraction or solid-phase extraction with a following concentration step in respect to low concentrated metabolites (Dettmer *et al.*, 2007).

1.4.3 Gas chromatography – mass spectrometry

Gas chromatography (GC) coupled to mass spectrometry (MS) is one of the most common approaches for high-throughput metabolome analyses (Dettmer *et al.*, 2007). With this analysis method, a wide range of metabolites (with masses up to 1000 Da) can be covered. Volatile compounds are analysed directly by the so called headspace technique and other compounds are derivatised to make them vaporisable. In this study, metabolites were silylated with *N*-methyl-*N*-(trimethylsilyl)-trifluoro-acetamide (MSTFA). The silylation reaction accords the introduction of a silyl group in place of a labile hydrogen atom (Figure 6 B). This substitution leads to an improved solubility in non-polar solvents and the disappearance of hydrogen bounds and thus to an increased volatility (Kashutina *et al.*, 1975). Since some metabolites exhibit more than one labile hydrogen, several derivatives of the same metabolite are possible, as, for example, shown for glycine (Figure 6 B, Kanani and Klapa, 2007). These derivatives have to be combined in the final data processing. To minimise the number of possible derivatives in the case of carbohydrates, an additional derivatisation step is conducted. Here, carbonyl groups are replaced by a methoxyamine group by the reaction with methoxyamine-hydrochlorid (Figure 6 A), which stabilises the open-chain structure of a sugar (Adams, 1999).

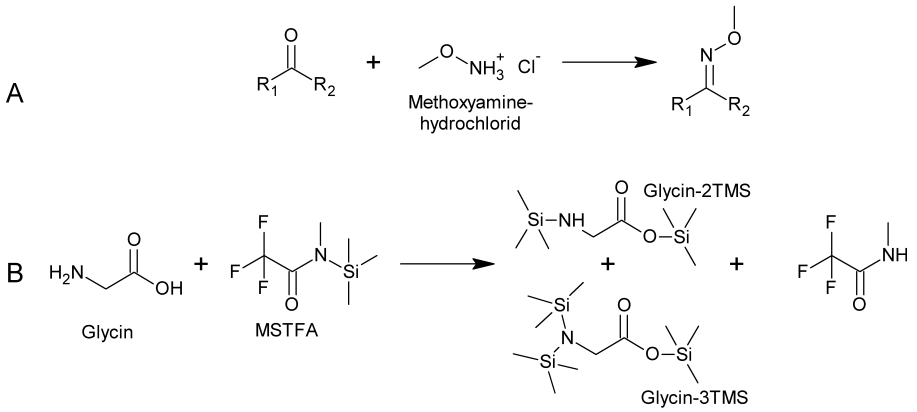

Figure 6: Derivatisation reactions used in the present study. A: Methoxyamination of a carbonyl compound, B: silylation of glycine by MSTFA (Kashutina *et al.*, 1975). MSTFA: *N*-methyl-*N*-(trimethylsilyl)-trifluoro-acetamide; TMS: trimethylsilyl.

Substances that have to be vaporised first, are often injected into the GC instrument by a programmed temperature vaporising (PTV) injector. Here, the derivatised substances are progressively vaporised by a temperature gradient and thus enter pre-separated the GC system (Stan and Linkerhägner, 1996).

The GC system is equipped with a temperature controlled and coated separation column and the compounds are transported by an inert carrier gas, such as helium. According to the mass, the steric configuration, the interaction with the column material and other parameters, the substances are separated individually. Usually, the separation is conducted by applying an additional temperature gradient.

By using MS, the separated substances have to be ionised. Usually, this is done with a standardised electron ionisation (EI), applying an electron energy of 70 eV. The ionisation with 70 eV is a so called hard ionisation technique and therefore, induces characteristic and complex but reproducible fragmentation reactions that are exchangeable between laboratories (Strehmel *et al.*, 2008). The ionised compounds are then detected with the mass spectrometer. The resulting spectra are individual for each compound and are used for the identification of these. For the GC-MS approach described, several open and commercial MS libraries are available that allow the identification of compounds (Dettmer *et al.*, 2007).

1.5 Structure analysis via atmospheric pressure chemical ionisation mass spectrometry

By using untargeted GC-MS approaches, unidentified substances are detected. The identification of these is often essential to confirm or deny their biological origin and to elucidate their potential metabolic role. Several instruments can be used for structure analysis such as NMR spectroscopy. However, NMR spectroscopy presuppose the isolation of large quantities of the compound of interest, which is in most cases very challenging. Therefore, the big advantage of using GC-APCI-MS (atmospheric pressure chemical ionisation) is the direct comparability to GC-EI-MS. Exactly the same sample preparation, derivatisation and GC separation can be conducted and only the ionisation technique is replaced. Thus, the assignment of the compound of interest is easily done.

In contrast to EI, APCI is a soft ionisation technique that leads to only slight fragmentation. Hence, the determination of the molecular ion is possible in most cases (Strehmel *et al.*, 2014). By using high mass resolution MS instruments, the accurate mass of each compound can be determined. With the accurate mass and some defined restrictions concerning the elemental composition (C, H, N, S, O, P and Si because of the derivatisation), sum formulae can be predicted. However, with increasing molecular mass the number of possible sum formula predictions increase, too. By using isotope abundance patterns as further constraint, the number of possible candidates can be reduced. The basis of these patterns, is that natural compounds reflect the natural abundance of stable elemental isotopes such as ^{13}C which is found at approximately 1.11 % of the most frequent ^{12}C (Kind and Fiehn, 2006).

On the basis of a predicted sum formula, modifications concerning the derivatisation and even the cultivation can be used to unravel the structure information of the compound of interest. By conducting the derivatisation without the methoxyamination step, carbonyl groups are revealed. The number of silylated groups and thus of labile hydrogen atoms of hydroxyl-, thiol- or amino groups, can be elucidated by MSTFA-*d9* (MSTFA-9-times deuterated) derivatised samples. By comparison of MSTFA and MSTFA-*d9* measurements a mass shift is observed, which provides information on the number of trimethylsilyl groups. The same is achieved by using two different derivatisation reagents that react equally. In the case of MSTFA, BSTFA (N,O-bis(trimethylsilyl)trifluoro-acetamide) can be

used alternatively. By using MSTFA, the labile hydrogen atom is replaced by a $Si(CH_3)_3$-moiety and by using BSTFA by a $Si(CH_2)C(CH_3)$-moiety. Again, the resulting mass shift provides information on the present groups exhibiting labile hydrogen atoms (Strehmel *et al.*, 2008). This approach is cheaper compared with the derivatisation with MSTFA-*d9*, but the changed retardation behaviour of the differently derivatised compound in the GC system, hinders the correct assignment of the compound of interest. Furthermore, the number, for example, of carbon atoms can be determined by providing the organism exclusively fully ^{13}C-isotope labelled substrates. Compared with standard ^{12}C-measurements, the detected mass shift accords the number of carbon atoms. Concomitantly, this approach ensures the biological origin of the compound of interest.

Lastly, the occurring specific fragmentation due to the ionisation can be used to unravel the structure of the compound. For the interpretation of fragmentation patterns, existing decision trees for substructure predictions or other sources are available (Hummel *et al.*, 2010).

However, even if a structure assumption evolved from the conducted analyses, a reference substance has to be analysed. Unfortunately, many substances are not available commercially.

1.6 Objectives

Marine bacteria have been shown to take over essential roles in the marine ecosystem as they promote growth of phytoplankton and higher organisms. Phytoplankton is assumed to fix about 50 % of the global carbon and thus stable populations are essential. Furthermore, the breakdown of dissolved organic matter by bacteria, contributes to the world's sulphur and nitrogen cycle. Thus, the understanding of marine bacteria is of great interest also in regard to rapid changing areas because of anthropological effects. So far, predominantly genomic and phylogenetic studies regarding marine heterotrophic bacteria were conducted as numerous marine strains are uncultivated. Since the globally distributed so called Roseobacter group exhibits cultivatable strains, members of this group got into focus in the last decades as models for heterotrophic marine bacteria and their ecological role.

The aim of this thesis was to get access to adaptation processes to changing environmental conditions of the Roseobacter member and model organism *Dinoroseobacter shibae* DFL12^T. On the basis of the complete genome sequence of *D. shibae* (Wagner-Döbler *et al.*, 2010), systems biology approaches were conducted in cooperation with several partners. My part was the metabolome analysis via GC-MS.

In the first experiment the transition of *D. shibae* from oxygen to nitrate respiration should be investigated. This scenario simulates anoxic conditions that, for example, can occur after the collapse of an algal bloom that is accompanied by the release of excess nutrients which leads to increased oxygen respiration.

The focus of the second study is the metabolic adaptation of *D. shibae* to different salinities in long-term adapted cells and cells exposed to a salt shock. In general, the marine environment is characterised by a high salinity which is influenced by several parameters such as seasons. These experiments presupposed the identification of so far unknown metabolites of *D. shibae*. Within the scope of this study, these were identified by GC-APCI(+)-MS analyses.

In the third experiment, as nitrogen is often limited according to season and region, the organism is analysed during the exposure to nitrogen-limitation in combination with the high salinity of the marine habitat.

2 Material and methods

2.1 Chemicals

If not indicated otherwise, chemicals and reagents of highest quality marked with the term “purest” or “for analytical purpose” were utilised. The substances were purchased from the manufacturers Carl Roth (Karlsruhe, Germany), CS GmbH (Langerwehe, Germany), Fisher Scientific (Schwerte, Germany) and Sigma-Aldrich (Steinheim, Germany).

2.2 Organisms

Table 3: Strains used in this study

Strain	Description	Reference
Dinoroseobacter shibae DFL12^T DSM 16493	Wild-type	(Biebl *et al.*, 2005)
Escherichia coli BL21 pET28a(+)	Expression mutant, with a pET28a(+) vector carrying *gpgS*	(Klähn *et al.*, 2010)

2.3 Media and solutions

All water based solutions were prepared with salt-free, particle filtered and sterile filtered ultra pure water (ddH_2O) from an ultra pure water system (arium®611VF, Sartorius). Sterilisation was achieved by autoclaving for 20 min at 121 °C and 1 bar overpressure, unless described otherwise.

2.3.1 Marine bouillon

The complex medium marine bouillon (MB) was purchased from Carl Roth and was prepared following the manufacturer's instruction.

2.3.2 Luria & Bertani medium

Luria & Bertani medium Luria/Miller (LB medium) was purchased from Carl Roth and was prepared following the manufacturer's instruction. Sterile kanamycin-solution was added to a final concentration of 50 µg/mL prior to inoculation.

2.3.3 Salt water minimal medium

The salt water minimal medium (SWM) was prepared immediately before the inoculation. Therefore, different high concentrated stock solutions: Basic SWM, KH_2PO_4, $CaCl_2$, $NaHCO_3$, Na_2-succinate, vitamins and trace elements were combined and sterile ddH_2O was added. All stock solutions were autoclaved, with the exceptions of the carbon source, the vitamins and the trace elements, which were sterilised by filtration.

For the experiment described in section 2.6.1 the SWM was additionally spiked with KNO_3, achieving a final concentration of 25 mM nitrate.

For the experiment section 2.7 Basic SWM without NaCl was prepared and the salt concentration was adjusted by a 166.75 g/L NaCl-stock solution.

Basic SWM: final concentration in the medium [g/L]

Na_2SO_4	4
NH_4Cl	0.25
NaCl	20
$MgCl_2$ x 6 H_2O	3
KCl	0.5

$CaCl_2$: final concentration in the medium[g/L]

$CaCl_2$ x 2 H_2O	0.15

KH_2PO_4: final concentration in the medium[g/L]

KH_2PO_4	0.2

$NaHCO_3$: final concentration in the medium[g/L]

$NaHCO_3$	0.19

Carbon source: final concentration in the medium [g/L]

Na_2-Succinate	2.74

Vitamins: final concentration in the medium [mg/L], sterile filtrated

Biotin	2
Nicotinic acid	20
4-Aminobenzoate	8

Trace elements: 2 mL/L medium

H_2O	50	mL
$Fe(II)SO_4$ x 7 H_2O	2.1	g
HCl, 25%ig	13	mL
(Na_2EDTA)	5.2	g

The pH was adjusted to 6 - 6.5 and the following trace salts were added [mg].

H_3BO_3	30
$MnCl_2$ x 4 H_2O	100
$CoCl_2$ x 6 H_2O	190
$NiCl_2$ x 6 H_2O	24
$CuCl_2$ x 2 H_2O	2
$ZnSO_4$ x 7 H_2O	144
Na_2MoO_4 x 2 H_2O	36

Filled up to 1000 mL with ddH_2O and sterile filtrated

2.3.4 Inoculation solutions for phenotype microarray analysis

Inoculation solution 1

IF10a GN Base (1.2x, Biolog inc., USA)	5 mL
ddH_2O	1 mL

Inoculation solution 2

IF10a GN Base (1.2x, Biolog inc., USA)	8.33 mL
Vitamins	120 µL
Trace elements	24 µL
Redox Dye Mix D(Biolog inc., USA)	120 µL
ddH_2O	1.406 mL

2.3.5 Alkane mix for retention index calibration

The following alkanes were dissolved in cyclohexane for the preparation of a stock solution.

Decane	12.5 mg, respectively 17.1 µL
Dodecane	12.5 mg, respectively 16.7 µL
Pentadecane	12.5 mg, respectively 16.2 µL
Nonadecane	12.5 mg

Docosane	12.5 mg
Octacosane	12.5 mg
Dotriacontane	12.5 mg
Hexatriacontane	12.5 mg

The stock solution was diluted 8-fold with cyclohexane, aliquoted and stored at -20 °C for GC-MS measurements.

2.4 Microbial techniques

2.4.1 Measurement of cell density

The cell density was determined photometrically at 578 or 600 nm. If needed, cultures were diluted with Basic SWM (section 2.3.3) accordingly.

2.4.2 Cultivation procedure

If not indicated otherwise, MB medium was inoculated with cells of a glycerol stock culture (storage at -80 °C) with an inoculating loop. The cultures were incubated for at least three days.

According to the set-up, a minimal medium pre-culture was inoculated with 2 % (v/v) of the MB medium culture or with a defined volume of a glycerol stock culture with previously adapted cells according to the final condition. In the exponential growth phase of the pre-culture, it was used to inoculate the main culture. Initial cell density was set to an OD_{600} of 0.05.

All incubations occurred at 150 rpm and 30 °C in darkness in Erlenmeyer flasks with three baffles (Certomat BS-1, orbit 50 mm, Sartorius), unless described otherwise.

2.4.3 Preparation of glycerol stocks of adapted cells

Glycerol stock cultures of adapted cells were prepared by using a main culture of the appropriate condition with a cell density of an OD_{600} of 1. 50 mL of the culture were concentrated by centrifugation (9000 x *g*, 3 min, 4 °C), the supernatant was discarded and the cells were resuspended with 5 mL medium and 1.25 mL glycerol. After mixing, the

solution was kept on ice for 20 min and afterwards aliquoted and quick-frozen with liquid nitrogen. Glycerol stock cultures were stored at -80 °C.

2.5 Phenotypic microarray analysis

Phenotypic microarray analysis of *D. shibae* was performed with an OmniLog-reader by using the PM9 micro plate (Biolog inc., USA) for osmolytes. Therefore, *D. shibae* cells of a MB-agar plate were transferred to inoculation solution 1 until achieving a turbidity of 13 %. 2 mL of inoculation solution 1 were added to inoculation solution 2 and each well of the micro plate was filled with 100 µL of this solution. Incubation time was 72 h at 30 °C. Every 15 min a photo was automatically taken. The gained data were processed in the Biolog vendor software with respect to the corresponding areas under the curves.

2.6 Main experiment: Adaptation processes during oxygen depletion

2.6.1 Cultivation conditions and experimental set-up

To investigate the adaptation processes of *D.* shibae during oxygen depletion, a continuous cultivation was performed in SWM (section 2.3.3) with a succinate concentration of 5 mM in an HT Multifors 2 reactor (Infors) at 30 °C, pH 8.0, with an aeration of 0.7 L_n of air/min and a stirring speed of 150 rpm. The working volume of each reactor was 1 L. The chemostat was protected from light to avoid aerobic anoxygenic photosynthesis. The reactors were inoculated and the organism was cultivated until the culture reached an OD_{578} of 0.5 and then the continuous cultivation was started. After 20 h of continuous cultivation the aeration was stopped, so that *D. shibae* consumed the residual oxygen itself (Ebert *et al.*, 2013; Laass *et al.*, 2014). The cultivations were performed in cooperation with Sebastian Laaß in the Institute of Microbiology (TU Braunschweig, AG Jahn).

For the metabolome analysis cells, according a cell dry weight (CDW) of 7 mg, were sampled by centrifugation (8819 x *g*, 3 min, 4 °C) and were washed twice with 20 mL of a

35 g/L NaCl-solution. Further preparation was done as described in section 2.12.1. The investigated time points were before (0 min) and 15, 30, 60 120 and 240 min after oxygen shut-down.

Additionally, samples were taken for PHB, transcriptome, proteome and electron microscopy analysis by Sebastian Laaß. Details of the sampling and the analyses are provided in (Laass *et al.*, 2014).

In general, the obtained data were compared always with the reference state, the culture state directly before the oxygen shut-down (0 min).

2.6.2 ATP determination in oxygen depleted D. shibae *DFL12^T cells*

To analyse the ATP supply of *D. shibae* cells during oxygen depletion, an additional cultivation in batch culture was performed to guarantee anaerobic harvesting conditions. Therefore, cultures were prepared according to standard conditions (section 2.4.2) in SWM (section 2.3.3). Cells were cultivated until an OD_{600} of 0.9 and were then filled to the brim in 50-mL falcons to minimise the residual air space. The cultures were transferred to an anaerobic chamber and the stirring was stopped.

In the following, 500 µL culture were harvested anaerobically and quick-frozen with liquid nitrogen. The investigated time points were before (0 min) and 15, 30, 60, 120, 180, 240, 300 and 360 min after oxygen shutdown.

For the quantification of ATP, the quick-frozen samples were diluted (5-fold; only reference (0 min) was diluted 20-fold). The determination was done with the BacTiter-Glo™ Microbial Cell Viability Assay (Promega) following the manufacturer's instructions, by using a sample volume of 50 µL. ATP content was quantified by using a calibration curve (range 1.25-20 pmol). Luminescence was measured with a Tecan Infinite® M200 (Tecan Group), which was controlled with the vendor software Tecan i-control 3.7.3.0.

2.7 Main experiment: Exposure to various salinity and nitrogen limitation

2.7.1 Cultivation conditions and experimental set-up of various salinity and nitrogen limitation

For the analysis of the metabolome of *D. shibae* DFL12^T under various salinity, it was cultivated according to the standard conditions (section 2.4.2). For the inoculation of the pre-cultures previously condition-adapted glycerol stock cultures were utilised. Salinity was regulated by a 166.75 g/L NaCl-stock solution. Minimal salinity was 0.3 % (w/v) due to necessary buffer substances etc. Investigated salinities were 0.3, 2.3, 3.5 and 5 %.

Additionally, cultures were cultivated with a salinity of 3.5 % and a limited nitrogen supply (1 mM ammonium instead of 4.7 mM ammonium).

Overall, for metabolome analysis cells according a CDW of 7 mg were harvested by centrifugation (9000 x *g*, 3 min, 4 °C). Afterwards, the cell pellets were washed twice with a 0.9, 2.3, 3.5 and 5 % NaCl solution respectively, according to the cultivation conditions 0.3, 2.3, 3.5 and 5 % salinity. The metabolome of cells in medium containing 3.5 % salt served as a reference for the interpretation of data.

For PHB determination 2 mL of the culture were centrifuged (12000 x *g*, 1 min) and the cell pellets were quick-frozen in liquid nitrogen. Further preparation was done as described in section 2.11.2.

In general, the investigated time points were at an OD_{600} of 1 (exponential growth) and at OD_{max}, with the exception of the nitrogen limited cultures. These were only sampled at a OD_{600} of 0.9.

2.7.2 Cultivation and experimental set-up for salt shock of cells

To study the metabolic and transcriptional response of *D.* shibae DFL 12^T after an osmotic up-shock, cells were cultivated under standard conditions (section 2.4.2) with a salt concentration in the medium of 2.3 %. For the inoculation of the pre-culture a previously condition-adapted glycerol stock culture was utilised. After the cultures reached

an OD_{600} of 1, 2.7 g sterilised solid NaCl was added each to half of the cultures. 10 and 90 min after the salt shock samples for metabolome and transcriptome analysis were taken.

For the metabolome analysis cells, according a CDW of 7 mg, were sampled by centrifugation (9000 x *g*, 3 min, 4 °C) and were then washed twice with 20 mL of a 2.3 or 3.5 % NaCl solution (w/v). Further preparation was done as described in section 2.12.1.

For the transcriptome analysis, 15 mL of the cultures were centrifuged (9000 x *g*, 30 min, 20 °C) and 1 mL RNAprotect™ (Qiagen) was added to the cell pellets and mixed for at least 30 s. After an incubation time of 5 min the mixture was centrifuged again (8000 x *g*, 20min, 20 °C) and the pellets were quick-frozen in liquid nitrogen. Further preparation of the samples was done as described in section 2.9.2.

2.7.3 Quantification of glutamate and glycosides

Quantification of glutamate and glycosides was achieved by measuring calibration lines of glutamate and β-glucosylglycerol in a range of 10 to 50 nmol by GC-MS. β-Glucosylglycerol was used for the quantification of α-glucosylglycerol and α-glucosylglycerate due to the absence of available standards. Measurements of the calibration lines were done at the same time as the metabolome analysis and only 0.5 µL of the sample were injected (section 2.13.1).

2.8 Synthesis of α-glucosylglycerate

Cultivation of the *E. coli* expression clone, purification of glucosylglycerate-3-phosphate synthase (GpgS) and the enzymatic synthesis of α-glucosylglycerate was adapted from the publication of Klähn et al. (2010). The *E. coli* clone contains a pET28a(+) vector, including the gene *gpgS* of *Synechococcus* sp. PCC 7002 and a sequence encoding an N-terminal His-tag.

2.8.1 Expression of glucosylglycerate-3-phosphate synthase

To express GpgS, a pre-culture of *E. coli* BL12, carrying the plasmid pET28a(+) possessing the gene encoding GpgS (Klähn *et al.*, 2010), was prepared by inoculation of

LB medium (section 2.3.2) in an Erlenmeyer flask with cells of a glycerol stock culture by using an inoculation loop. The cultivation occurred at 150 rpm and 37 °C (Certomat BS-1, orbit 50 mm, Sartorius). With the actively growing cells of the pre-culture in sum 1600 mL LB medium were inoculated (1 % v/v) and incubated for six hours as described before. Then isopropyl-β-D-thiogalactopyranosid was added achieving a final concentration of 1 mM and the incubation temperature was reduced to 20 °C.

Cells were harvested by centrifugation for 10 min at 9820 x *g*. The cell pellets were stored at -20 °C until further preparation.

2.8.2 Purification of glucosylglycerate-3-phosphate synthase

Half of the obtained cell pellets of section 2.8.1 were utilised for protein extraction. The extraction was done by sonication (3 times 2 min with mode 6 and 2 times 2 min with mode 7, amplitude 60 %; Bandelin Sonoplus HD 2070) on ice in 20 mM NaH_2PO_4-buffer (pH 7.8) containing 1 mg/mL lysozyme and 50 µg/L of the serine protease inhibitor phenylmethanesulfonyl fluoride (PMSF). After centrifugation (18514 x *g*, 30 min, 4 °C), the supernatant was utilised for affinity chromatography.

Affinity chromatography was performed with a ÄKTAprime plus (GE Healthcare Life Sciences) on a Protino®Ni-NTA column (Macherey-Nagel). The system was equilibrated with a 20 mM NaH_2PO_4-buffer containing 10 mM imidazole, 50 µg/L PMSF and 50 % glycerol (v/v). Proteins were eluted with increasing imidazole concentration (gradient: 10 – 250 mM) by using a flow rate of 1 mL/min.

Purity of the protein was confirmed with a standard 12 % sodium dodecyl sulphate polyacrylamide gel electrophoresis (appendix A1)

2.8.3 Enzymatic synthesis of α-glucosylglycerate

α-Glucosylglycerate was synthesised in a 100 µL assay containing 2.5 mM ADP-glucose, 2.5 mM 3-phosphoglycerate, 5 mM $MnCl_2$ and about 10 µg purified recombinant protein in 25 mM HEPES buffer (pH 7.5) supplemented with 1.25 mg/mL bovine serum albumin. The reaction mixture was incubated for 30 min at 30 °C and the reaction was stopped by heating for 15 min at 100 °C. The obtained α-glucosylglycerate-phosphate was

dephosphorylated with alkaline phosphatase (Thermo Scientific) for 2 h at 37 °C. Proteins were precipitated by the addition of 400 µL acetone (-20 °C) and the supernatant was lyophilized and stored at -80 °C until measurement.

2.9 Transcriptomic analyses

2.9.1 Transcriptional adaptation to oxygen depletion

Transcriptomic analysis for the experiment section 2.6.1 was conducted by cooperation partners from the Institute of Microbiology at TU Braunschweig. Transcripts were analysed by using a whole genome microarray. The data have been deposited in the NCBI Gene Expression Omnibus (Edgar *et al.*, 2002) and are accessible through GEO Series (GSE47445). Details of the methods and results are provided in the corresponding joint publication (Laass, Kleist *et al.*, 2014).

2.9.2 Transcriptional response to salt shock

Transcriptomic analysis for the salt shock of *D. shibae* DFL12^T described in section 2.7.2 was conducted by cooperation partners from the HZI in Braunschweig (Dr. Robert Geffers). The quality and integrity of the total RNA was controlled on an Agilent Technologies 2100 Bioanalyzer (Agilent Technologies). The RNA sequencing library was generated from 1000 ng total RNA after rRNA depletion by RiboZero followed by ScriptSeq v2 RNA-Seq Library Preparation Kit (Epicentre) according to the manufacturer's protocols. The libraries were sequenced on Illumina HiSeq2500 by using TruSeq SBS Kit v3-HS (50 cycles, single ended run) with an average of 3 x 10^7 reads per RNA sample. Reads were aligned to the reference genome (*Dinoroseobacter shibae* DFL 12 uid58707) by using the open source software Rockhopper. Statistical analysis was done by using Bioconductor/R. Results are provided in the corresponding joint publication (Kleist *et al.*, 2016).

2.10 Proteomic analysis

Proteomic analysis for the experiment section 2.6.1 was conducted by cooperation partners from the ICBM in Oldenburg (research group of Prof. Ralf Rabus). Proteins were analysed by using 2D-DIGE with cyano dyes for quantification. Identification of peptide sequences was performed on a MASCOT server searching against the genome of *D. shibae* DFL 12^T. Details of the methods and results are provided in the corresponding joint publication (Laass, Kleist *et al.*, 2014).

2.11 poly-(R)-3-Hydroxybutanoate analyses

2.11.1 poly-(R)-3-Hydroxybutanoate share during adaptation to oxygen depletion

Quantification of PHB for the experiment section 2.6.1 was conducted by cooperation partners from the IBVT at TU Braunschweig (research group of Prof. Christoph Wittmann). PHB was analysed by using a high performance liquid chromatograph equipped with an UV-detector. Details of the methods and results are provided in the corresponding joint publication (Laass, Kleist et al., 2014).

2.11.2 poly-(R)-3-Hydroxybutanoate share under various salinities

Quantification of PHB for the experiment section 2.7.1 was performed via GC-MS. Therefore, the obtained cell pellets were treated with 1 mL 2 M HCl for 60 min at 90 °C to achieve PHB extraction and hydrolysis. After cooling down, the samples were neutralised with 1 mL 2 M NaOH solution, centrifuged (15900 x *g*, 5 min) and the supernatant was used for PHB determination. 25 µL of the supernatant were lyophilised and utilised for the PHB quantification of exponential growth phase samples and 10 µL for OD_{max} samples.

2.12 Sample preparation for GC-MS analyses

2.12.1 Extraction of intracellular metabolites

The washed cells were resuspended in 750 µL ethanol, containing 15 µL/mL of a 0.2 mg/mL adonitol aqueous solution. Then the cells were digested in an ultrasonic bath for 15 min at 70 °C. After cooling down on ice, 750 µL water were added and the mixture was homogenised. Non-polar substances and proteins were removed by a chloroform (1 mL) extraction. Phase separation was achieved by centrifugation (14000 x *g*, 5 min, 4 °C). In each case, 750 µL of the polar phase were lyophilised in 2 mL reaction tubes or 1.2 mL crimp glass vials in case of automated derivatisation and stored at -80 °C until further preparation. In the case of experiment section 2.7 additionally 250 µL of the polar phase were lyophilised.

2.12.2 Derivatisation reaction

The two-step derivatisation included a substitution of carbonyl groups with a methoxyl group in the first step and a silylation of amino- and hydroxyl groups in the second step. Therefore, 40 µl methoxyamine/pyridine solution (20 mg/mL) were added to the dried sample and incubated for 90 min at 30 °C with constant agitation. Then 60 µl MSTFA were added and samples were incubated for 30 min at 37 °C followed by 2 h at 25 °C with constant agitation. Manually derivatised samples were centrifuged at 14000 × *g* for 5 min and the supernatants were transferred into glass vials for GC-MS analysis. In the case of automated derivatisation, a MPS 2 XL autosampler (Gerstel) coupled to the Leco Pegasus 4D GC × GC TOF MS system was used. Here, the final incubation temperature was reduced to 18 °C and no agitation was applied.

In the case of measurements of standard substances, these were directly derivatised as described above or were first lyophilised, when a prior dissolving was necessary.

2.13 Gas chromatography – mass spectrometry analyses

For metabolic analyses two different GC-MS systems were used. In general, samples were analysed with the Leco Pegasus 4D GC × GC TOF MS and for the identification of unknown substances the Bruker micrOTOF-QII MS was used.

2.13.1 Leco Pegasus 4D GC x GC TOF mass spectrometer

Metabolic analyses were performed by using the Leco Pegasus 4D GC × GC TOF MS (vendor software: ChromaTOF 4.24) in GC-EI-TOF mode, equipped with a MPS 2 XL autosampler (vendor software: Maestro 1.4.24.2, Gerstel). As time standard an alkane mix (section 2.3.5) was analysed to allow comparability of the measurements. Calibration of the mass spectrometer was conducted according to the manufacturer with perfluorotributylamine. Samples were injected in splitless mode into a programmed temperature vaporising (PTV) injector (controlled by the software Maestro, Gerstel), which was equipped with a 71 × 1 mm CIS 4 glass liner, filled with silanized glass wool (Gerstel). The sample volume was 1 µL for each sample. In the case of 250 µL lyophilised polar phase (section 2.12.1) the injection volume was reduced to 0.5 µL. After an initial time of 0.02 min at 70 °C the temperature of the PTV was increased with 12 K/s to 330 °C, which was then held constant for 5 min. Gas chromatography was performed in a 7890 Agilent GC, equipped with a ZB-5MS column (Phenomenex). The helium flow was set at 1.2 mL/min. After 1 min at 70 °C the GC oven temperature was increased by 10 K/min to 330 °C, which was then held constant for 3 (experiment section 2.6.1) or 5 min (experiment section 2.7). The transfer line was set to 275 °C, the ion source temperature was 250 °C and the detector voltage was adjusted according to the sample concentration and the daily performance of the instrument. Overall the detector voltage was set 200 V higher than the output of the automatic tuning. Solvent delay was adjusted according to the deterioration of the column. After solvent delay time, full mass spectra were collected from 45 to 600 *m*/*z* at 4 scans/s.

2.13.2 Bruker micrOTOF-QII mass spectrometer

For the identification of unknown compounds the Bruker micrOTOF-QII MS (vendor software micrOTOFcontrol 3.0) coupled to a GC (CTC) was used, equipped with a GC PAL autosampler (CTC). For controlling and synchronising the GC and the MS the vendor software Hystar 3.2 was used. Calibration of the mass spectrometer was conducted according to the manufacturer with an APCI/APPI Calibrant Solution (Fluka). Samples were injected in split mode, with a ratio of 1:10-1:50 according to the requirements of the sample. The injection system was a PTV injector (CTC), which was equipped with a 71 × 1 mm baffled CIS 4 glass liner (Gerstel). The sample volume was 1 µL for each sample. After an initial time of 0.1 min at 70 °C the temperature of the PTV was increased with 12 K/s to 330 °C, which was then held constant for 5 min. Gas chromatography was performed in a 7890 Agilent GC, equipped with a VF-5ms column (Agilent Technologies). The helium flow was set at 1.2 mL/min. After 1 min at 70 °C the GC oven temperature was increased by 10 K/min to 325 °C, which was then held constant for 2.5 min. The transfer line was set to 300 °C. Spectra were obtained in positive mode by using a mass range of 100...1550 *m/z* and a spectra rate of 0.4 Hz. The settings of the MS instrument were set to:

end plate offset	-500 V;
capillary	-1000 V;
corona	3000 nA;
nebuliser	4 bar;
dry gas	4 L/min and dry temperature, 180 °C;
funnel 1/2 RF	200 Vpp;
in-source CID energy	0 V;
hexapole RF	150 Vpp;
quadrupole ion energy	5 eV;
collision energy	7 eV;
collision RF	140 Vpp;
transfer time	80 µs
and pre puls storage	5 µs.

2.13.3 DSQ II GC-MS

PHB determination for the experiment section 2.7 was performed by using the DSQ II 2.0.1 (Thermo Fisher Scientific, controlled by the vendor software: Xcalibur 2.0.7) in GC-EI-TOF mode, equipped with a AI/AS 3000 2.0 autosampler (Thermo Fisher Scientific, software: Xcalibur 2.0.7). As time standard an alkane mix (section 2.3.5) was analysed to allow comparability of the measurements. Calibration of the mass spectrometer was conducted according to the manufacturer with perfluorotributylamine. Samples were injected in split mode (1:15) into a PTV injector (vendor software: Xcalibur 2.0.7), which was equipped with a 1 x 2.75 x 120 mm Trace 2000 glass liner, filled with silanized glass wool (Thermo Fisher Scientific). The sample volume was 1 µL for each sample. After an initial time of 0.2 min at 70 °C the temperature of the PTV was increased with 14 K/s to 330 °C, which was then held constant for 5 min. Gas chromatography was performed with a TRACE GC Ultra 2.0, equipped with a VF-5ms column (Agilent). The helium flow was set at 1.2 mL/min. After 1 min at 70 °C the GC oven temperature was increased by 1 K/min to 76 °C, than the temperature was increased by 6 K/min to 185 °C and last by 20 K/min to 325 °C, which was then held constant for 4 min. The transfer line was set to 275 °C and the ion source temperature was 220 °C. Solvent delay was adjusted according to the deterioration of the column. After solvent delay time, full mass spectra were collected from 40 to 460 *m*/*z* at 4 scans/s.

2.14 GC-EI-MS data processing and analysis

Raw data from the GC-EI-MS instrument were exported as NetCDF (network common data format), to allow access of the software MetaboliteDetector (Hiller *et al.*, 2009), which was under development until 2013 by Christian Nieke (TU Braunschweig). The software converts the NetCDF data in a *.bin-format and deconvolutes all mass spectra from a chromatogram. For each data set an alkane mix was measured, which is used as time standard, allowing the calculation of instrument independent retention indices (RI) modelled on Kováts (1958), based on formula 1.

$$RI^T = 100\left[(y-x)\frac{(\log(t_i)-\log(t_x))}{(\log(t_y)-\log(t_x))}+x\right]$$ Formula 1

RI^T: retention index in a temperature gradient
x: number of carbon atoms of the alkane eluting before the analyte
y: number of carbon atoms of the alkane eluting after the analyte
t_i: retention time of the analyte
t_x: retention time of the alkane eluting before the analyte
t_y: retention time of the alkane eluting after the analyte

Additionally, the calculated retention indices of the analytes of each chromatogram were corrected by an alignment to the internal standard adonitol. Compounds were automatically identified by comparison of mass spectra and retention indices with an institute internal library, by using in general a cut-off score of 70 % similarity. The substances were quantified with one certain fragment ion so called quantification ion (QI). This was either defined in the library or manually curated. Moreover, a non-targeted approach was used, so that potentially new metabolites could be found, which were then added to the library.

To reduce the number of zero-values of several compounds, more than one batch analysis were performed with various settings to satisfy compounds of low or very high abundance, respectively. The results of the batch analyses were merged. Zero values left, were added manually, if possible. Finally, data were normalised to the internal standard, the

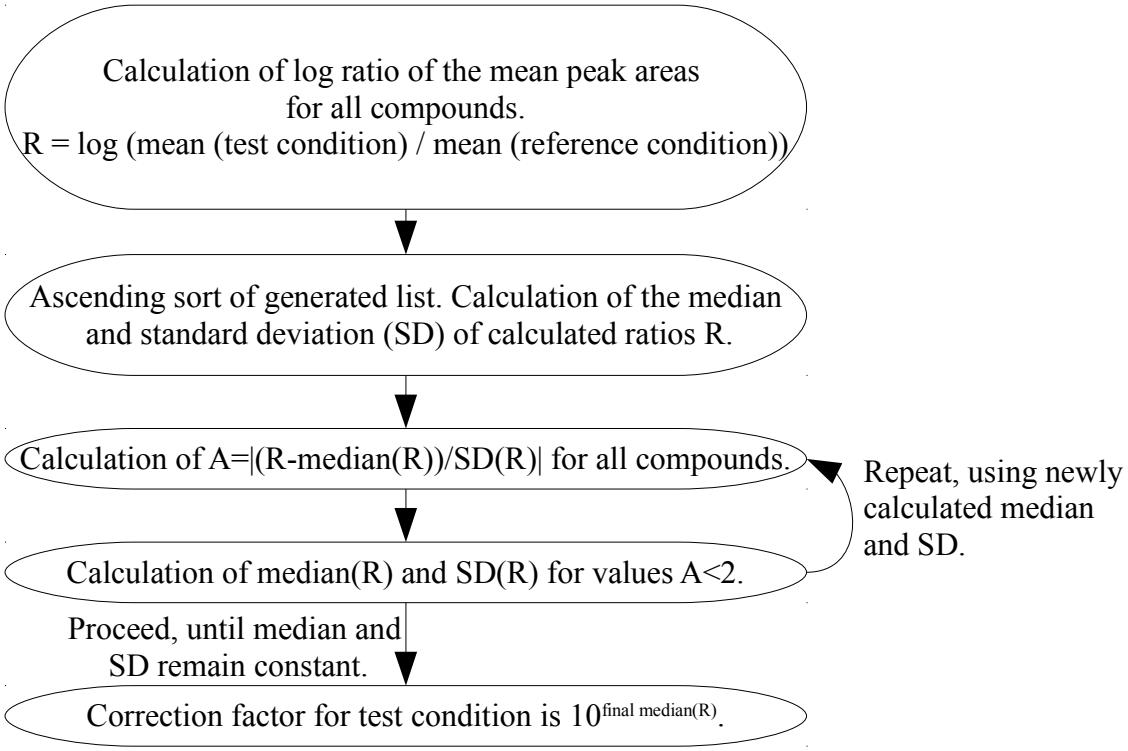

Figure 7: Procedure for central normalisation.

utilised cell dry weight and by a central normalisation (Figure 7), if necessary. With the itool (BIBC, TU Braunschweig), derivatives of one metabolite were summed and the means and errors of each defined group were calculated.

As the semi-quantitative analyses of metabolites require a relative comparison, fold changes referring to a certain reference condition were calculated for further interpretation. The errors of changes were calculated based on propagation of uncertainty (formula 2).

$$\text{error of fold change} = \sqrt{\left(\frac{SE(t)}{mean(t)}\right)^2 + \left(\frac{SE(r)}{mean(r)}\right)^2} \cdot \frac{mean(t)}{mean(r)} \qquad \text{Formula 2}$$

SE: standard error
t: test state
r: reference

2.15 Statistical data analysis

2.15.1 Significance test

Metabolome analyses are challenging because of the necessity to guarantee an immensely quick and reproducible sampling procedure. Additionally, a large culture volume is needed compared with, for example, transcriptome analyses. Therefore, the number of sample replica is in most cases limited. Due to this, the data sets achieved are usually not normally distributed, which was confirmed by using the Shapiro-Wilk test (Shapiro and Wilk, 1965). Hence, appropriate non-parametric statistical tests have to be used. In this study, the rank-sum test according to Mann-Whitney-Wilcoxon (Mann and Whitney, 1947) was used for the examination of affiliation of various conditions. A p-value of 0.05 was set as the level of significance. To prevent false positive results when conduction multiple comparisons, as they are needed for statistical analyses of metabolome data, the false discovery rate according to the Benjamini-Hochberg (Benjamini and Hochberg, 1995) procedure was used. This procedure is based on the correction of the level of significance. All these tests were performed with the MultiExperiment Viewer 4 (MeV4) (Saeed *et al.*, 2003).

2.15.2 Visualisation of datasets

Correlation matrices and corresponding heat maps were generated with R by using Spearman correlation coefficient.

Hierarchical cluster analyses (HCA) were performed with the software MeV4 (Saeed *et al.*, 2003). Therefore, the data loaded were first normalised based on formula 3.

$$\text{value} = \frac{\text{value} - \text{mean}(\text{metabolite})}{\text{SD}(\text{metabolite})} \qquad \text{Formula 3}$$

SD: standard deviation

The cluster analyses underlying correlation was Spearman or Pearson correlation coefficient. HCA's were presented in dendrograms which enables an intuitive understanding of the relations of the conditions and metabolites tested. Concomitantly, colour coded heatmaps were generated, so correlating metabolite groups could easily be detected.

2.16 GC-APCI-MS data analysis

For the analysis of the GC-APCI-MS chromatograms the raw data were used to work in the vendor software DataAnalysis 4.0. Deconvolution was achieved by using the software implemented *Dissect*-algorithm. Here, all mass traces with a maximum at the same retention time are merged in one spectrum and it is assumed that these masses are associated with one compound. The assignment of compounds found by GC-APCI-MS measurements and GC-EI-MS measurements was achieved through the relative retention times and comparison of the fragment patterns of the different ionisation methods. In general, the highest mass of an APCI spectrum equates the base peak and in most cases the molecule ion. In case of strong fragmentation, the identification of the molecule ion was carried out on the mass difference of 16.03 Da. This is a typical loss for molecule ions and accords to a loss of a methyl-group plus H^+, originating from a trimethylsilyl moiety.

In the following, the software implemented tool *SmartFormula3D* was used to calculate possible sum formulae on the basis of the accurate mass and the isotope pattern. Therefore, several constraints were set: $n_C \geq 3\ n_{Si}$, $2\ n_N + n_O + n_S \geq n_{Si}$, n_P min $3\ n_O$ (n: number of; C, N,

O, P and Si: elements); mass tolerance: 10 ppm; limit mSigma: 40. The results of the tool were checked manually and probable sum formulae were further verified, if possible, with ^{13}C-labelled samples, MSTFA-*d9*-labelled samples or standard substances.

3 Results

3.1 Adaptation processes during oxygen depletion

Data and contents of the following chapter 3.1 were published in the *Journal of Biological Chemistry* (Laass, Kleist *et al.*, 2014).

D. shibae is capable of growing anaerobically by denitrification (Piekarski *et al.*, 2009). During denitrification, nitrate is gradually reduced to elemental nitrogen and, similar to oxygen respiration, a proton-motive force is generated. This force enables ATP synthesis by ATPase.

D. shibae was continuously cultivated in SWM supplemented with nitrate. During the cultivation, the aeration was stopped in order to force the cells to switch from oxidative phosphorylation to denitrification. This scenario simulates the survival of the organism after the sinking into the sediment or in layers that are low in oxygen. To gain comprehensive access to the adaptation processes, a collaborative systems biology approach was performed including metabolome, proteome and transcriptome analyses. The contributions covered in this work consists of the analysis of small soluble polar metabolites by GC-MS and the quantification of ATP by luminescence measurements, as well as the cultivations and sampling required for these analyses. Proteome data, consisting of a shotgun and membrane protein data set as well as a 2D-DIGE set of soluble proteins, were collected by the working group of Prof. Ralf Rabus (ICBM, Oldenburg). Sampling and cultivation for proteome, transcriptome and PHB analysis were performed by Sebastian Laaß (Institute for Microbiology, Braunschweig), in addition to the microarray based transcriptome analysis. The PHB analysis was conducted by Annekathrin Bartsch (IBVT, Braunschweig) and the electron microscopy pictures were taken by Prof. Manfred Rohde (HZI, Braunschweig).

3.1.1 Set-up of the systems biological approach and observations during the transition to anoxic condition

For the systems biological approach, the sampling points for the different methods were chosen considering expected adaptation processes (Figure 8) in a period of 240 min after oxygen shut-down.

During cultivation, the optical density and the oxygen supply were observed. After oxygen shut-down, *D. shibae* consumed the residual oxygen within 30 min. Also the optical density and the cell count were slightly affected. It decreased in the first 60 min after oxygen shut-down and stabilised in the ongoing cultivation, though to a lower level compared with the starting condition (Figure 8).

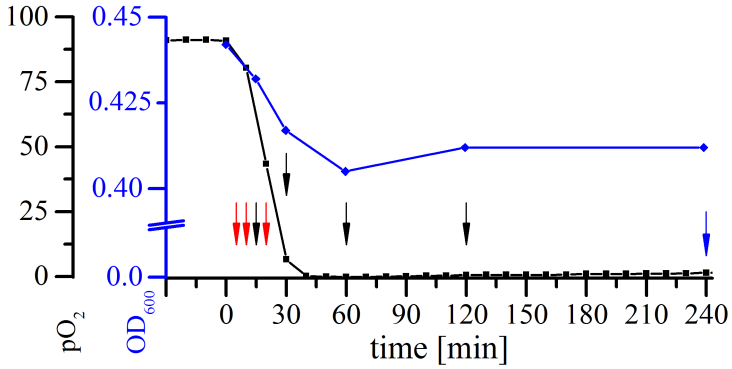

Figure 8: Continuous cultivation of *D. shibae* under oxygen depleted condition. *D. shibae* was cultivated aerated in a chemostat in salt water minimal medium supplemented with 25 mM nitrate. At time point 0 min the aeration was stopped. The oxygen partial pressure pO_2 is visualised by the black curve and the optical density of the culture by the blue curve. Red arrows indicate sampling time points of transcriptome; black arrows indicate sampling time points of metabolome, proteome and transcriptome; the blue arrow: indicates sampling time point of metabolome and proteome.

3.1.2 Energy supply during the adaptation to anoxic conditions in batch cultures

To study how decreased oxygen supply affects the respiratory chain, the concentration of ATP, one of the crucial end products of respiration, was determined.

As some pretests showed, a completely anaerobic sampling had to be guaranteed while sampling for the ATP measurements. Otherwise, the short period of time under oxygenated conditions affected the ATP concentration enormously, probably due to the extremely high formation rate of ATP under these circumstances. Hence, in addition to the chemostat

cultivation, *D. shibae* was cultivated in batch cultures. Initially, the cells were cultivated under standard conditions, but during their active growth, ensuring that sufficient nutrients were left, they were transferred to an anaerobic chamber to enable an anoxic sampling. Compared with the chemostat cultivation (section 3.1.1) growth inhibition was clearer in batch culture (Figure 9).

Prior to the shift to anoxic conditions, an ATP concentration of about 1300 pmol/mg CDW was determined, which decreased during a time period of 120 min continuously, reaching a minimum at 440 pmol/mg CDW. Afterwards, the concentration increased again (Figure 9). Concomitantly, the growth of *D. shibae* stopped for about 120 min then started again with the regeneration of ATP (Figure 9), both to a lower extent compared with oxic conditions.

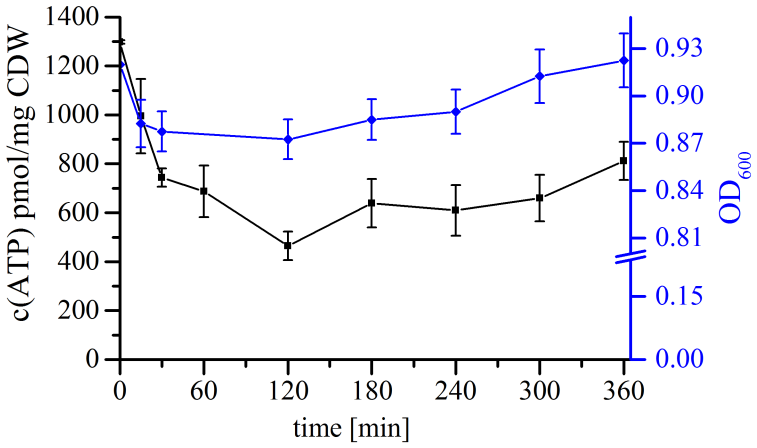

Figure 9: ATP concentration over time of *D. shibae* batch cultures shifted from oxic (0 min) to anoxic conditions. ■ ATP concentration; ♦ OD, optical density measured at 600 nm; CDW: cell dry weight. n=6.

3.1.3 Metabolic response during the shift to anaerobic conditions

Metabolome analyses of *D. shibae* cell extracts during the adaptation of the organism to the anoxic condition revealed immense changes in the central metabolism. In sum 92 metabolites were detected of which 72 were identified. A complete list of all metabolites and their fold changes compared with the metabolic state under oxic condition can be found in appendix A2.

A correlation analysis of the metabolite profiles resulted in three groups (Figure 10). The first group comprised the oxic state and time-point 15 min, the second the time points 30 and 60 min and the last time-points 120 and 240 min with at least high correlation

values of 0.95 in all cases.

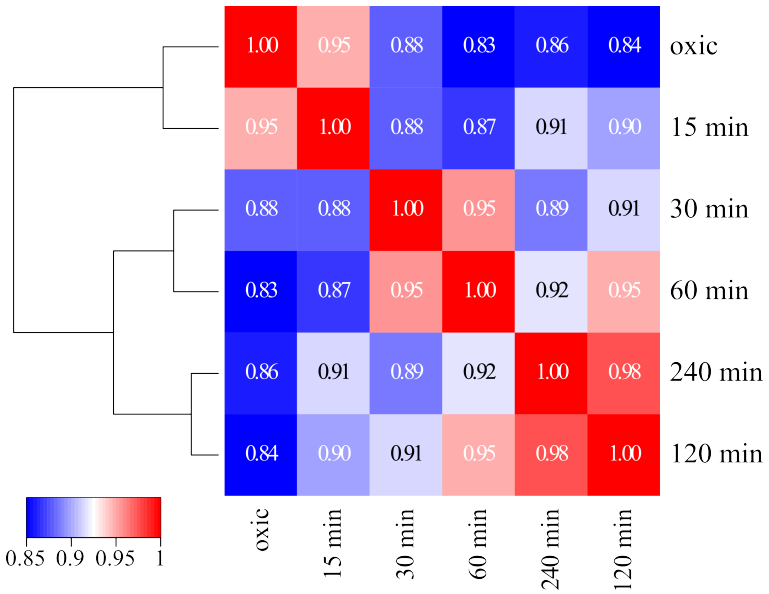

Figure 10: Correlation matrix of intracellularly detected metabolites during the adaptation of *D. shibae* to anaerobic conditions. Metabolite profiles of *D. shibae* cells during oxic state and 15, 30, 60, 120 and 240 min after oxygen shutdown. A Spearman correlation was performed and visualised in a heat map. The dendrogram is based on euclidean distance.

An overview of the acquired data gives the hierarchical cluster analysis of significantly changed metabolites (tested in a prior ANOVA) (Figure 11). The Spearman based analysis of the significantly changed metabolites resulted in a slightly changed clustering of the time-points tested compared with Figure 10, but not in a relevant way. The heat map nicely shows the four resulting metabolite clusters. Metabolites were grouped according to their abundance changes throughout the experiments. Most metabolites were low in abundance under oxic conditions and 15 min after the oxygen shut-down and reached a maximum 60 min after the shift (cluster III, Figure 11). A small group of metabolites decreased throughout the experiment (cluster I). Contrarily, some metabolites were increased at the time-points 120 and 240 min (cluster II) or changed similar to metabolites of cluster III but with the highest abundance 30 min after oxygen shut-down (cluster IV).

Selected metabolites and their actual changes are shown in Table 4. In particular, TCA cycle intermediates (cluster III, Figure 11) were strongly upregulated up to 18-fold 60 min after oxygen shut-down. Furthermore, the branched chain amino acids with their precursors 2-isopropylmalate and 2-methylmalate were strongly increased with a maximum 60 min after the oxygen shut-down. Intermediates of the gluconeogenesis and the Entner-Doudoroff pathway were also affected, predominantly in the same manner as described, but to a much lower extent.

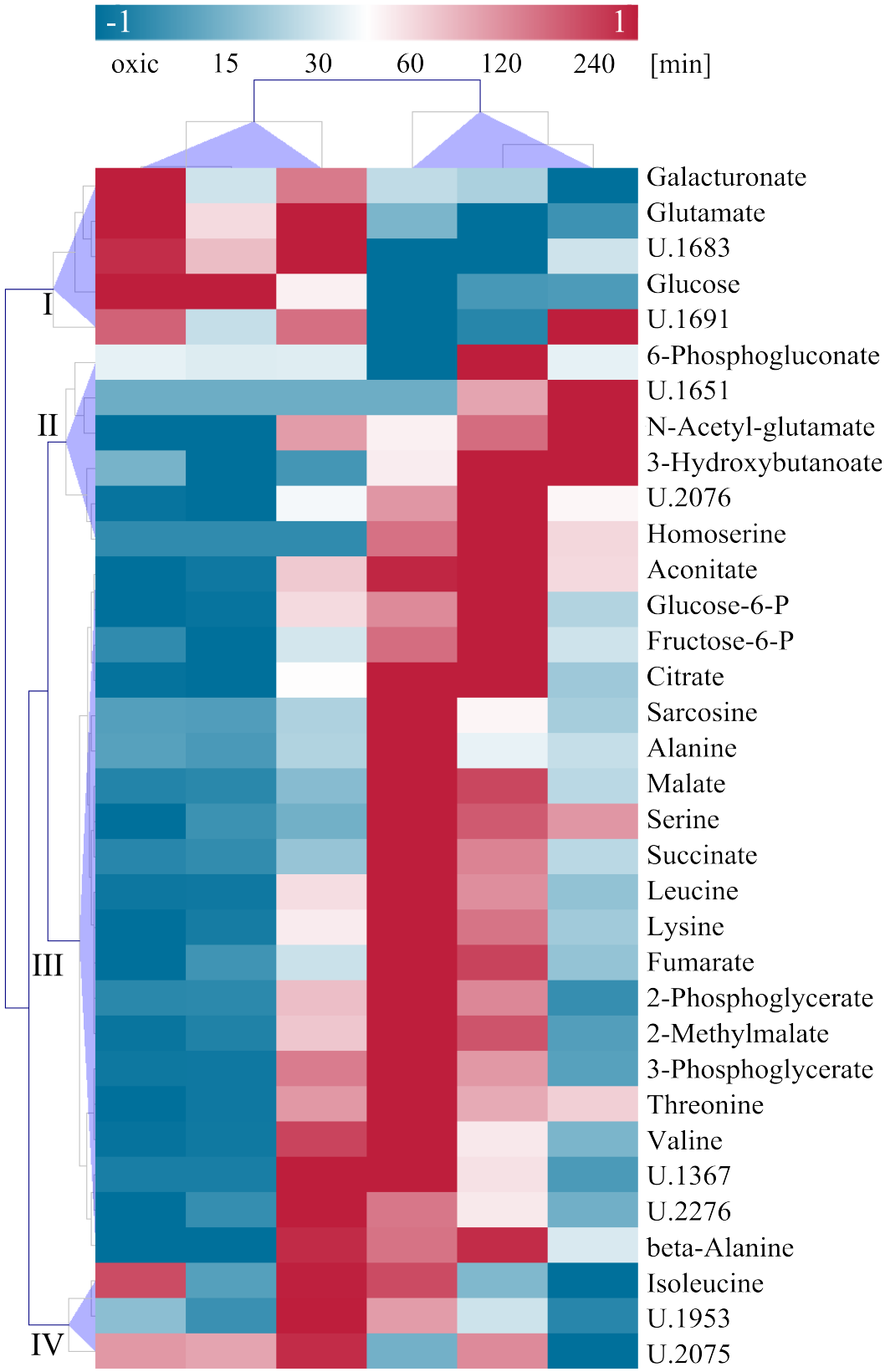

Figure 11: Hierarchical cluster analysis based on metabolite concentrations significantly changed during adaptation to anoxic condition. Shown are the time points oxic conditions and 15, 30, 60, 120, 240 min after oxygen shut-down. I-IV: Resulting metabolite cluster. Cluster analysis was done by using Spearman correlation.

Table 4: Selected metabolites of *D. shibae* intracellularly regulated after oxygen shut-down. Fold changes were computed by comparison with the oxic state of cells. *: significantly changed (α=0.05; Wilcoxon-Mann-Whitney-Test with false discovery rate control according to Benjamini/Hochberg). ": Not detected under oxic condition, hence the fold changes were computed by comparison with the first time-point detected (error of fold changes appendix A2). n.d: not detected; TCA: tricarboxylic acid; KDG: 2-keto-3-deoxy-gluconate.

Metabolites	time after oxygen shut-down [min]				
	15	30	60	120	240
Amino acids and derivatives					
Alanine	0.77	2.54	12.58 *	3.50 *	2.89 *
Glutamate	0.76	1.03	0.59 *	0.41 *	0.52 *
Homoserine"			1.00	1.68 *	0.68 *
Isoleucine	1.43	8.34	7.26 *	8.31 *	4.68 *
Leucine	1.08	11.15	25.11	14.41 *	5.83 *
Lysine	1.07	1.67	2.58 *	1.99 *	1.40 *
N-Acetyl-glutamate	0.97	1.99	1.76	2.12	2.47
Serine	1.75	2.07	5.03 *	4.08 *	3.66 *
Threonine	1.71	3.78	5.03 *	3.66 *	3.41 *
Valine	1.51	24.27	32.69 *	14.88 *	6.92 *
Amino acid metabolism					
2-Isopropylmalate	0.66	62.45	27.71 *	12.21 *	4.64 *
2-Methylmalate	1.91	13.31	25.83 *	18.45 *	3.92 *
TCA Cycle					
Aconitate"	1.00	3.34	4.78 *	4.86 *	3.20 *
Citrate	0.76	5.61	10.88 *	11.30 *	3.80 *
Fumarate	1.98	3.84	9.87 *	7.39 *	3.11 *
Malate	1.20	3.71	17.99 *	12.58 *	5.08 *
2-Oxoglutarate	0.85	2.26	1.10	1.04	1.09
Succinate	1.20	3.21	14.24 *	8.09 *	3.91 *
Gluconeogenesis and Entner-Doudoroff pathway					
Dihydroxyacetone phosphate	1.03	1.05	0.51	0.96	1.07
Fructose-6-phosphate	0.59	1.88	3.02	4.36 *	1.85
Glucose	0.93	0.58	0.20 *	0.31 *	0.32 *
Glucose-6-phosphate	1.09	2.72	3.23 *	4.79 *	2.05 *
KDG	1.15	2.08	2.63 *	1.32	1.87
Phosphoenolpyruvate	0.75	4.19	4.05 *	1.74	1.26
6-Phosphogluconate	0.97	0.98	n.d.	2.52	1.00
2-Phosphoglycerate	1.00	1.83	2.83 *	2.02	1.03
3-Phosphoglycerate	1.00	2.99	4.18 *	2.83 *	1.37
Pyruvate	2.97	0.69	3.11	4.40 *	4.21
scale for fold changes	< 0.1	0.2 – 0.5	0.5 – 2	2 – 5	5 – 10	> 10

3.1.4 Response during the transition to anoxic conditions on the protein and transcriptional level

This chapter provides the most relevant results for the interpretation of the metabolome analysis from complementary transcriptomic and proteomic analyses conducted by cooperation partners. These results are discussed in detail in the corresponding sections. Sampling for the transcriptome and proteomic analysis were done as described in section 3.1.1.

In general, the increase of genes transcripts involved in denitrification started (appendix A3) immediately after oxygen shut-down and reached the highest values at time-point 30 min. The first corresponding changes were observed in the proteome 30 min after oxygen shut-down, which were still ongoing at time-point 240 min (Laass, Kleist *et al.*, 2014). Most gene transcript levels of oxidative phosphorylation started to decrease, whereas, for example, high oxygen affinity *cbb*$_3$-type cytochrome oxidase type systems were upregulated.

Table 5: Selected transcripts of genes encoding stress proteins of *D. shibae* with corresponding log$_2$ fold changes 5 -120 min after oxygen shutdown. A whole genome microarray analysis of *D. shibae* was conducted. Ratios were computed by comparison with cells under oxic conditions.

Locus tag	Product	5	10	15	20	30	60	120
		[min]						
Dshi_0009	cold-shock DNA-binding domain-containing protein	0.0	-0.1	-0.3	-0.4	-0.7	-0.9	-0.1
Dshi_0737	heat shock protein DnaJ domain-containing protein	0.0	0.1	0.4	0.5	0.8	0.9	0.5
Dshi_1338	UspA domain-containing protein	0.7	1.3	2.6	3.4	3.8	3.2	2.4
Dshi_2213	UspA domain-containing protein	0.3	0.7	1.7	2.9	3.7	2.8	2.0
Dshi_2219	cold-shock DNA-binding domain-containing protein	0.0	-0.1	-0.3	-0.4	-0.9	-0.5	-0.1
Dshi_2686	UspA domain-containing protein	0.3	0.6	1.7	2.8	3.3	2.5	1.3
Dshi_2796	heat shock protein Hsp20	0.5	1.3	2.3	2.9	3.8	3.3	2.8
Dshi_2892	heat shock protein Hsp20	0.0	0.0	0.1	0.1	0.4	1.3	1.0
Dshi_2919	chaperonin GroEL	-0.1	0.0	-0.1	-0.3	-1.8	-1.9	-0.8
Dshi_2920	chaperonin Cpn10, GroS	0.0	0.0	-0.1	-0.1	-1.6	-1.6	-0.7

The general stress responses observed on the transcriptional level are summarised in Table 5. Most corresponding translation products were then detected in the ongoing experiment (Supplement: Laass, Kleist *et al.*, 2014).

Selected gene transcripts and their $\log_2$ fold-changes compared with the oxic state of cells can be found in appendix A3.

3.1.5 Concentration changes of poly-(R)-3-hydroxybutanoate during the adaptation process

In addition to the metabolome analysis, the influence of the shift to anoxia on PHB formation was investigated.

The data presented in Figure 12 show the strong accumulation of PHB throughout the whole investigated time period. The quantitative analysis required an alkaline-hydrolysation of the polymer so that the resulting monomer 3-hydroxybutanoate could be quantified by HPLC measurements. Under oxic conditions a PHB concentration of 0.02 pg/cfu (colony forming units) was determined, which continuously increased under anoxic conditions up to a level of 0.16 pg/cfu. This PHB accumulation could be supported by electron microscopy, which revealed formation of granula due to storage of PHB (Figure 12).

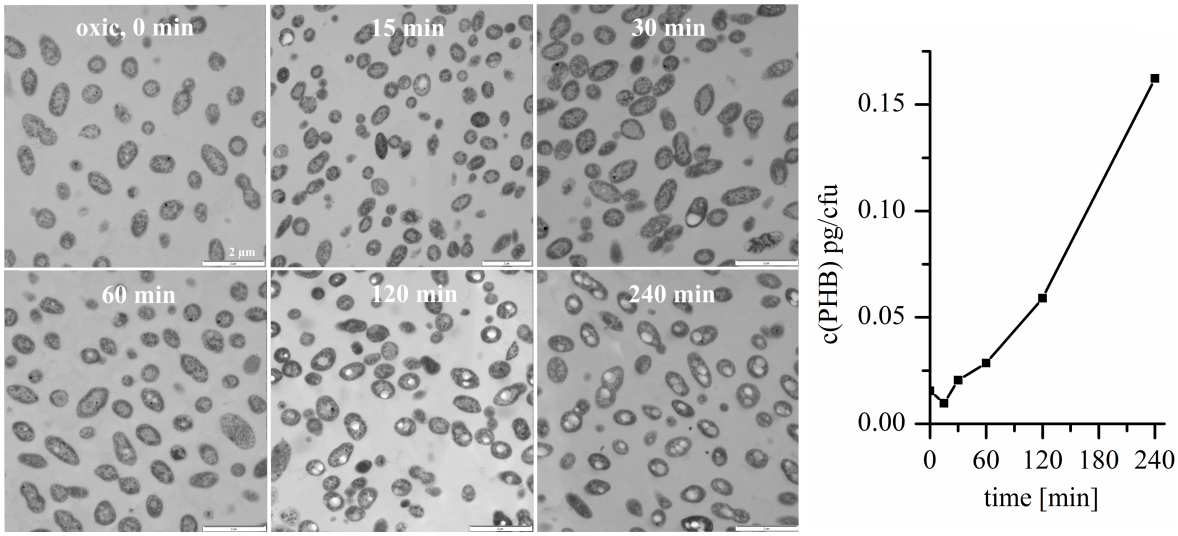

Figure 12: poly-(R)-3-Hydroxybutanoate (PHB) accumulation during the adaptation to anoxia, monitored over 240 min after oxygen shut-down. PHB granula are indicated as light spots in the cells visible in the electron microscopy pictures (Manfred Rohde). Quantification of PHB via the monomer was performed by HPLC (Annekathrin Bartsch). cfu: colony forming units.

3.2 Identification of unidentified compounds of D. shibae

Data and contents of the following chapter 3.2 were partially published in the journal *Environmental Microbiology* (Kleist *et al.*, 2016).

Depending on the condition and growth phase, four compounds dominate the metabolome analyses of *D. shibae* cell extracts (Figure 13). One of these is glutamate, the others are substances with no entries in established GC-MS databases. Their EI-MS spectra are very similar. In the following these substances are called *unknown#2251-dsh_1*, *unknown#2288-dsh_2* and *unknown#2309-dsh_3*. Since the concentrations of the unknown compounds achieved remarkable values, these substances have to play a decisive role for *D. shibae*.

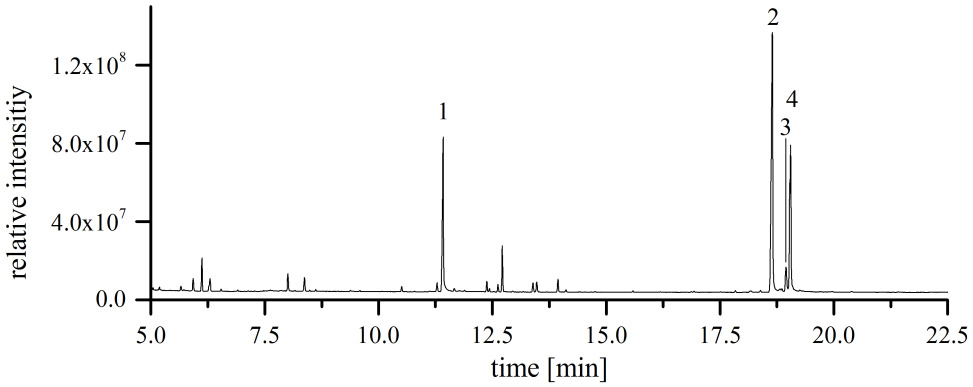

Figure 13: Chromatogram cut-out of a GC-EI-MS measurement of a *D. shibae* cell extract (stationary growth phase). Derivatives of 1: glutamate (2TMS), 2: *unknown#2251-dsh-1*, 3: *unknown#2288-dsh_2* and 4: *unknown#2309-dsh_3*.

For the identification of these unknown compounds, GC-APCI(+)-MS measurements were performed following the method of Strehmel *et al.* (2014) in parallel with GC-EI-MS measurements. The assignment of the relevant compounds was achieved via comparison of the retention times (Jäger, 2011) and the corresponding spectra. Although APCI is considered a soft ionisation technique, strong in-source fragmentation of the investigated compounds was observed (Figure 14B). Usually, in an APCI(+) spectrum one base peak, equating the molecule ion $+H^+$ $[M+H]^+$, is assumed. Figure 14 shows a comparison of an EI and an APCI(+) spectrum of *unknown#2309-dsh_3*. Due to the strong fragmentation detected by APCI(+), similar fragments as by EI were obtained. This allowed a direct assignment of the different ionisation techniques via characteristic fragments, e.g.: *m/z* 217, 351 and 361, but hampers the identification of the $[M+H]^+$. Additionally, the fragmentation

leads to very low intensities of higher masses which enormously reduce the quality of according isotope patterns and therefore hinders the prediction of potential sum formulae.

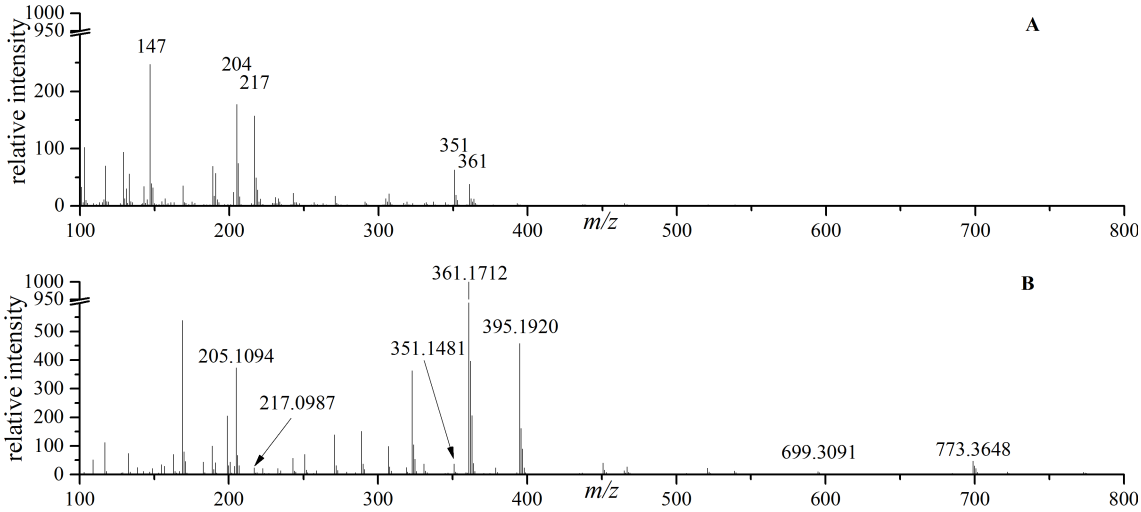

Figure 14: Spectra of the unknown substance *unknown#2309-dsh_3*. A: EI spectrum, B: APCI(+) spectrum.

EI spectra of the unknown compounds showed fragmentation patterns typical for pyranoses (*m/z* 191, 204 and 217). Additionally, the fragment *m/z* 361 indicates a glycosidic linkage with a further moiety, *e.g.* a further monosaccharid (Simoneit *et al.*, 2004). Regarding the fragment *m/z* 361: its relative intensity is too low for a disaccharid, as an exemplary comparison of trehalose and the *unknown#2309-dsh_3* indicates (Figure 15). The fragment *m/z* 361 results from the cleavage of the glycosidic bondage and an additional loss of a TMS- and methyl-moiety (Simoneit *et al.*, 2004). In the case of disaccharids, this fragment can be formed twice leading to a high abundance in the spectra. Because of this, it was assumed that the three unknown compounds possess a glycosidic bondage to a carbohydrate similar moiety, as no further peculiarities for other substance classes were apparent in the spectrum.

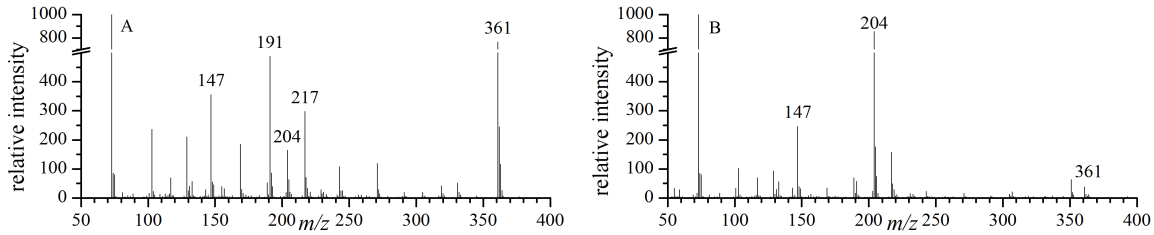

Figure 15: EI spectra of A: trehalose (8TMS) and B: the unknown substance *unknown#2309-dsh_3.*

Additionally, the retention indices (RI) of the substances (*unknown#2251-dsh_1*: RI 2251, *unknown#2288-dsh_2*: RI 2288, *unknown#2309-dsh_3*: RI 2309) could not be

assigned to common carbohydrate classes, whose RI ranges are shown in Table 6. Due to this, a molecular mass ranging between a monosaccharid and a disaccharid was suggested. The only entry in our metabolite library with a carbohydrate moiety in this RI range was mannosylglycerate (RI 2230), which was conform with all information discovered so far.

Table 6: Retention index (RI) ranges of carbohydrates with various carbon number.

Substance class	RI range
Tetroses (C4)	1430 - 1460
Pentoses (C5)	1630 - 1710
Hexoses (C6)	1830 - 1915
Unknown substances	2250 - 2310
Disaccharids (C12)	2600 - 3000
Trisaccharids (C18)	3200 - 3600

As previously mentioned, the unknown compounds underlay a strong fragmentation by APCI(+). Due to this, neutral losses, as they are known from chemical ionisation in positive mode (Warren, 2011), were expected - in particular the neutral loss CH_4. However, it had to be noticed that the resulting $[M\text{-}CH_4]^+$-ion could not be found for the relevant compounds. $[M\text{-}CH_4]^+$ corresponds to the loss of a methyl-group plus H of a TMS-moiety and is indicated by a mass loss of 16.03 Da. Instead, in all spectra one ion could be identified along with an ion with a mass discrepancy of 14.01 Da, which probably corresponds with a loss of CH_2 (Figure 16). Interestingly, a further but low concentrated unknown substance, which was clearly associated with *unknown#2288-dsh_2* and *unknown#2309-dsh_3* (occurrence and spectrum), showed two masses in the area of the molecule ion with a difference of 2.0138 Da, which corresponds to two hydrogen atoms (2.0151 Da)(Figure 16D). Accordingly, a $[M\text{-}CH_4]^+$ fragment (613.2510 Da) could be identified for the higher mass (629.2780 Da) and a $[M\text{-}CH_2]^+$ fragment for the lower mass (627.2642 Da), as described before for the other unknown substances.

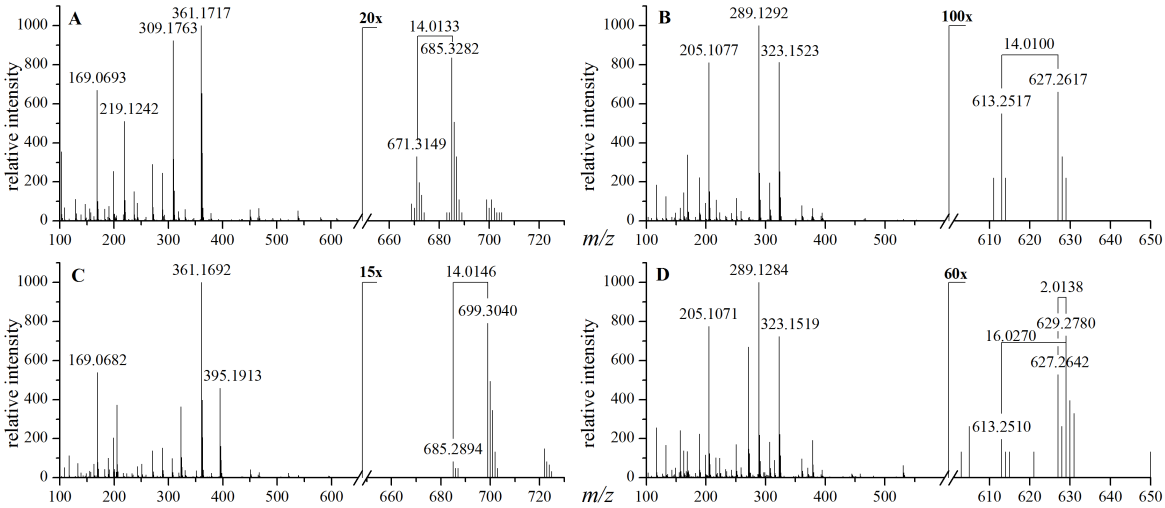

Figure 16: APCI(+) spectra of the unknown substances A: *unknown#2251-dsh_1*, B: *unknown#2288-dsh_2*, C: *unknown#2309-dsh_3*, D: a B and C associated unknown. Each marked with relevant mass differences.

To test whether the unknown substances possess methoxyamine-groups, the first derivatisation step was conducted without methoxyamine but with pyridine only (section 2.12.2). Since the substances were still detected unchanged (RI and MS spectrum), they are free of methoxyamine-groups. In the following, cell extracts of *D. shibae* were derivatised with 9-times deuterated MSTFA (MSTFA-*d*9, Sigma-Aldrich) and analysed by GC-APCI(+). Moreover, fully ^{13}C-labelled samples were analysed. For this approach, the organism was cultivated under standard conditions, supplying 25 mM [U-^{13}C]-glucose (Eurisotop) as sole carbon source, instead of unlabelled succinate (section 2.3.3). Exemplary results for these approaches are shown for *unknown#2309-dsh_3* in Figure 17. Under common conditions the highest mass detected was 699.2952 Da, in MSTFA-*d9* derivatised samples 753.6394 Da and in the ^{13}C-labelled samples 708.333 Da. Assuming that these are the corresponding $[M+H]^+$, the complete carbon backbone is included. Therefore, the mass difference of the relevant ions, compared with the control, provides information on the number of TMS-moities or carbon atoms, respectively. In the case of MSTFA-*d9* treated samples a mass shift of 54.38 Da was observed which accords to six TMS-*d9*-moieties, as each moiety possesses nine deuterium (Figure 17). The spectrum resulting from fully ^{13}C-labelled cell extract showed a mass difference of 9.04 Da which accords nine carbon atoms (Figure 17). By using these approaches, it was revealed that the three substances contain nine carbon atoms and that *unknown#2251-dsh_1* and *unknown#2309-dsh_3* possess 6 TMS-groups and *unknown#2288-dsh_2* possesses 5 TMS-moities.

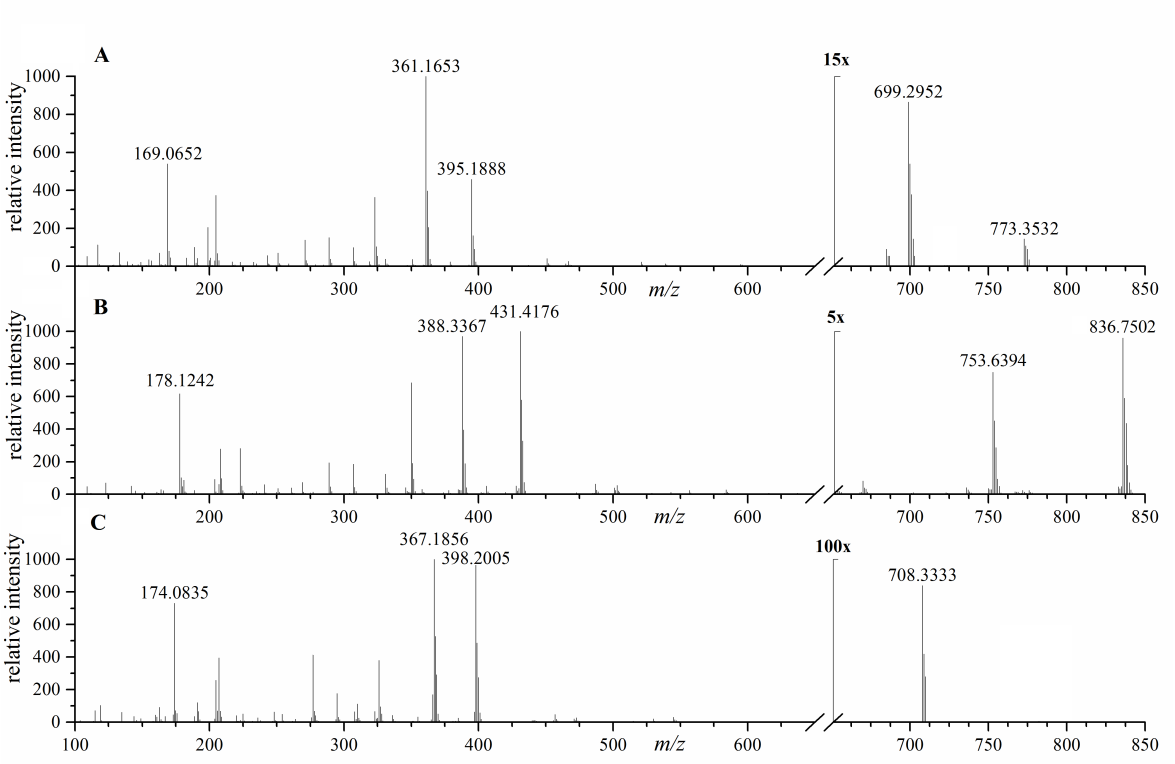

Figure 17: APCI(+) spectra of the unknown substance *unknown#2309-dsh_3*. A: unlabelled, B: derivatised with MSTFA-*d*9, C: from cultivation with [U-^{13}C]-glucose.

Furthermore, the previous assumption of the assignment of the $[M+H]^+$ ions could be enhanced, because of detected masses greater than the suggested molecule ions. The highest masses detected in the spectra of Figure 17 were 773.3532 (A: standard treatment), 836.7502 (B: MSTFA-*d9* derivatisation) and 782.3893 Da (C: ^{13}C-cultivation) which accords to mass differences of 74.06, 83.11 and 74.06 Da, respectively. Since the mass difference between the common sample treatment and the fully ^{13}C-labelled is the same, the data indicate that this additional fragment does not contain carbon of biological origin, whereas the fragment must originate from one TMS-moiety because of the mass shift of 9.05 Da in the MSTFA-*d9* derivatised samples. Strehmel *et al.* reported on $M+C_3H_9Si$ fragments (+ 72.04 Da) in APCI(+) measurements (Strehmel *et al.*, 2014). Because, as suggested before, exclusively $[M-2H]^+$ ions but no $[M+H]^+$ ions were detected for the investigated substances, this fits into the picture. Thus, the additional higher mass is not only 72.04 Da increased but 74.06 Da and concomitantly the commonly present $[M-CH_4]^+$ ion is only a $[M-CH_2]^+$ ion. Hence, the higher masses detected are $[M+C_3H_9Si]^+$ fragments, which are formed during the ionisation process.

On the basis of these information, the protonated molecule ions were defined, disregarding the mass discrepancy of the two protons. The accurate masses $[M+H]^+$ of the unknown substances, a prediction of their sum formulae, and further parameters are summarised in Table 7. The data indicated that the *unknown#2288-dsh_2* and *unknown#2309-dsh_3* are presumably two derivatives (5- and 6-TMS -moieties) of one substance.

Table 7: Sum formula predictions of the unknown substances *unknown#2251-dsh_1*, *unknown#2288-dsh_2* and *unknown#2309-dsh_3* with corresponding mass error, mSigma and a postulated sum formula, with respect to the derivatisation reagents. Results were obtained by the software DataAnalysis 4.0.

Unknown compound	mass [Da]	sum formula derivative	Δmass [mDa]	mSigma[a]	sum formula compound
unknown#2251-dsh_1	685.3290	$C_{27}H_{65}O_8Si_6$	0.75	8.8	$C_9H_{16}O_8$
unknown#2288-dsh_2	627.2687	$C_{24}H_{55}O_9Si_5$	0.90	50.6	$C_9H_{14}O_9$
unknown#2309-dsh_3	699.3084	$C_{27}H_{63}O_9Si_6$	0.22	10.0	$C_9H_{14}O_9$

a: The smaller this quality parameter is the more matches the isotope pattern the predicted sum formula.

Following the results from the GC-MS analyses, the genome of *D. shibae* was screened for potential enzymes involved in the biosynthesis of pyranoses glycosidically linked to a C_3-moiety. A gene annotated as glucosylglycerol-phosphate synthase (Dshi_3832) was identified. Based on this, the dephosphorylated enzyme product α-glucosylglycerol ($C_9H_{18}O_8$) was assumed to be *unknown#2251-dsh_1*, regardless of the mass discrepancy of two protons. Correspondingly, the second unknown substance was assumed to be a pyranoseglycerate, probably α-glucosylglycerate. Therefore, the isomers mannosylglycerate, galactosylglycerol and β-glucosylglycerol of the assumed substances were measured via GC-APCI(+)-MS. In all cases, only the molecule ions with a loss of two protons were detected. To confirm the predicted substances, it was necessary to analyse standard substances. α-Glucosylglycerol and α-glucosylglycerate were not commercially available. Hence, α-glucosylglycerol was supplied by bitop AG (Witten, Germany), which uses this substance as a supplement for a vanishing crème (Luley-Goedl and Nidetzky, 2011) and α-glucosylglycerate was enzymatically synthesised by an *E. coli* expression clone and the method of Klähn *et al.* (2010) (section 2.8). The analysis of these reference substances via GC-ACPI(+)-MS also showed sum formulae with a loss of two protons. This, the identical spectra and RI and spiking experiments confirmed the presence of α-glucosylglycerol and α-glucosylglycerate (two derivatives) in the metabolome of

D. shibae. *Unknown#2251-dsh_1* is accordingly α-glucosylglycerol-6TMS and *unknown#2288-dsh_2* and *unknown#2309-dsh_3* α-glucosylglycerate-5TMS and α-glucosylglycerate-6TMS, respectively. The identified derivatives were added to our metabolite library.

In this context, homologues of genes for the biosynthesis of α-glucosylglycerol and α-glucosylglycerate were found in the genome of *D. shibae*. For α-glucosylglycerol Dshi_3832 already is annotated as glucosylglycerol-phosphate synthase, *ggpS*, and the neighbouring gene Dshi_3831 is currently annotated as sucrose-6F-phosphate phosphohydrolase. The latter is assumed to be glucosylglycerol-phosphate phosphatase, *ggpP*. The genome of *D. shibae* was blasted with NCBI BLASTp 2.2.32.+ against the glucosylglycerol synthase gene, *ggpPS*, of the γ-proteobacterium *Azotobacter vinelandii* (Table 8). This gene combines the synthase (glycosyltransferase GTB type superfamily) and phosphatase in one transcript and the synthesis of α-glucosylglycerol by this organism was experimentally confirmed (Mikkat *et al.*, 2000; Hagemann *et al.*, 2008; Klähn *et al.*, 2009). Additionally, the phosphatase domain of *A. vinelandii* was identified as the sucrose-6F-phosphate phosphohydrolase domain. The synthase domain could be assigned to Dshi_3832 the phosphatase domain to Dshi_3831. Thus, the genes for α-glucosylglycerol biosynthesis are coded on chromid 153 kb.

Table 8: BLASTp results of the amino acid (AA) sequences of glucosylglycerol synthase (GgpPS) and glucosyl-3-phosphoglycerate synthase (GpgS) assigned to the genome of *D. shibae*.

Blasted AA sequences of	Domain	Assigned genes of *D. shibae*	E-value	Identity [%]	Coverage [%]
GgpPS[a]	S6PP[d]	Dshi_3831	4·e-44	41	31
	gluc_glyc_Psyn[e]	Dshi_3832	1·e-143	45	65
GpgS[b]		Dshi_1821	3·e-125	44	99
GpgP[c]		Dshi_1820	1·e-33	31	98

a: AvCA6_34680 of *Azotobacter vinelandii* CA6; b: PERMA_1582 of *Persephonella marina* DSM 14350; c: PERMA_1578 of *Persephonella marina* DSM 14350; d: Sucrose-6F-phosphatase phosphohydrolase; e: glucosylglycerol-phosphate synthase.

For potential genes for α-glucosylglycerate biosynthesis, the genome of *D. shibae* was blasted with NCBI BLASTp 2.2.32.+ against the glucosyl-3-phosphoglycerate synthase, GpgS, and glucosyl-3-phosphoglycerate phosphatase, GpgP, of the aquificae *Persephonella marina,* whose functions were experimentally confirmed (Table 8; Costa et

al., 2007). GpgS could be assigned to Dshi_1821, a so far hypothetical protein. The neighbouring gene Dshi_1820, in the same chromosomal operon as Dshi_1821, was annotated as mannosyl-3-phosphoglycerate phosphatase. As the formation of mannosylglycerate is unlikely because of the GC-MS measurement of the reference substance, this gene was assumed to be a glucosyl-3-phosphoglycerate phosphatase. The BLASTp analysis also supported the assignment to this gene (Table 8).

The assigned genes encoding the biosynthesis of α-glucosylglycerol and α-glucosylglycerate allow the definition of the exact stereoisomerism of the two newly identified substances. This results in the structures shown in Figure 18.

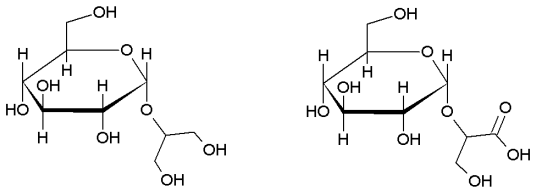

Figure 18: Structures of the newly identified substances in *D. shibae* extracts, A: 2-*O*-(α-D-glucopyranosyl)-glycerol and B: 2-*O*-(α-D-glucopyranosyl)-glycerate.

3.3 Exposure to various salinities and nitrogen limitation

Data and contents of the following chapter 3.3 were partially published in the journal *Environmental Microbiology* (Kleist *et al.*, 2016).

3.3.1 Phenotypic microarray experiment of osmolytes

For the determination of required or growth promoting osmolytes for *D. shibae*, a phenotypic microarray analysis was performed. In this context, twelve different salts with various concentrations and 23 osmolytes in combination with 6 % NaCl (B2-C12) were tested (Figure 19).

The principle of the phenotypic microarray analysis is the monitoring of a colour change as an indicator for respiratory activity. The colour change occurs due to the reduction of a tetrazolium dye. The resulting kinetic plots are analysed regarding their area under the curve and the slope of curves. However, a strong colour change does not necessarily mean that growth is possible.

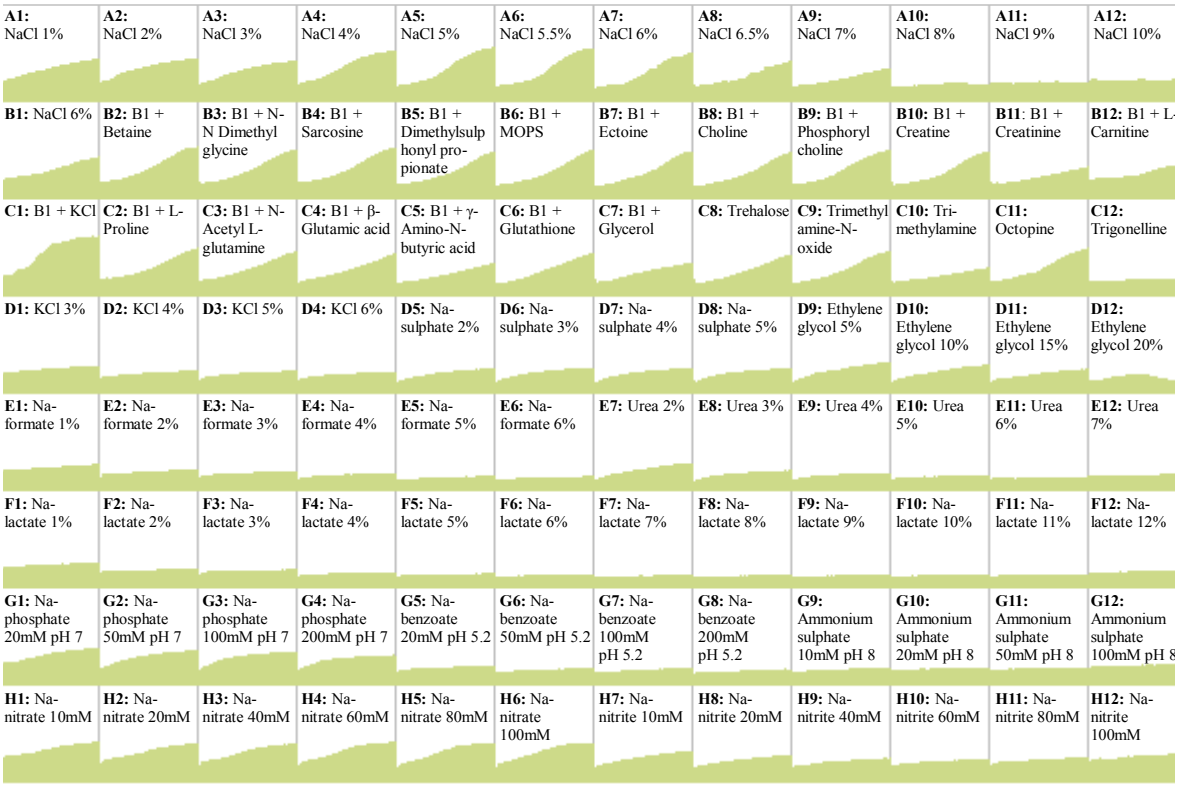

Figure 19: Phenotypic microarray analysis of osmolytes. The curves represent respiratory activity on the basis of the reduction of a colour indicator monitored for 72 h. The experiment was performed with an OmniLog-reader by utilising a PM9 micro plate. MOPS: (3-N-morpholino)propanesulfonic acid.

The average level of salinity in marine habitats is 3.5 %. In general, respiration was observed in a NaCl concentration range of 1 to 7 % (A1-A9), in which the biggest slope was present between 4 and 5.5 % NaCl. Strongest respiratory activity was observed with 6 % NaCl supplemented with potassium chloride (C1).

6 % NaCl is challenging for many organisms, hence uptake of known osmolytes and their potential improvement in growth was tested under these conditions. In the case of *D. shibae*, a strong respiratory activity was detected for 6 % NaCl without further supporting substances (A7, B1). A clear negative effect was observed for creatinine, L-carnitine, trimethylamine and trigonelline (B11, B12, C10 and C12). With the exception of potassium chloride (C1), no clear supporting influence on respiration was detected for the remaining osmolytes tested.

Very weak responses were detected for single supplied substances potassium chloride (D1-D4), sodium sulphate (D5-D8), ethylene glycol (D9-D11), low concentrated urea (E7 and E8) and for all sodium phosphate concentrations tested (G1-G4).

D. shibae possesses the entire equipment necessary for denitrification. The phenotypic microarray analysis revealed a positive response for all sodium nitrate concentrations tested (10 - 100 mM, H1-H6). Additionally, the toxic sodium nitrite, in the concentrations 10 and 20 mM, led to a weak response (H7 and H8).

No respiration was observed with sodium formate (E1-E6), sodium lactate (F1-F12), sodium benzoate (pH 5.2, G5-G8) and ammonium sulphate (pH 8, G9-G12), independent of their concentration.

3.3.2 Salt shock

The marine environment is a more or less stable environment regarding physico-chemical parameters. Very short-term changes are less probably, although a local change from *e.g*. brackish water to open sea water is possible, which causes several changes including increased salinity. *D. shibae* was challenged by a rapid NaCl increase in the medium. This extreme treatment was used to unravel general key elements to cope with high salt concentrations. Therefore, metabolic and transcriptional analyses were performed during the adaptation to the new conditions.

Starting from an initial salinity of 2.3 %, solid NaCl was added to a final salinity of 5 %. As previously mentioned, α-glucosylglycerate, α-glucosylglycerol and glutamate are highly abundant in *D. shibae* extracts and therefore have to play a major role in its metabolism. With respect to this, these three substances were quantified absolutely whereas other metabolites were analysed regarding their changes compared with the reference condition.

3.3.2.1 Impact of salt shock on growth

Interestingly, growth of salt shocked *D. shibae* cells was only slightly affected. Exponentially growing cells transferred from an initial salinity of 2.3 % to 5 % interrupted growth for about 30 min and continued replication with a slightly reduced growth rate (76 %). Additionally, the same maximal optical density was achieved (Figure 20).

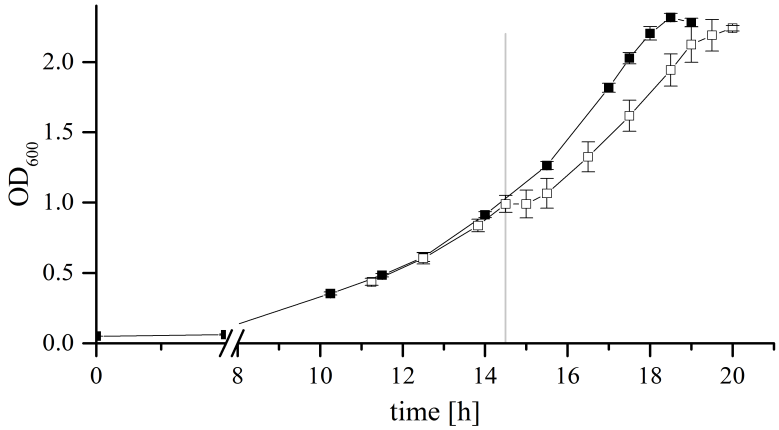

	μ [h^{-1}]	t_D [h]
■	0.25 ± 0.004	2.8 ± 0.04
□	0.19 ± 0.010	3.6 ± 0.18

Figure 20: Growth behaviour of *D. shibae* cultures under reference condition and after a salt shock with the according growth rate (μ) and doubling time (t_D). ■: 2.3 % salinity culture, □ culture shocked from initial 2.3 % to 5 % salinity; the vertical line marks the time point of salt shock. n = 3.

3.3.2.2 Metabolic response to salt shock

D. shibae cells in exponential phase shifted from a low salt level (2.3 %) to a high level (5 %) were analysed 10 and 90 min after the shock. All compounds and their according fold changes compared with the reference condition are listed in the appendix A4.

A closer look was taken at the generally highly abundant substances glutamate, α-glucosylglycerol and α-glucosylglycerate. Cell extracts of the reference condition (2.3 % salinity) contained exclusively glutamate in contrast to the shocked cultures (Figure 21). Just 10 min after the shock, α-glucosylglycerol was detected intracellularly, whereas the glutamate concentration decreased about 30 % compared with untreated cells. In the following 80 min, the concentration of α-glucosylglycerol increased constantly and a small

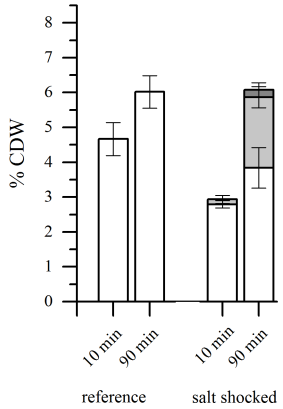

Figure 21: Intracellular concentrations of glutamate (white), glucosylglycerol (light grey) and glucosylglycerate (dark grey) of *D. shibae* 10 and 90 min after a salt shock. Initial salinity 2.3 % and a final salinity 5 %.

amount of α-glucosylglycerate was detected (Figure 21). Glutamate retained its low level.

Regarding the metabolites detected in this approach, glutamate was not the sole amino acid to be reduced. Actually, 10 min after the shock, amino acids were regulated in particular. Along with glutamate, aspartate, asparagine, lysine and tyrosine were at least two-fold decreased or detected in the reference only, whereas the branched chain amino acids as well as alanine, serine and threonine were at least two-fold increased (Figure 22, Table 9). 80 min later, exclusively alanine and serine were still increased and asparagine was only detected in extracts of the reference culture (Figure 22, Table 9).

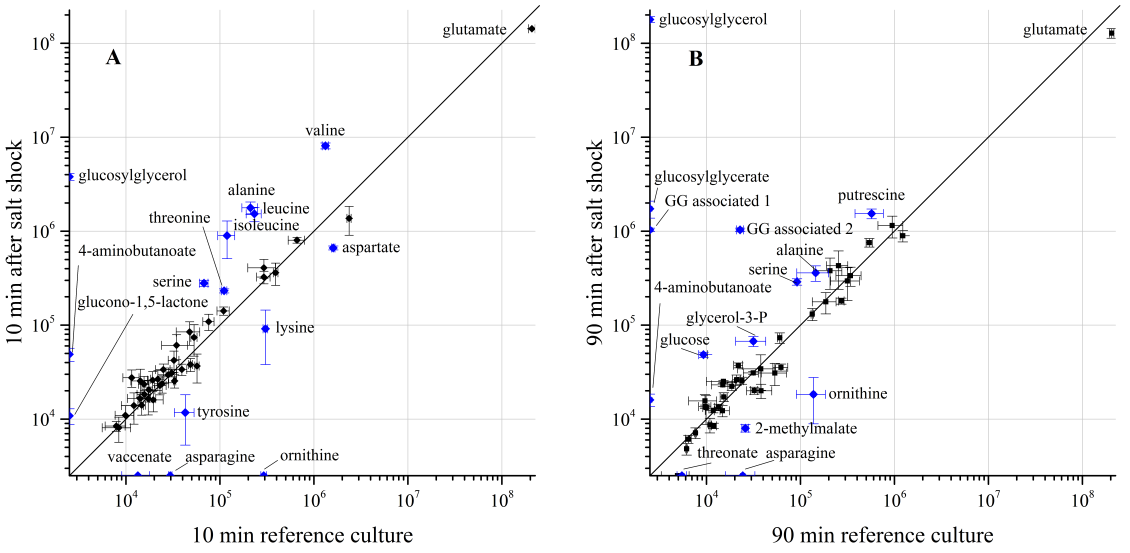

Figure 22: Intracellular metabolic changes of *D. shibae* A: 10 min and B: 90 min after a salt shock. Comparison between cultures continuously cultivated in medium containing 2.3 % salt and salt treated cultures, shocked from initial 2.3 % salt to 5 %. Normalised peak areas of metabolites plotted in double-logarithmic scale. Blue: metabolites changed with a fold change greater than 2 or less than 0.5. GG: α-glucosylglycerol.

Some metabolites were only detected in one single condition. In particular, 4-aminobutanoate was associated with the salt shock culture as well as the previously

Table 9: Selected metabolites of *D. shibae* intracellularly regulated 10 and 90 min after a salt shock. Fold changes were computed by comparison with the respective reference time points of untreated cultures. GG: α-glucosylglycerol.

	Fold change			Fold change	
Metabolites	10 min	90 min	Metabolites	10 min	90 min
Alanine	8.4 ± 2.06	2.5 ± 1.04	Isoleucine	7.5 ± 3.60	1.7 ± 0.86
Asparagine	0.4 ± 0.03	0.7 ± 0.11	Leucine	6.6 ± 1.66	1.8 ± 0.91
GG associated 1	1.8 ± 0.75	63.1 ± 22.0	Serine	4.1 ± 0.52	3.2 ± 0.25
GG associated 2	1.8 ± 0.71	45.4 ± 4.26	Threonine	2.1 ± 0.18	1.0 ± 0.15
Glucose	2.4 ± 0.69	5.2 ± 0.66	Tyrosine	0.3 ± 0.16	0.9 ± 0.54
Glycerol-3-P	1.4 ± 0.53	2.1 ± 0.8	Valine	6.1 ± 0.65	1.2 ± 0.48

mentioned substances α-glucosylglycerol, associated unknowns and α-glucosylglycerate. In contrast, ornithine was increased or only detected in untreated cells (Figure 22).

An important increase was observed for the α-glucosylglycerol precursors glucose (5.2 fold change) and glycerol-3-phosphate (2.1 fold change) (Figure 22, Table 9) after the adaptation to the changed conditions (time point: 90 min).

3.3.2.3 Transcriptional response to salt shock

Transcriptome analysis of *D. shibae* cells shocked with NaCl were done by a RNASeq analysis to unravel major responses to the shock and to elucidate the adaptation to the changed conditions. Salt treated cultures were investigated 10 and 90 min after the shock, were compared with the untreated reference cultures at the same time points and $\log_2$ ratios were determined.

For the interpretation of the comprehensive transcriptome data, some restrictions were defined. For the decision if a transcript is regarded to be reliably detected, a threshold of 4 was set, which accorded 10 % of the median over all expression values. Transcripts with an expression value less than 4 were therefore excluded from further interpretation. Hence, the computation of a $\log_2$ ratio was only allowed when both conditions met the restriction. In the special cases when transcripts were only reliably detected in one of the compared conditions, a differentiation between regulated and highly regulated transcripts was done. Regulated transcripts were assumed when the expression value was between 4 and 40 (d) and highly regulated transcripts were assumed when the expression value was greater than 40 (dd). Transcriptome data were published in the journal *Environmental Microbiology* and are available there.

A general overview of the number of regulated gene transcripts is presented in Table 10. Here, it is striking that the expression values of about 42 % of genes located on chromid 153 kb were upregulated after 10 min and still 23 % of these 90 min after the salt shock. This indicates an essential role of the 153 kb chromid in the adaptation to a higher salinity, which carries the genes encoding the α-glucosylglycerol biosynthesis, numerous transporters and channels and some hypothetical proteins. In contrast, most expression values of genes of the chromosome and the other extrachromosomal elements returned to initial levels again or inverted during the adaptation process (time point 90 min).

Table 10:Number of up- and downregulated gene transcripts of *D. shibae* (cut-off: log_2 ratio of ± 2) 10 and 90 min after the salt-shock.

Location	upregulated		downregulated		% regulated	
	10 min	90 min	10 min	90 min	10 min	90 min
chromosome	172	21	100	73	8.1	2.8
plasmid 191 kb	18	1	3	1	10.8	1.1
chromid 153 kb	57	13	-	-	41.9	9.6
plasmid 126 kb	12	-	-	-	17.1	-
plasmid 86 kb	2	-	3	-	8.5	-
chromid 72 kb	15	4	1	-	26.2	6.6

The short-term response to salt shock can be classified in four major groups. The first group includes genes encoding general stress proteins, the second includes genes encoding enzymes involved in α-glucosylglycerol biosynthesis, the third consists of genes encoding enzymes of the Entner-Doudoroff pathway and last of genes encoding all kinds of exchange systems such as transporters or channels (Table 11). Transcription levels of these genes were increased compared with untreated cells. Furthermore, the expression values of uncharacterised transcriptional regulators and Dshi_3834, a signal transduction histidine kinase (log_2 fold-change 5.6), were increased.

Regarding the entire transcriptome analysis, 90 min after the salt shock most transcriptional levels were back to the levels of the reference or were inverted. Expression of genes for the α-glucosylglycerol biosynthesis, some stress proteins and some transporters and channels were still upregulated. These genes are mainly located on the 153 and 72 kb chromid.

The strong regulations of gene transcripts of the Entner-Doudoroff pathway along with the regulations of the gluconeogenesis and glycerol-3-phosphate synthesis are shown in detail in Figure 23. Gene expressions of gluconeogenesis enzymes were unaffected by the salt shock.

Furthermore, the high expression levels throughout the entire experiment of the two glycerol-3-phosphate dehydrogenases (*glpD* and Dshi_3830) of *D. shibae* were remarkable. Expression of *glpD* was increased by a log_2 fold change of 6.0 and 5.4 and expression of Dshi_3830 was increased by 7.9 and 3.6 10 and 90 min after the salt shock (Figure 23). Dshi_3830 is located in the same operon as the two genes for α-glucosylglycerol biosynthesis (Dshi_3831 and Dshi_3830).

Table 11: Selected gene transcripts of *D. shibae* with corresponding log_2 fold changes 10 and 90 min after the salt shock. Ratios were computed using a reference culture at the same time points. a: primary annotation: sucrose-6F-phosphate phosphohydrolase; b: only transcripts with a fold change ≥ 3 are shown or "d" transcripts only reliably detected under shock conditions (threshold: expression value 4).

			log_2 fold change	
Locus Tag	**Gene**	**Product**	**10 min**	**90 min**
Genes encoding general stress proteins				
Dshi_0107		ferritin-like protein	0.9	2.7
Dshi_0169		glutathione S-transferase	4.0	0.0
Dshi_0617	*clpB*	chaperone protein clpB	1.8	2.8
Dshi_2892		small heat shock (HSP20) protein	1.8	4.9
Dshi_3839		ferritin Dps family protein	6.1	1.2
Dshi_3912		ferritin Dps family protein	6.1	0.9
Dshi_4184		CsbD family protein	9.8	2.9
Genes encoding enzymes involved in glucosylglycerol biosynthesis				
Dshi_0630	*glpD*	glycerol-3-phosphate dehydrogenase	6.0	5.4
Dshi_1742	*gap1*	glyceraldehyde-3-phosphate dehydrogenase	5.4	-2.0
Dshi_3830		glycerol-3-phosphate dehydrogenase	4.8	3.6
Dshi_3831		glucosylglycerol-3-phosphatase[a]	4.7	4.0
Dshi_3832		glucosylglycerol-phosphate synthase	5.1	3.4
Genes encoding enzymes of the Entner-Doudoroff pathway				
Dshi_1682	*pgi*	glucose-6-phosphate isomerase	3.1	-0.7
Dshi_1683		putative 6-phosphogluconolactonase	3.6	0.2
Dshi_1684	*zwf*	glucose-6-phosphate 1-dehydrogenase	3.9	-0.3
Dshi_1768	*eda*	KHG/KDPG aldolase	5.5	-0.6
Dshi_1769	*edd*	phosphogluconate dehydratase	5.7	-1.5
Genes encoding transporters or channels[b]				
Dshi_0144	*amtB*	ammonium transporter	d	-
Dshi_0743	*mscS*	MscS mechanosensitive ion channel protein	d	-
Dshi_3001	*dctM2*	TRAP dicarboxylate transporter subunit DctM	3.3	0.2
Dshi_3036		efflux transporter	3.6	-0.2
Dshi_3884		multi anti extrusion protein MatE	d	-
Dshi_3897		MgtC/SapB transporter	d	d
Dshi_3902		RND family efflux transporter MFP subunit	d	-
Dshi_3905		MscS mechanosensitive ion channel	5.0	0.6
Dshi_3906		SSS family solute/sodium (Na+) symporter	7.1	-0.2
Dshi_3907		sodium/calcium exchanger membrane region	5.1	1.1
Dshi_3913		TrkA domain-containing protein	3.6	0.6
Dshi_3914		cation transporter	d	1.6
Dshi_3922		transport protein, putative	5.7	1.7
Dshi_4182		MscS mechanosensitive ion channel	d	-

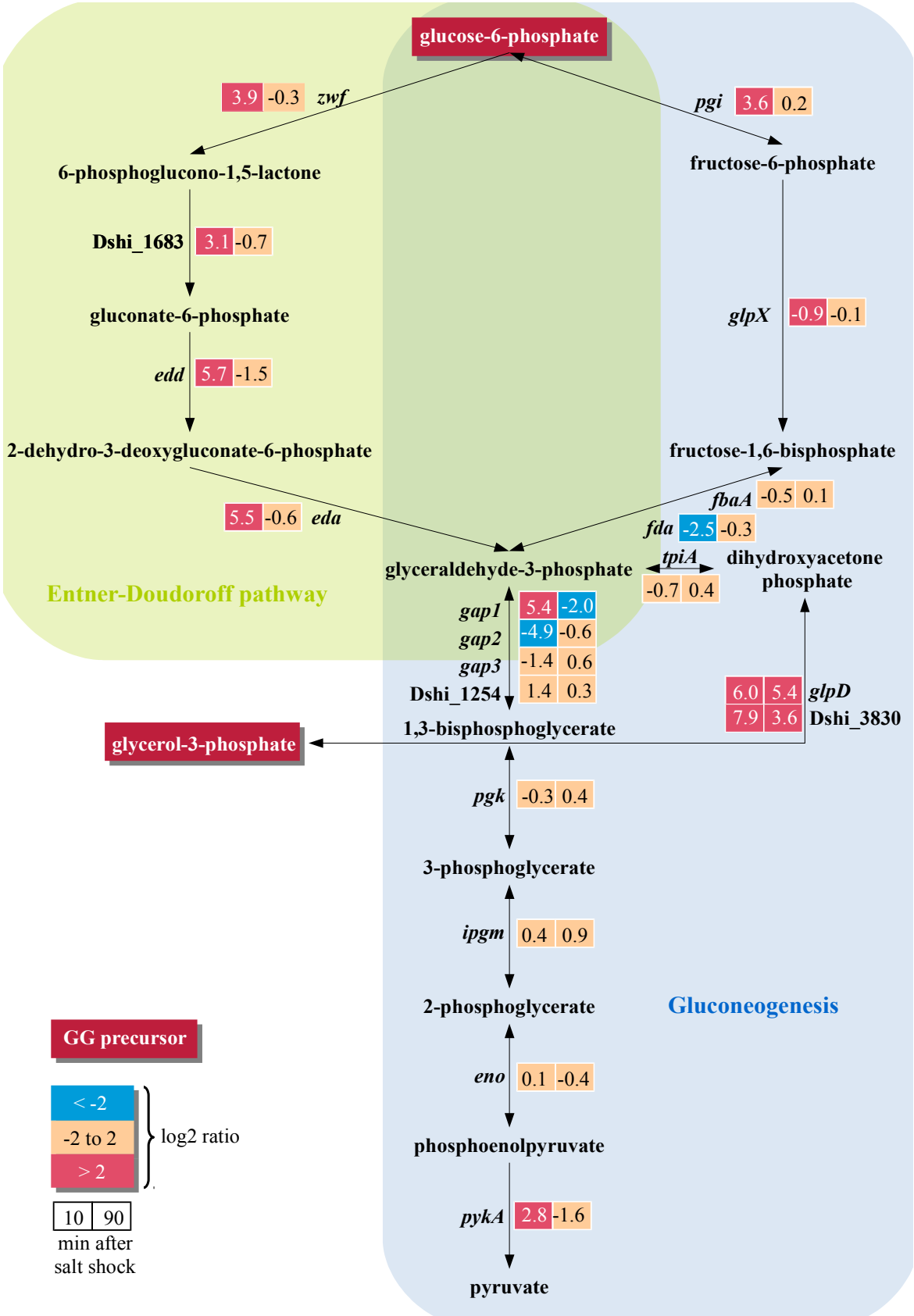

Figure 23: Transcriptional changes of *D. shibae* 10 and 90 min after a salt shock (2.3 to 5 % salinity) in gluconeogenesis and Entner-Doudoroff pathway. GG: α-glucosylglycerol.

3.3.3 Long-term adapted cells under various salinities

The metabolome of *D. shibae* was investigated under various salinities in its exponential growth phase and at its maximal optical density (OD_{max}) to unravel the metabolic adaptation needed to maintain a functional metabolism and the capability for replication. As mentioned previously, glutamate, α-glucosylglycerate and α-glucosylglycerol were quantified absolutely because of their generally conspicuous high concentrations in *D. shibae* extracts whereas other metabolites were analysed regarding their changes compared with defined reference conditions.

3.3.3.1 Influence of medium salinity on the growth behaviour

Growth of *D. shibae* was observed in a range from almost fresh water conditions, 0.3 % salinity, up to 5 % (Figure 24). Fastest growth occurred in medium containing 2.3 % salt (doubling time 2.8 h), which is only about 65 % of that of sea water. With rising salt concentrations the growth rate decreased up to a level where the growth of cells was strongly restricted (7 % salinity). A very low salinity led to a strongly impaired growth (doubling time 6.4 h). Surprisingly, the OD_{max} values were unaffected by salinity.

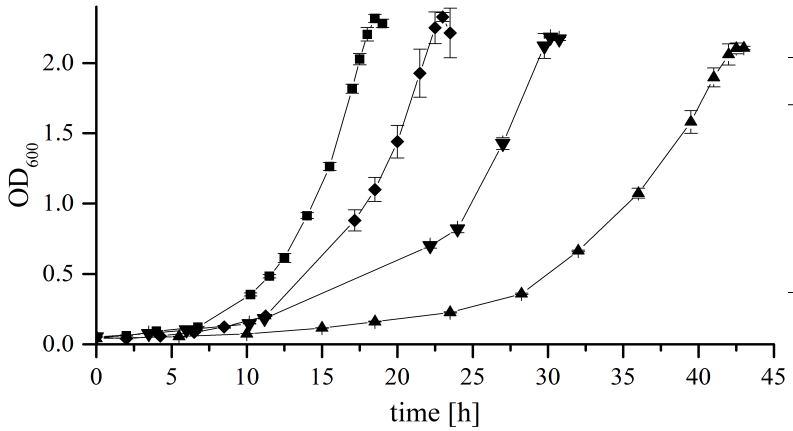

	μ [h^{-1}]	t_D [h]
▲	0.12 ± 0.002	6.4 ± 0.12
■	0.25 ± 0.004	2.8 ± 0.04
♦	0.20 ± 0.002	3.5 ± 0.04
▼	0.12 ± 0.003	5.7 ± 0.14

Figure 24: Growth behaviour of *D. shibae* under various salinities with the according growth rate (μ) and doubling time (t_D). ▲: 0.3 % salinity, ■: 2.3 % salinity, ♦: 3.5 % salinity, ▼: 5 % salinity. n=3, each.

3.3.3.2 Influence of salinity and growth phase on the metabolome

As the growth experiments resulted in a growth range from 0.3 % to 5 % salinity, the following four salinities were chosen for investment in long-term adapted *D. shibae* cells: 0.3 % salinity simulates almost freshwater conditions, 2.3 % corresponds to brackish water, 3.5 % corresponds to the average salinity of the oceans and 5 % were chosen to trigger a strong metabolic response. Metabolome analyses were conducted in the exponential growth phase and at OD_{max}, because the latter leads to metabolic rearrangements in the transient phase of cells. Nevertheless, an adequate turgor pressure must be maintained under these circumstances. Fold changes of the various conditions were computed by comparison with the according time points of *D. shibae* cultures cultivated at 3.5 % salinity.

Concerning the in detail investigated compounds glutamate, α-glucosylglycerate and α-glucosylglycerol, striking observations were made. Under all conditions tested, glutamate was the most abundant compound in *D. shibae* cells, independent of growth phase and salinity. While glutamate showed little differences in the exponential phase under 2.3, 3.5 and 5 % salinity (about 5 mg/100 mg CDW), it was more than 5-fold decreased in cultures grown under 0.3 % salinity (Figure 25A). Interestingly, α-glucosylglycerate and α-glucosylglycerol were not detected under the two low concentrated salt conditions. At OD_{max}, glutamate was strongly reduced under all conditions tested, except the culture grown in medium containing 5 % salt, where the effect was not that strong (Figure 25B). Remarkably, under 0.3 % salinity exclusively glutamate was detected.

α-Glucosylglycerol was first detected in cells grown under environmental conditions (3.5 % salts) during the exponential phase, and its concentration increased with increasing salinity (Figure 25). Moreover, it was detected at OD_{max} under all conditions, with the exception of 0.3 % salinity.

In contrast to α-glucosylglycerol, α-glucosylglycerate seems to be less affected by salinity but rather by growth phase. It was detected in minor concentrations in the exponential phase of the 3.5 and 5 % salinity cultures; for the latter the concentration stayed unchanged at OD_{max}. In contrast, the α-glucosylglycerate concentration was increased at OD_{max} in the culture with 3.5 % salinity, but the highest concentration of 0.9 mg/100 mg CDW was achieved at OD_{max} of the 2.3 % salinity culture (Figure 25).

Overall, glutamate, α-glucosylglycerate and α-glucosylglycerol together represented in minimum 0.3 mg of 100 mg CDW (0.3 % salinity, OD_{max}) and in maximum about 7.7 mg of 100 mg CDW (5 % salinity, exponential phase). In general, the share was reduced at OD_{max} with a maximal amount of 5.8 mg/100 mg CDW (5 % salinity, OD_{max}, Figure 25).

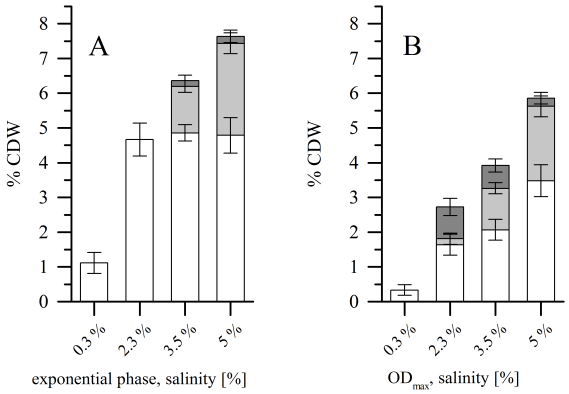

Figure 25: Intracellular concentrations of glutamate (white), glucosylglycerol (light grey) and glucosylglycerate (dark grey) of *D. shibae,* A: exponential phase and B: at OD_{max} under various salinities. CDW: cell dry weight.

A complete list of all metabolites and their changes compared with the 3.5 % salinity culture in exponential phase respective at OD_{max} is available in the supplementary material in appendix A4.

Besides the partly remarkable changes described above, the metabolic differences of the 2.3 % and 5 % compared with 3.5 % salinity cultures in the exponential phase were generally less extreme. Certain amino acids were increased compared with the 3.5 % salinity reference state, only valine was decreased (2-fold) during the cultivation at 5 % salinity. In both cases 2-methylmalate was clearly decreased (2.2 and 2.6-fold). Oppositely regulated were putrescine and ethanolamine. Cultures cultivated at 2.3 % salinity showed a 3.8 and 2.4-fold increase of these compounds and at 5 % salinity a reduction of 2.3- and 2.9-fold was observed (Table 12).

In contrast, the differences in the metabolome of cells in exponential phase at 0.3 % salinity was more distinct (Table 12, appendix A4). Here, the concentrations of almost all detected amino acids were strongly reduced just as the concentrations of citrate (3.3-fold), fumarate (2.1-fold), 2-oxoglutarate (3.0-fold) and malate (1.7-fold), although the latter was less clear. Contrarily, the concentrations of putrescine (7.4-fold), glycerol-3-phosphate (8.1 fold) and the fatty acid vaccenate (3.2-fold) were strongly increased (Table 12). Furthermore, the level of a few compounds decreased under the detection limit.

Table 12: Selected metabolites of *D. shibae* intracellularly influenced by salinity and growth phase. Fold changes were computed by comparison with the cultures cultivated at 3.5 % salt in according growth phase. * significantly changed (α=0.05; Wilcoxon-Mann-Whitney-Test with Benjamini/Hochberg correction). d: detected; TCA: tricarboxylic acid.

Metabolites	Fold change, exponential phase			Fold change, OD_{max}		
salinity [%]	0.3	2.3	5	0.3	2.3	5
Amino acids						
Alanine	0.15 *	0.71	1.03	0.56 *	1.93	10.53 *
Asparagine		0.73	1.73 *			d
Aspartate	0.04 *	0.84 *	1.03		0.27	11.24 *
Glycine	0.30 *	1.13	1.56 *	1.39	1.52 *	2.00 *
Isoleucine	0.28 *	0.75	0.78	0.64	3.08	1.28
Leucine	0.22 *	0.95	0.93	0.11 *	1.41	0.23 *
Lysine	0.56 *	1.08	2.45 *		0.10 *	22.96 *
Methionine	0.35 *	1.18	0.79 *			0.94
Ornithine	0.24 *	2.51 *	0.61 *			1.51
Phenylalanine	0.17 *	1.25	1.19	0.01 *	0.65	0.12 *
Proline	0.89 *	1.01	0.86 *	0.60 *	0.70	1.14
Serine	0.38 *	0.81	2.47 *	1.14	1.23	5.16 *
Threonine	0.50 *	1.27 *	1.26	0.32 *	0.70	1.87 *
Valine	0.14 *	0.89	0.49	0.05 *	1.14	0.12 *
Amino acid metabolism						
2-Isopropylmalate	0.85	1.13	0.67 *		0.80	0.61 *
2-Methylmalate	0.50 *	0.45 *	0.39 *	0.43 *	1.04	0.85
3-Aminoisobutanoate		1.32	0.85	0.61 *	0.64 *	0.63 *
Phenylpyruvate				0.55 *	3.72 *	
Putrescine	7.36 *	3.75 *	0.43 *	17.91 *	4.81 *	3.29
Fatty acids & Lipids						
Ethanolamine	1.20	2.39	0.34 *	1.33	3.90 *	0.74
Glycerol	0.93	0.90	1.28 *	1.25	0.62	0.68 *
Glycerol-3-P	8.07 *	1.64 *	0.94	2.78 *	0.87	0.69 *
Vaccenate	3.21 *	1.30		3.53 *	0.75	
TCA cycle						
Citrate	0.30 *	0.99	0.70 *		0.86	0.40 *
Fumarate	0.47 *	1.23	1.06	0.69	0.85	1.20
2-Oxoglutarate	0.33 *	1.10	0.85	0.08 *	2.10 *	0.15 *
Malate	0.60 *	1.00	0.98	0.36 *	0.80	1.35
Succinate	1.25 *	1.10	0.62 *	1.39	1.14	1.01

< 0.1	0.1 – 0.2	0.2 – 0.5	0.5 – 2	2 – 5	5 – 10	> 10

Concerning the culture at 0.3 % salinity, the comparison of the metabolic levels at OD_{max} showed only a slightly changed picture. Most changes previously observed in the exponential growth phase were intensified at OD_{max}, which led to an immensely increased putrescine concentration of 17.9-fold (Table 12).

D. shibae cultures at 5 % salinity showed a strong increase in the concentrations of the amino acids alanine (10.5-fold), aspartate (11.2-fold), lysine (23.0-fold) and serine (5.2-fold) whereas leucine (4.3-fold), phenylalanine (8.3-fold) and valine (8.3-fold) were decreased as well as the TCA cycle intermediates citrate and 2-oxoglutarate (Table 12).

3.3.4 Exposure to nitrogen limitation

As it is known that compatible solutes are often nitrogen-containing substances, a nitrogen limited *D. shibae* culture was investigated to unravel potential suitable responses. Therefore, the ammonium concentration of the SWM was reduced from 4.7 to 1 mM and the metabolome was analysed.

3.3.4.1 Influence of nitrogen limitation on growth

The growth behaviour of nitrogen limited *D. shibae* cultures differed clearly from that of unlimited cultures (Figure 26). The nitrogen limited cultures showed a comparable lag phase as their reference culture (both 3.5 % salinity), but showed a strongly hampered growth in the ongoing cultivation. In the first 19 h of cultivation the doubling time was 4 h

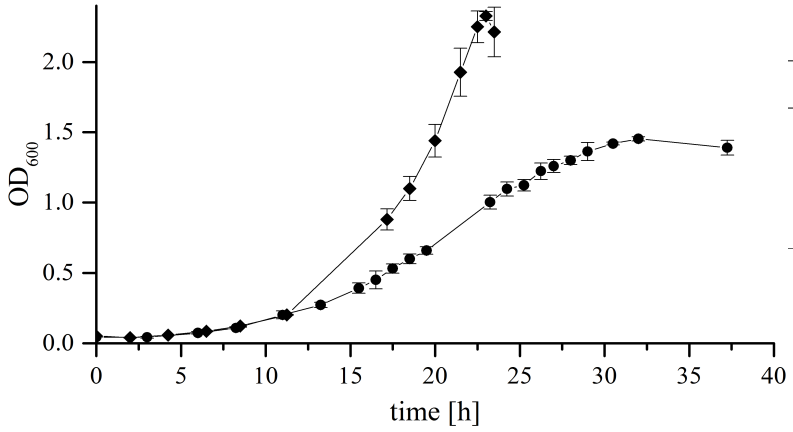

	μ [h^{-1}]	t_D [h]
♦	0.20 ± 0.002	3.5 ± 0.04
● a	0.17 ± 0.005	4.0 ± 0.02
● b	0.05 ± 0.005	13.9± 0.07

Figure 26: Growth behaviour of *D. shibae* during exposure to nitrogen limitation and reference culture with the according growth rate (μ) and doubling time (t_D). ♦: 3.5 % salinity (4.7 mM ammonium), ●: 3.5 % salinity, nitrogen limited (1 mM), a: first 19 h of cultivation, b: last 9 h of active growth. n=3.

which was later immensely prolonged to 13.9 h, indicating the initiation of the limitation. Additionally, the OD_{max} of the nitrogen limited culture was strongly reduced from 2.3 to 1.5 (Figure 26).

3.3.4.2 Influence of nitrogen limitation on the metabolome

D. shibae cells under nitrogen limited conditions and a salinity of 3.5 % were analysed in their active growth phase (OD 0.9, Figure 26). All compounds and their according fold changes compared with the reference condition (3.5 % salinity in exponential growth phase) are listed in appendix A4.

The first remarkable change in the metabolome of *D. shibae* under nitrogen limited conditions was the extremely high amount of α-glucosylglycerate of 1.7 mg/100 mg CDW. This accords a 259-fold increased level compared with the reference conditions (Table 13, Figure 27A). Concomitantly, the glutamate concentration decreased 15-fold. The α-glucosylglycerol concentration seemed to be unaffected of the nitrogen supply (Figure 27).

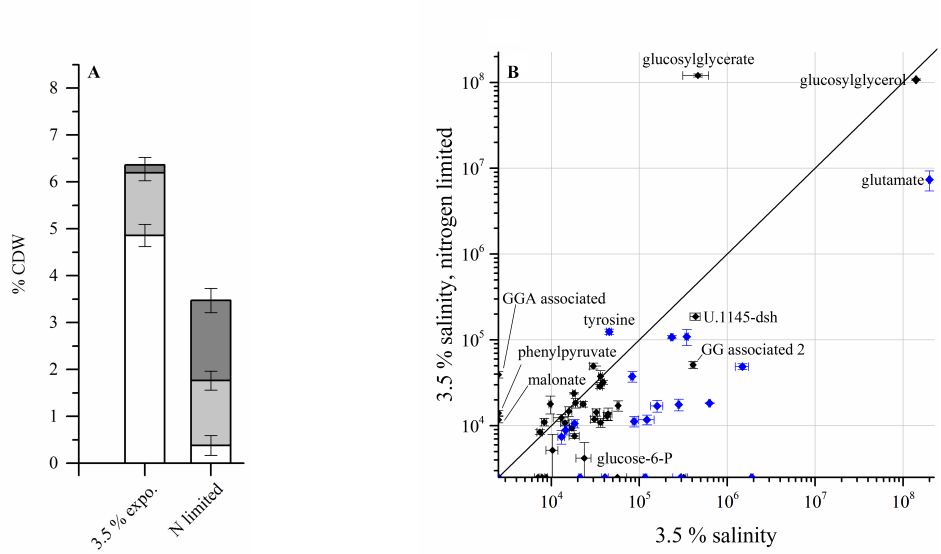

Figure 27 Intracellular metabolic changes of *D. shibae* during nitrogen limitation. A: Intracellular concentrations of glutamate (white), glucosylglycerol (light grey) and glucosylglycerate (dark grey). Reference condition 3.5 % salinity, 4.7 mM ammonium in exponential phase and nitrogen limitation 3.5 % salinity, 1 mM ammonium during active growth. **B:** Comparison between cultures in exponential growth phase in medium containing 3.5 % salt, 4.7 mM ammonium and cultures during active growth in medium containing 3.5 % salt and only 1 mM ammonium. Normalised peak areas of metabolites plotted in double-logarithmic scale. Blue: nitrogen-containing substances. GGA: α-glucosylglycerate; GG: α-glucosylglycerol; U.: unknown substances with corresponding ID.

The strong reduction of nitrogen-containing substances observed, is shown in Figure 27B. However, these were not the only metabolites decreased. Tyrosine was the single known nitrogen-containing substance with an increased concentration of 2.7-fold (Table 13).

Table 13: Selected metabolites of *D. shibae* intracellularly regulated during exposure to nitrogen limitation (3.5 % salinity, 1 mM ammonium). Fold changes were computed by comparison with the according reference culture (3.5 % salinity, 4.7 mM ammonium). α-glucosylglycerol: glucosylglycerol; U.: unknown substances.

Metabolites	Fold change	Metabolites	Fold change	Metabolites	Fold change
Citrate	0.3 ± 0.04	Isoleucine	0.1 ± 0.02	Tyrosine	2.7 ± 0.27
Ethanolamine	0.1 ± 0.02	Lysine	0.06 ± 0.01	U.1145-dsh	0.4 ± 0.07
GG associated 2	0.1 ± 0.01	Malate	0.04 ± 0.01	U.1226-pin	0.3 ± 0.06
Glucose-6-P	0.2 ± 0.10	2-Methylmalate	0.3 ± 0.01	U.1385-pae	0.4 ± 0.06
Glucosylglycerate	259 ± 85.4	Phenylalanine	0.5 ± 0.03	Vaccenate	0.5 ± 0.28
Glutamate	0.04 ± 0.01	Putrescine	0.03 ± 0.00	Valine	0.08 ± 0.01
Glycerol-3-P	0.44 ± 0.06	Serine	0.5 ± 0.07		
Glycine	0.31 ± 0.07	Threonine	0.13 ± 0.02		

An α-glucosylglycerate associated substance, malonate and phenylpyruvate were exclusively detected in in cell extracts of nitrogen limited cultures. In contrast, alanine, asparagine, aspartate, methionine, ornithine, 2-isopropylmalate and a few more substances (appendix A4) were only detected under reference conditions.

3.3.5 General observations to changing salt concentrations and nitrogen-limitation

Throughout the experiments of section 3.3.2 to 3.3.4 the concentrations of 55 identified and 10 unidentified metabolites were monitored. A complete list of the detected metabolites and their fold changes compared with defined reference conditions is available in the appendix (appendix A4).

3.3.5.1 Hierarchical cluster analysis of performed experiments

For the determination of correlations between all experiments performed (section 3.3.2 to 3.3.4) a hierarchical cluster analysis was performed. These resulted in four major clusters (Figure 28).

Cluster I comprises the exponential phase and OD_{max} samples at 0.3 % salt. Cluster II comprises the three conditions: OD_{max} of 2.3 and 3.5 % salinity cultures and nitrogen limitation. Cluster III consists of the three conditions: 5 % salt (exponential and OD_{max}) and 90 min after salt shock and finally, cluster IV includes the four conditions: exponential phase of 2.3 and 3.5 % salinity cultures, 10 min after salt shock and the 90 min reference culture (Figure 28). Overall, this indicates only slight metabolic differences between the moderate salt concentrations of 2.3 and 3.5 %. The more extreme conditions of 0.3 and 5 % salinity are clearly separated, and thus indicate distinct adaptation processes needed.

In particular, the high correlations between the conditions 2.3 % salinity, exponential phase and 90 min shock reference as well as the conditions 90 min after shock and 5 % salinity, exponential phase have to be noticed.

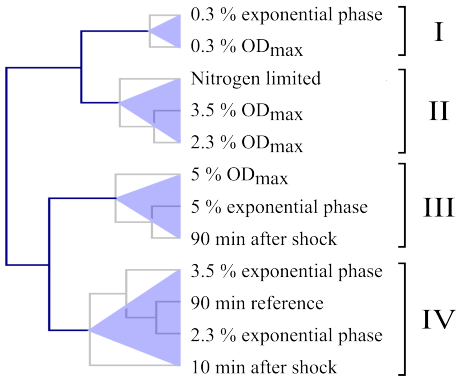

Figure 28: Hierarchical cluster analysis based on metabolite concentrations. All metabolome data generated in the experiments section 3.3.2 to 3.3.4 were processed. Cluster analysis was done based on the Pearson correlation.

3.3.5.2 poly-(R)-3-Hydroxybutanoate share under various salinities and nitrogen limitation

In addition to the metabolome analyses in the experiments section 3.3.2 to 3.3.4 by GC-MS, the accumulation of the storage compound poly-(R)-3-hydroxybutanoate was quantitatively investigated. Therefore PHB was alkaline-hydrolysed and the resulting monomer 3-hydroxybutanoate was quantified via GC-MS measurements.

The data indicated a general PHB share between 20 and 35 % of cell dry weight, with a low tendency of an increasing share with increasing salinity (Figure 29). At OD_{max}, the PHB content was slightly higher, which was more extreme for cells cultivated in 0.3 % salt medium.

Remarkable was the high PHB amount under nitrogen-limited conditions. Here, about 60 % of the cell dry weight consists of PHB (Figure 29).

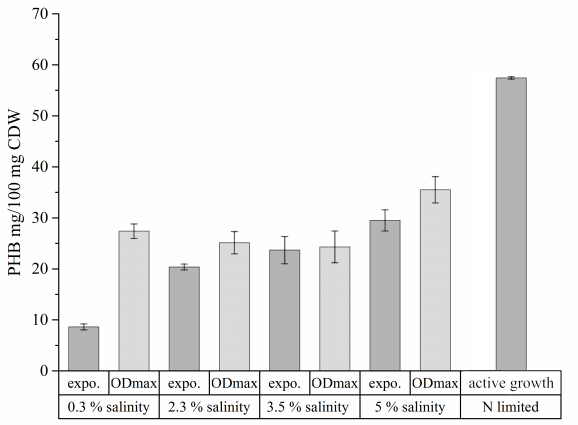

Figure 29: poly-(R)-3-Hydroxybutanoate (PHB) share of *D. shibae* under various salinities in exponential phase and maximal optical density (OD_{max}) as well as under nitrogen-limited conditions during active growth. CDW: cell dry weight; expo.: exponential growth phase.

4 Discussion

4.1 Adaptation processes of D. shibae during oxygen depletion

To get access to adaptation processes of *D. shibae* during oxygen depletion, the organism was shifted from oxic to anoxic conditions. Throughout the cultivation the alternative electron acceptor nitrate was supplied. The shift was applied by stopping the oxygen supply of an initially aerobic culture. Hence, *D. shibae* was forced to switch from oxygen respiration to denitrification to facilitate proliferation. This set-up was applied to simulate the sinking of *D. shibae* into sea layers that are low in oxygen or even in the sediment. A cooperative systems biology approach, including metabolome, proteome and transcriptome analyses, was performed to get an almost all-encompassing picture of the adaptation processes, which might serve as a model for other denitrifying bacteria.

4.1.1 General observations

After the oxygen shut-down a slight decrease in OD was observed (Figure 8) that lasted about 60 min and afterwards the OD stabilised again. This indicated an interrupted growth immediately after oxygen shut-down and a decreased OD as result of the continuous dilution caused by the chemostat. Between the time-points 60 and 120 min a sufficient shift to denitrification had to be accomplished to allow replication again, which was covered by the obtained transcriptome and proteome data (section 3.1.4). According to this, denitrification is probably possible after 60 min of oxygen depletion, even if the final level of enzymes was not reached yet. This is remarkable, as after reaching the actual state of anoxia (Figure 8) less than 30 min were needed to establish an operable denitrification machinery.

Concerning the time-resolved metabolome analysis during the adaptation to oxygen depletion, the correlation analysis (Figure 10) revealed in a clear differentiation between the oxic and still oxic state of cells (time-points 0 and 15 min), a state of metabolic crisis due to the not yet sufficiently established denitrification (time-points 30 and 60 min) and a slowly normalising metabolism due to the strengthened denitrification 120 and 240 min after oxygen shut-down.

4.1.2 Energy supply during oxygen depletion on the basis of ATP concentration

Under oxic conditions, *D. shibae* forms ATP via the respiratory chain. Electrons of reducing equivalents are transferred to a redox chain and finally these are transferred to the electron acceptor oxygen. The initiated redox cascade induces a proton-motive force which is used for ATP formation via oxidative phosphorylation. Alternatively, nitrate can serve as electron acceptor. Nitrate is stepwise reduced to nitrogen and thus different enzymes are required. By stopping the oxygen supply, the final electron acceptor of the respiratory chain was removed. Therefore, until compensated by established denitrification, a strong negative effect on ATP regeneration was expected.

To investigate this effect, a batch culture was required to guarantee anoxic sampling conditions. Since the revival of growth started after a comparable period of time, in batch and chemostat culture, also the adaptation process should be comparable (Figure 8 and Figure 9).

The ATP quantification showed a clearly hampered ATP formation triggered by the shift to anoxic conditions (Figure 9). Similar was also observed for *Saccharomyces cerevisiae*. The ATP/ADP concentration of the yeast was strongly affected during the shift to anoxic conditions and after reaching the anoxic state (Gonzalez *et al.*, 2000), which is in good agreement with the observations done for *D. shibae*.

The obtained data could prove that the oxidative phosphorylation was indeed interrupted in *D. shibae* resulting in a declined ATP concentration. Efficient ATP regeneration will only be possible after the formation of enzymes of the denitrification chain. Predominantly by the proteome analysis, it became clear that denitrification first was possible 60 min after oxygen shut-down, as discussed previously. This is reflected by an increase of ATP (Figure 9).

Since the respiratory chain was interrupted, concomitant accumulation of NAD(P)H is very probable as has also been shown for hepatocytes of rats under hypoxia (Obi-Tabot *et al.*, 1993). ATP and reducing equivalents are essential for several reactions in the cell. Hence, the strong decreased ATP concentration and the accumulation of reducing equivalents in their reduced form lead to a strongly affected or even disrupted metabolism, which is discussed detailed in the following chapters.

4.1.3 Changes in central metabolism

Tricarboxylic acid cycle: The intermediates of the TCA cycle showed three different types of concentration patterns caused by the oxygen shut-down (Figure 30) that can be assigned to: 1: Citrate and aconitate, 2: 2-oxoglutarate and 3: succinate, fumarate and malate. The TCA cycle could be covered almost completely by the conducted method with exception of succinyl-CoA and oxaloacetate. The directly dependent intermediates citrate and aconitate showed a very similar concentration pattern with highest concentrations 60 and 120 min after oxygen shut-down. Quite different is the pattern of 2-oxoglutarate, the next intermediate in the TCA cycle. At this point, the cycle was disrupted for several reasons. The turnover of aconitate by isocitrate to 2-oxoglutarate requires $NADP^+$ which is missing due to the strongly decreased redox potential present in the cell during adaptation to anoxia. Additionally, isocitrate dehydrogenase is probably inhibited by accumulated NADPH as have been shown for *Phormidium laminosum*, *Chlorobium limicola* and *Rhodopseudomonas palustirs* (Pardo *et al.*, 1999; Lebedeva *et al.*, 2002). The reverse reaction is unlikely, because 2-oxoglutarate is formed by a decarboxylation step. As consequence, 2-oxoglutarate concentration is hardly affected throughout the adaptation process. In addition, 2-oxoglutarate can be balanced by the conversion to glutamate and further connected metabolites. Although the decarboxylation product, succinyl-CoA, is not detectable by GC-MS, its NAD^+ dependent formation is unlikely, because the oxoglutarate dehydrogenase is probably product inhibited by NADH as has been shown for *Acinetobacter* (Weitzman, 1972).

Succinate, fumarate and malate showed the same concentration patterns implying their direct conversion. Their concentrations strongly increased up to 20-fold with a maximum 60 min after the oxygen shut-down (Figure 30). This was unexpected as the conversion by succinate dehydrogenase is ubiquinone dependent. Ubiquinone is part of the interrupted respiratory chain and therefore assumed to be existent in its reduced form only. Succinate, the sole carbon source, seems to be absorbed also during the crisis caused by the missing oxygen. Thus, succinate and its conversion products strongly accumulated. As in the first 30 min after oxygen shut-down residual oxygen is present, the metabolic response is strongest 60 min after oxygen shut-down which is mirrored by several concentration patterns of detected metabolites, reaching highest concentrations at this time point.

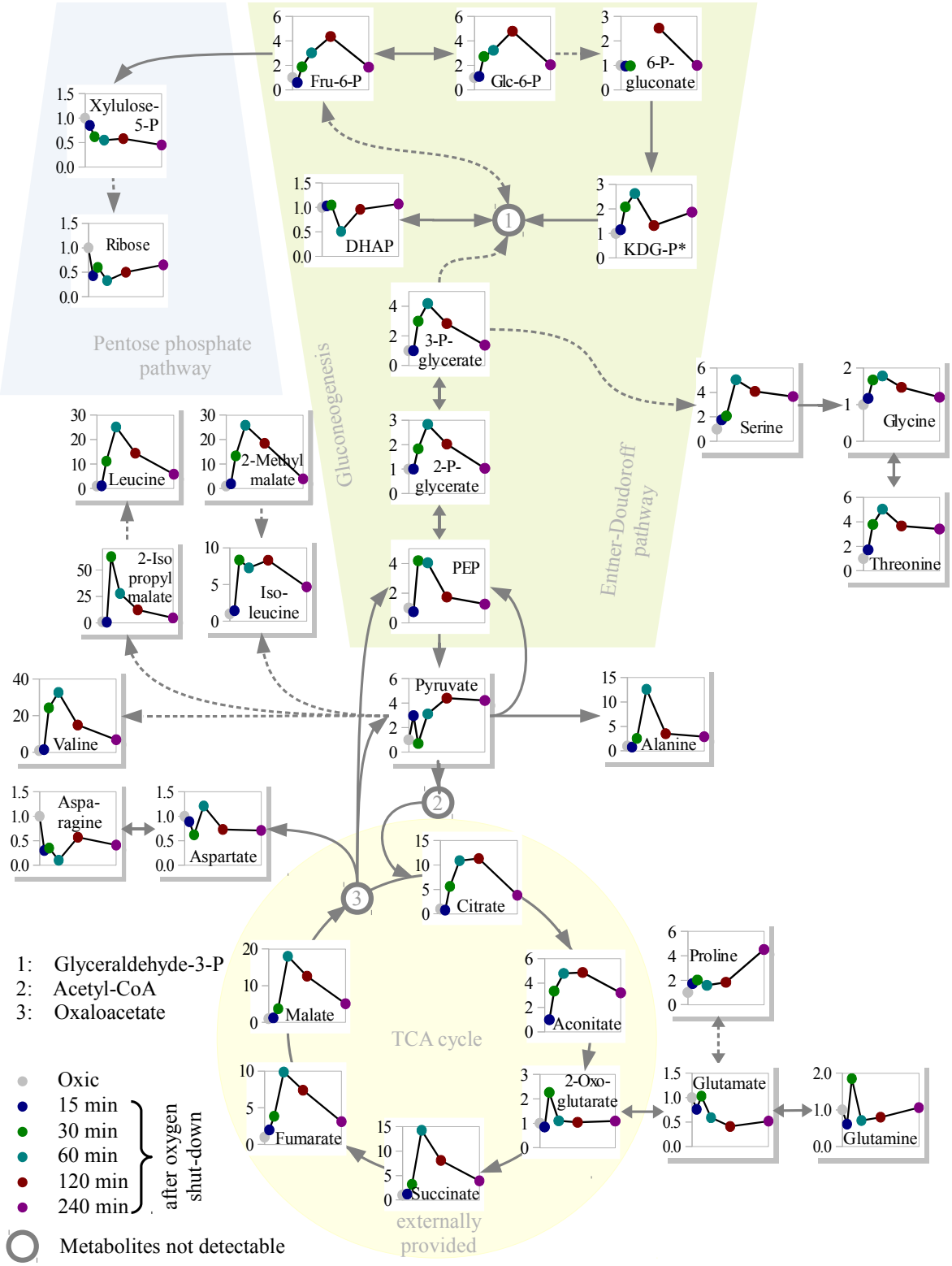

Figure 30: Overview of metabolic changes in the central metabolism of *D. shibae* during adaptation to denitrifying conditions. Shown are fold-changes compared to the oxic reference state. CoA: coenzyme A, DHAP: dihydroxyacetone phosphate, Fru: fructose, Glc: glucose, KDG-P: 2-keto-3-deoxy-gluconate (* detected dephosphorylated), P: phosphate, PEP: phosphoenolpyruvate.

In the following, oxaloacetate might show a different concentration pattern again because the conversion of malate to oxaloacetate requires NAD^+ which is probably not present in a sufficient amount. Additionally, for *Streptomyces coelicolor* a substrate inhibition of malate dehydrogenase was reported (Ge *et al.*, 2010) which is probably also applicable for *D. shibae*.

One of the main purposes of the TCA cycle is the generation of NAD(P)H. Since NAD(P)H are present in excess, the TCA cycle is strongly affected. During the first 60 min after oxygen shut-down, the TCA cycle seemed to has lost its function in energy metabolism and is rather used for biosynthesis only. Enzymes of the TCA cycle showed no crucial changes in abundance, suggesting that no adaptation of the cycle is needed for the anaerobic lifestyle. Also on the transcriptional level only slight changes were observed. The transcriptional levels of genes encoding enzymes which can form succinyl-CoA (*sucA*, *sucB*, *sucC*, *sucD1*) were slightly increased. Succinyl-CoA is a precursor for heme and bacteriochlorophyll biosynthesis. As bacteriochlorophyll synthesis is up-regulated, the regulations of *sucABCD* are probably associated with it (Laass, Kleist *et al.*, 2014).

Overall, during the adaptation to denitrification, transient changes in the TCA cycle could be determined probably controlled by several feedback inhibitions. The effect was exclusively observed on the metabolic level and was strongest 60 min after oxygen shut-down and reversed with the establishment of the denitrification apparatus.

***Gluconeogenesis, Entner-Doudoroff and pentose phosphate pathway*:** The metabolic regulations of gluconeogenesis, Entner-Doudoroff and pentose phosphate pathway were not as distinct compared with changes of the TCA cycle. *D. shibae* is only capable of the non-oxidative pentose phosphate pathway.

Generally, the succinate feeding condition requires gluconeogenesis for the formation of carbohydrates in particular C_5-bodies to enable nucleotide biosynthesis. These intermediates are formed in the pentose phosphate pathway and were decreased (Figure 30), indicating a reduced flux into the pentose phosphate pathway. This is supported by downregulated transcript levels of genes involved in this pathway, as well as by the observed low concentration of TktA (transketolase), the central enzyme of the pentose phosphate pathway (Laass, Kleist *et al.*, 2014). These observations indicate clearly the decreased nucleotide synthesis and consequently a reduced genome replication. This

agreed with the hampered growth of *D. shibae* during the first 60 min after oxygen shut-down (Figure 8).

Gluconeogenesis includes two ATP demanding steps. First, the formation of the entry metabolite phosphoenolpyruvate requires ATP, regardless of whether oxaloacetate or pyruvate is utilised as precursor (Cannata and Stoppani, 1963; Cooper and Kornberg, 1965). Secondly, the conversion of 3-phosphoglycerate to glyceraldehyde-3-phosphate via 1,3-bisphosphoglycerate consumes one ATP (Rao and Oesper, 1961). As ATP availability has been shown to be limited, these are two critical steps in gluconeogenesis. The intermediates phosphoenolpyruvate as well as 2- and 3-phosphoglycerate were detected, the intermediates which connect these steps. The concentration patterns of these metabolites were similar to those of the TCA cycle intermediates *e.g.* fumarate (Figure 30), but the fold-changes were less distinct. Obviously, phosphoenolpyruvate is formed in high amounts just 30 min after the oxygen shut-down, when ATP concentration did not reach its minimum, yet. Accordingly, the subsequent intermediates 2- and 3-phosphoglycerate were accumulated. In the following, 3-phosphoglycerate is not further metabolised because of the consecutive ATP demanding step. This is supported by the reduced dihydroxyacetone phosphate level (Figure 30), the balanced tautomer of glyceraldehyde-3-phosphate.

The accumulation of fructose- and glucose-6-phosphate (Figure 30) is a result of the decreased efflux towards the pentose phosphate and the Entner-Doudoroff pathway. In general, the Entner-Doudoroff pathway is assumed to play a minor role under succinate feeding conditions. Additionally, the conversion by glucose-6-phosphate dehydrogenase to 6-phosphogluconate is probably inhibited by accumulated NADPH as have been shown for several bacteria (Lessmann *et al.*, 1975; Schaeffer and Stanier, 1978; Hansen *et al.*, 2002). The sugar phosphates showed a slightly delayed decline compared with other metabolites. This is probably due to the renewed ATP generation which leads to an increased flux towards these intermediates.

Summarised, similar to the TCA cycle, gluconeogenesis and the Entner-Doudoroff pathway are dominated by several feedback inhibitions initiated by the energy and redox crisis. These changes are primarily limited to the metabolome. This means that no basic adaptations of the central metabolism are needed for the transition to denitrification.

The pentose formation by the pentose phosphate pathway is downregulated at all levels analysed. Consequently, the formation of nucleotides is probably downregulated (Hove-

Jensen *et al.*, 1986). This indicates a diminished genome replication in accordance with the diminished cell proliferation.

***Amino acids*:** Protein biosynthesis from amino acids is very ATP demanding. The transcriptome and proteome data showed an immediate down-regulation of the protein biosynthesis in the first minutes after oxygen shut-down. Several aminoacyl-tRNA synthetases (Laass, Kleist *et al.*, 2014) were detected only under oxic conditions or their concentrations were found strongly diminished after oxygen shut-down. Even more extreme was the effect on transcription of genes encoding ribosomal proteins (Laass, Kleist *et al.*, 2014).

Most amino acids accumulated in the metabolome after 60 min. This is the result of a decreased protein biosynthesis during the transition phase to anoxia. Especially, the concentrations of the branched-chain amino acids and their associated precursors 2-methylmalate and 2-isopropylmalate were extremely increased (Figure 30). The synthesis of branched-chain amino acids by ketol-acid reductoisomerase consumes excess NADPH and contributes thus to a more balanced redox state of the cell. However, the observed accumulation was unexpected as the biosynthesis of the branched-chain amino acids has been shown to be product inhibited in some cases in several organisms (Kohlhaw *et al.*, 1969; Blatt *et al.*, 1972; de Carvalho *et al.*, 2009). Furthermore, serine, glycine and threonine were highly abundant (Figure 30), indicating a channelling of accumulated 3-phosphoglycerate towards these metabolites.

Nitrogen is mainly assimilated by the transfer of ammonium to 2-oxoglutarate by the formation of glutamate in *D. shibae*. Glutamate is thus the main nitrogen donor for every nitrogen containing metabolite and in particular for amino acids. The reduced glutamate concentration (Figure 30) indicates a decreased ammonium assimilation. This supports again the downregulated protein biosynthesis.

With the establishment of the denitrification, amino acid concentrations started to decrease again and concomitantly the expression of genes involved in protein biosynthesis and amino acid metabolism increased again. Overall, the results indicate that protein biosynthesis in *D. shibae* is hampered in the first hour of oxygen depletion. This is a result of a disturbed redox state and energy balance of the cells, accompanied with a metabolic crisis.

4.1.4 PHB formation during oxygen depletion

During the adaptation of *D. shibae* from oxic to anoxic conditions a short term energy crisis was confirmed as described previously (section 4.1.2). The formation of the storage compound PHB is assumed to be dependent on the energy metabolism of cells (Senior and Dawes, 1971; Miura *et al.*, 1997; Trautwein *et al.*, 2008; Xiao and Jiao, 2011). Therefore, the cellular PHB content was quantified throughout the adaptation process. Here, a continuous increase of PHB concentration starting 30 min after the oxygen shut-down was determined (Figure 12). In accordance, an increase towards PHB formation could be confirmed by the transcriptome and 2D-DIGE analysis (Laass, Kleist *et al.*, 2014).

As discussed previously, the reducing equivalents NAD(P)H accumulated in their reduced form, since the consumption by the respiratory chain or by anabolism was inhibited within the first minutes after stopping the oxygen supply. The first step of PHB formation is the reduction of acetoacetyl-CoA to 3-hydroxybutanoyl-CoA by the consumption of NAD(P)H. NADPH is preferred 5-fold compared with NADH, at least in *Azotobacter beijerinckii* (Ritchie *et al.*, 1971). Due to this, *D. shibae* is able to diminish the excess of reducing equivalents enabling essential processes. Similar was reported for oxygen limited cultures of *A. beijerinckii* (Senior and Dawes, 1971). Here, PHB was first discussed as electron and carbon sink. An increased PHB formation was also observed for *Dinoroseobacter* sp. JL1447 cultivated in a day and night cycle. Under these conditions NADH is saved, since the utilisation of light energy shares the same electron transfer system as the oxidative phosphorylation (Xiao and Jiao, 2011).

After establishment of the denitrification apparatus most metabolites returned to levels similar to those prior to oxygen shut-down. Contrarily, the PHB formation was unresisted, still 240 min after oxygen shut-down (Figure 12). This effect is probably a result of the changed energy metabolism. For the β-proteobacterium *Aromatoleum aromaticum* the potential electron supply provided by the organic substrates was assumed to exceed the electron-accepting capacity of nitrate, under denitrifying conditions (Trautwein *et al.*, 2008). Also a study investigating the light driven production of hydrogen of *Rhodovulum sulfidophilum* W-1S observed a competition between the formation of hydrogen and PHB, as both are in a direct or indirect way electron acceptors (Miura *et al.*, 1997). Taking these information togehter, PHB might also serve as an electron sink for *D. shibae.*

4.1.5 Conclusion

The acquired results show the capability of *D. shibae* to shift very quickly and specifically from oxygen to nitrate respiration. This, together with the ability of using light as additional energy source (Wagner-Döbler and Biebl, 2006; Tomasch *et al.*, 2011) is very advantageous also compared with obligate aerobic competitors. *D. shibae* was isolated from the benthic dinoflagellate *P. lima* which occurs, amongst others, in sand and sediment (Fukuyo, 1981). Additionally, nutrient rich areas are often low in oxygen. Therefore, *D. shibae* might be compelled into nitrate respiration due to various circumstances.

Nevertheless, the oxygen shut-down first leads to a distinct metabolic crisis. Due to the removal of oxygen, the respiratory chain stagnates. This leads to a hampered oxidative phosphorylation and thus also ATP formation, which could be proven by the metabolic analyses. Concomitantly, the transfer of electrons of the reducing equivalents NAD(P)H to enzymes of the respiratory chain is suppressed. ATP and reducing equivalents are essential for several reactions of cells. The ATP lack induced energy crisis and the disturbed redox state dominate the metabolic responses of *D. shibae*. This is revealed primarily by the accumulation of most intermediates of the central metabolism. Interestingly, changes of the central metabolism were restricted to the metabolome. On the one hand this indicates that no basic adaptation of the central metabolism is needed for the transition to denitrification and on the other hand that the adaptation process of *D. shibae* is very target-oriented towards nitrate respiration.

However, during the establishment of the denitrification apparatus *D. shibae* shows several responses to overcome the disturbed redox state. Probably, $NADP^+$ is partly regenerated by the NADPH demanding formation of branched-chain amino acids indicated by their enormous accumulation. Additionally, NADH but mainly NADPH are most likely consumed by the formation of the storage compound PHB. This polymer has been shown to strongly accumulate throughout the entire adaptation process.

The changed abundance of amino acids and intermediates of the pentose phosphate pathway are mainly based on the interrupted cell proliferation. This resulted in accumulation of most amino acids as the energy demanding protein biosynthesis is hampered. In accordance, the probably reduced metabolic flux into the pentose phosphate pathway indicates a reduced formation of nucleotides and thus a reduced gene replication.

The proteome and transcriptome data support the observed metabolic changes as corresponding enzyme abundances and expression levels decrease in the first phase of adaptation.

Most of the described changes in the metabolome but also in the proteome and transcriptome reversed after the establishment of denitrification. As the physiological data suggest, and in particular the proteome data show, denitrification is first possible 60 min after the oxygen shut-down. This means, just 30 min after reaching the actual state of anoxia the metabolism starts to relax which was observed on all levels analysed.

4.2 Exposure to various salinity and nitrogen-limitation

4.2.1 Phenotypic MicroArray analysis

Phenotypic MicroArray was applied to test adaptation capabilities of *D. shibae* to various salts and to 6 % NaCl in combination with known osmolytes. This analysis was performed to gain overview of possibly growth promoting or inhibiting substances, respectively. Since only respiratory activity is monitored false positive results cannot be excluded.

Overall, respiration was tested under various NaCl concentrations ranging from 1 % to 10 %. Respiration was observed in a NaCl concentration range from 1 to 7 % and the putative best growth conditions for *D. shibae* elucidated by the microarray analysis are 4 - 5.5 % NaCl. The growth range is generally in accordance with the observations in batch cultures (section 3.3.3.1, Figure 24). Contrarily, in batch culture best growth was observed at a salinity of 2.3 % and cultivation at 5 % led to a clear growth inhibition, showing the discrepancy between respiration and growth. On the basis of the gained data, *D. shibae* can be assigned to slight halophilic organisms that show most rapid growth at 2 to 5 % NaCl. Extreme halophiles prefer 20 to 30 % NaCl (Ollivier *et al.*, 1994).

The respiration activity of *D. shibae* at 6 % NaCl was one of the strongest observed (Figure 19). Because of this, the additional growth promoting function of the supplied osmolytes in combination with 6 % NaCl cannot be confirmed or denied in most cases. Nevertheless, a promotion can be assumed for KCl in combination with 6 % NaCl as KCl led to an increased respiration. This is probably the result of the substitution of toxic

Na^+-ions with less toxic K^+-ions (Hagemann, 2011). This means that not only the absolute salt concentration but the composition of the salt is decisive, whereas the role of the anions is relatively minor (McCarty and McKinney, 1961). Interestingly, solely supplied KCl did not result in any respiration (D1-D4). Respiratory activity was reduced compared with pure NaCl when chloride was replaced by sulphate, lactate, phosphate, benzoate, nitrate or nitrite (Figure 19). Nitrite and benzoate are common preservatives utilised by the food industry as they are toxic for most bacteria, at least at a certain concentration (Barbour and Vincent, 1950; Roberts, 1975).

Surprisingly, the compatible solutes creatinine, carnitine and trigonelline seem to inhibit the respiration of *D. shibae*. As has been shown by Chambers *et al.* (1999), trigonelline did not improve the growth of *E. coli* under hypertonic conditions and an interference of trigonelline with cell function was assumed (Chambers *et al.*, 1999). Additionally, trigonelline and other betaines inhibit trehalose synthesis (Giæver *et al.*, 1988a; Chambers *et al.*, 1999). As the enzymes for trehalose and α-glucosylglycerol synthesis are closely related, the inhibition of α-glucosylglycerol formation by these compounds is possible. Consequently, respiration at 6 % NaCl with additional supplied trigenolline is possibly inhibited, since the batch culture experiments indicated the necessity to form α-glucosylglycerol at least from 3.5 % salinity (section 3.3.3.2, Figure 25). Similar could be true for the betaine carnitine.

D. shibae is assumed to require a minimal salt concentration ((Biebl and Wagner-Döbler, 2006) and following sections). Obviously, uncharged substances such as urea are not suitable to replace ions, whereas ethylene glycol led to a slight respiratory activity. Otherwise, urea, which can pass the cell by uncontrolled passive diffusion, is known to stress cells and exerts a greater antibacterial effect than equimolar concentrations of *e.g.* NaCl (Kaye, 1968; Randall *et al.*, 1996).

Overall, this analysis revealed that *D. shibae* is well adapted to its natural environment, as cultivation with NaCl, the most abundant salt in the oceans (Sommer, 2005), was the most suitable salt for respiratory activity as indicator for growth. Other salts investigated here are present in marine habitats, but are assumed to play a minor role for osmoregulation of *D. shibae* in its natural environment.

4.2.2 Salt shock

D. shibae was exposed to a NaCl-shock to trigger a strong osmoregulative response. Conducted metabolome and transcriptome analyses should unravel key elements for osmoprotection. In this context, the three highly abundant substances glutamate, α-glucosylglycerol and α-glucosylglycerate were examined more closely, as their high concentrations indicate an important role in the metabolism of *D. shibae.* In particular, glutamate is known as compatible solute in various bacteria (Tempest *et al.*, 1970; Measures, 1975; Makemson and Hastings, 1979; Botsford, 1984) and serves primarily as a counter-ion for intracellular cations (Csonka, 1989; Goude *et al.*, 2004).

The initiated salt shock from 2.3 to 5 % salinity affected the growth of *D. shibae* only slightly (Figure 20). Indeed, the growth was interrupted for about 30 min but continued almost undiminished again and the same OD_{max} compared with untreated cultures was achieved. The spontaneous increase of the extracellular salinity causes an enormous influx of ions into the cells. Biochemical functions rely on specific inorganic ions. However, when a certain concentration is exceeded, these functions can disrupt as salts affect the catalytic rate and the Michaelis constant of enzymes (Yancey *et al.*, 1982). Without a fully functional metabolism, biochemical processes and thus replication are strongly affected. This has been shown for *Lactococcus lactis*, which continued growth but with a clearly reduced growth rate and OD_{max} after a salt shock, indicating the absence of an effective adaptation capability to such conditions (Kilstrup *et al.*, 1997). Contrarily to this, *D. shibae* is obviously able to overcome the crisis caused by the salt shock after a certain time of adaptation, which is discussed detailed in the following sections.

4.2.2.1 Salt shock induced metabolic changes

After the salt shock, several metabolic changes became obvious. In extracts of the reference cultures (continuously cultivated at 2.3 % salinity), glutamate was detected in a high concentration, whereas α-glucosylglycerol and α-glucosylglycerate were not detected (Figure 21). However, just 10 min after the shock α-glucosylglycerol was detected in salt treated cultures and after further 80 min additionally α-glucosylglycerate (Figure 21).

α-Glucosylglycerol is known to be a dominant compatible solute in cyanobacteria (marine and non-marine), but has also been found in heterotrophic genera as

Stenotrophomonas and *Pseudomonas* (Pocard *et al.*, 1994; Mikkat *et al.*, 2000; Roder *et al.*, 2005; Hagemann *et al.*, 2008; Hagemann, 2011) and even in the plant *Myrothamnus flabellifolia* and the fungus *Aspergillus oryzae* (Bianchi *et al.*, 1993; Takenaka and Uchiyama, 2000). One family member of *D. shibae*, *R. sulfidophilum* DSM 1374 was reported to exhibit α-glucosylglycerol (Severin *et al.*, 1992). In *Synechocystis* sp. PCC 6803, α-glucosylglycerol is synthesised in a two-step reaction starting from glycerol-3-phosphate and ADP-glucose via the intermediate glucosylglycerol phosphate (Hagemann and Erdmann, 1994).

Equivalently, α-glucosylglycerate is formed with 3-phosphoglycerate as a precursor and either ADP- or UDP-glucose (Costa *et al.*, 2006, 2007). α-Glucosylglycerate has been found in cyano- and γ-proteobacteria, the archaeon *Methanohalophilus portucalensis*, the aquificae *Persephonella marina* and recently in the plant *Selaginella moellendorffii* (Robertson *et al.*, 1992; Cánovas *et al.*, 1999; Goude *et al.*, 2004; Costa *et al.*, 2007; Empadinhas and da Costa, 2008; Nobre *et al.*, 2012). Accordingly, this study provides the first experimental evidence of the occurrence of α-glucosylglycerate in *D. shibae*, and thus in the class of α-proteobacteria. In some cases, the function of α-glucosylglycerate as compatible solute has been shown (Kollman *et al.*, 1979; Goude *et al.*, 2004; Klähn *et al.*, 2010).

The genomic capacity of *D. shibae* to form α-glucosylglycerol and α-glucosylglycerate is described in section 3.2. Since enzymes for the synthesis of ADP-glucose are not annotated for *D. shibae*, the organism probably uses UDP-glucose as precursor for α-glucosylglycerol and α-glucosylglycerate. This agreed with the upregulation of GalU (Dshi_3577), UTP-glucose-1-phosphate uridylyltransferase and in the same operon a glucosyl transferase family 1 protein (Dshi_3578) after the salt shock. On the basis of the newly identified substances α-glucosylglycerol and α-glucosylglycerate in *D. shibae*, a comparative genomics study within the family *Rhodobacteraceae* in cooperation with Marcus Ulbrich (BIBC, TU Braunschweig) was conducted. This study revealed that the synthesis of these substances is restricted to marine *Rhodobacteraceae*. Out of 101 marine *Rhodobacteraceae*, 16 organisms were predicted to be capable to form α-glucosylglycerol, 41 organisms to form α-glucosylglycerate and 9 organisms were capable to form both. Some genera lacked both synthesis pathways (Kleist *et al.*, 2016).

During the shift to increased salinity, α-glucosylglycerate played a minor role for *D. shibae*, unlike α-glucosylglycerol which increased throughout the cultivation to a biomass concentration of 2 %, supporting its role as compatible solute. As α-glucosylglycerol was detected immediately after the shock, enzymes for its biosynthesis had to be present already under reference conditions. Additionally, transcript levels of genes encoding glucosylglycerol-phosphate synthase (GpgS) and glucosylglycerol 3-phosphatase (GpgP) were strongly increased 10 and still 90 min after the salt shock (Table 11). Supportingly, an immediate α-glucosylglycerol formation due to an osmotic shock was reported before for *Synechocystis* sp. PCC 6803 (Hagemann and Erdmann, 1994), in which a basal level of glucosylglycerol-phosphate synthase (GgpS) was detected in later studies (Marin *et al.*, 2002). Meanwhile it is known, that activation of GgpS and GgpP proceeds via formation of a complex that is induced in direct correlation to increasing ion strength (Hagemann and Erdmann, 1994; Schoor *et al.*, 1999; Stirnberg *et al.*, 2007). Whether the described activation is transferable to *D. shibae* is unclear. In the genome of *D. shibae*, GgpS and GgpP are organised in one operon along with a glycerol-3-phosphate dehydrogenase (Dshi_3830), contrary to the according genes of cyanobacteria (Hagemann *et al.*, 1997). Bacteria of the family *Pseudomonadaceae*, capable of α-glucosylglycerol synthesis, possess one single gene encoding GgpPS (combines GgpS and GgpP) (Hagemann *et al.*, 2008; Klähn *et al.*, 2009). GgpPS has been shown to form α-glucosylglycerol in one step (Hagemann *et al.*, 2008). GgpS and GgpP of *D. shibae* showed high similarities to GgpPS genes of *Pseudomonadaceae* (Table 8), only the number of genes differs. Hence, apart form activation by ion-induced formation of a complex also an already present complex, comparable with GgpPS, is possible for *D. shibae*.

Concerning further metabolic changes, 10 min after the salt shock mainly amino acids were regulated. Most of the amino acids accumulated at this time point (Table 9, Figure 22). Immediately after the applied salt shock, the cells were exposed to massive inflow of ions. Because of this, essential processes such as the protein biosynthesis possibly were hampered as indicated by the short growth interruption (Figure 20). First, when sodium ions are exchanged by potassium ions and when further adaptive processes were applied, basic cell mechanisms can start again. Therefore, the observed accumulation is possibly the result of a short-term interrupted protein biosynthesis. Besides, the entire amino acid pool

seems to be affected by the osmolarity of the medium as have been shown for several bacteria, in which generally the amino acid pool increased with increasing osmolarity (Tempest *et al.*, 1970; Killham and Firestone, 1984). However, some amino acids particularly the charged amino acids glutamate, aspartate and lysine were less abundant after the salt shock in *D. shibae* cell extracts (Table 9, Figure 22). A lower concentration of glutamate and aspartate due to increasing salinity was also observed for two *Streptomycetes* (Killham and Firestone, 1984). The reason for this observation is still unclear. In addition to the changed amino acid concentrations, 4-aminobutanoate was only detected in cultures after salt shock (Figure 22). 4-aminobutanoate is assumed to be a compatible solute in some bacteria (Measures, 1975; Csonka, 1989; Shelp *et al.*, 1999). Thus, this role is also assumed for *D. shibae*, although it has possibly only a limited influence because of the low concentration detected.

90 min after the salt shock, the concentrations of most amino acids had returned to levels, similar to the reference culture (Table 9, Figure 22). Otherwise, the α-glucosylglycerol precursors glucose and glycerol-3-phosphate and α-glucosylglycerol associated unknown substances were increased (Table 9, Figure 22). Therefore, the adaptation processes of *D. shibae* needed to overcome the changed salinity were mainly limited towards the α-glucosylglycerol formation. This underlines the key role of this compatible solute.

4.2.2.2 Salt shock induced transcriptional changes

The transcriptional analysis of *D. shibae* after a salt shock revealed an important role of the 153 kb chromid in osmoregulation. 42 % of the chromid genes were upregulated 10 min after the shock and 23 % of these genes were still upregulated 90 min after the shock (Table 10). The chromid carries numerous genes encoding transporters and channels, the genes for α-glucosylglycerol biosynthesis (Dshi_3830-3832) as well as some genes encoding hypothetical proteins, whose transcripts were upregulated. Furthermore, the histidine kinase located on the 153 kb chromid was strongly upregulated (Table 11). For *Synechocystis* sp. PCC 6803, histidine kinases are known to regulate the expression of many salt-inducible genes (Marin *et al.*, 2003). In general, the 153 kb chromid is obviously essential for the survival of *D. shibae* in the marine environment. Thus, in this study a extrachromosomal element of *D. shibae* could be assigned a certain function. Recently,

three further extrachromosomal elements of the organism were assigned to certain functions. The 72 kb chromid has been shown to play an essential role during starvation while applying a light/dark cycle (Soora *et al.*, 2015) and the 86 and 191 kb plasmids have been shown to be crucial for anaerobic growth (Ebert *et al.*, 2013). Moreover, curing of the 191 kb plasmid led to the loss of the ability to kill the algal host (Wang *et al.*, 2015).

As expected and previously mentioned, the genes encoding the enzymes for α-glucosylglycerol biosynthesis – glucosylglycerol-phosphate synthase and glucosylglycerol-3-phosphatase - were strongly upregulated immediately after the shock, as well as genes encoding enzymes for the synthesis of glyceraldehyde-3-phosphate and glycerol-3-phosphate (Figure 23). Glyceraldehyde-3-phosphate is the precursor for glycerol-3-phosphate which is directly utilised for α-glucosylglycerol biosynthesis. Since succinate was used as the sole carbon source in this study, an upregulation of gluconeogenesis would be expected in order to increase the formation of the α-glucosylglycerol precursor glucose. However, only the enzymes of the Entner-Doudoroff pathway were upregulated (Figure 23). This pathway consumes glucose, but produces glyceraldehyde-3-phosphate, to be utilised again for glucose or glycerol-3-phosphate formation. Due to the upregulation of the Entner-Doudoroff pathway, a kind of production cycle for the educts of α-glucosylglycerol seems to be present. In accordance, the transcriptional regulations were reflected by the corresponding metabolic changes as glucose (fold-change 5.2) and glycerol-3-phosphate (fold-change 2.1) were increased 90 min after the salt shock (Table 9). Also the increased α-glucosylglycerol concentration together with α-glucosylglycerol associated substances (GG associated 1 and 2) correlates with the observed transcriptional changes (Table 9).

In addition, at least seven genes encoding known general stress proteins were upregulated throughout the experiment. The gene transcripts of the two chaperones *clpB* (Dshi_0617) and Dshi_2892, encoding the small heat shock (HSP20) protein, were still increased 90 min after the salt shock (Table 11). Since chaperones assist in the correct folding of proteins or mediate the disaggregation of stress-damaged proteins (Parsell *et al.*, 1994) they are common stress responses, also to osmotic stress. Further chaperones of *D. shibae* were not strongly regulated on the transcriptional level, but had generally high expression values (e.g. *groEL, groES, dnaJ* and *dnaK*). In particular, GroEL and GroES

have been shown to be upregulated under osmotic stress conditions in some bacteria (Kilstrup *et al.*, 1997; Fulda *et al.*, 2006).

Furthermore, transcripts of two ferritin Dps family proteins and a ferritin-like protein were strongly upregulated (Table 11). Dps is known to protect against oxidative stress, nucleases and other stressful conditions including osmostress (Weber *et al.*, 2006; Zhang *et al.*, 2010). Dps interacts with DNA and leads to an excellent protection of the DNA regarding several environmental stresses (Wolf *et al.*, 1999). In the case of *D. shibae*, a strong imbalance regarding intracellular ions including the Mg^{2+}-concentration has to be assumed after the salt shock. Mg^{2+}-ions are known to protect several macromolecules and in particular DNA (Hartwig, 2001). Thus, Dps can be used to counteract such effects. Additionally, gene transcripts of a glutathione-S-transferase were upregulated (Table 11). Glutathione-S-transferases can be part of detoxifying processes and were reported to play a role during exposure to oxidative stress (Penninckx, 2000; Vuilleumier and Pagni, 2002). Its function and whether the upregulation in *D. shibae* is salt specific remains unclear. Also the transcriptionally increased Csb family protein (Table 11) is known as a general bacterial stress response, but its role in salt stress is yet unclear (Prágai and Harwood, 2002).

The strongest salt-specific regulations in *D. shibae* concern transporters and channels, especially 10 min after the salt shock. In particular, transcripts of mechanosensitive channels, proteins of the family solute/sodium symporter and of the multi anti extrusion protein MatE were strongly upregulated or reliably detected under shock conditions only (Table 11). By this, the cells reacted to the rapidly changed conditions including *e.g.* water efflux, changed turgor pressure and ion concentrations. The crucial role of transporters has also been shown in other studies of several organisms, such as *Bacillus subtilis*, *E. coli* and *Synechocystis* sp. PCC 6803 (Fulda *et al.*, 2006; Hahne *et al.*, 2010; Marin *et al.*, 2004; Roeßler and Müller, 2001).

An upregulation of t-RNAs was observed which implies the expected increase in protein biosynthesis during the adaptation process.

Overall, the transcriptional responses after the salt shock could be classified in three groups. Firstly, a general stress response was observed with particularly upregulated chaperones probably to protect existing macromolecules or to support their formation. Secondly, the synthesis of α-glucosylglycerol and its precursors were upregulated which

was supported by the metabolome data. Lastly, several import and export systems were regulated as response to the rapid influx of sodium ions. In most cases, the described regulations were observed only at the sample time point 10 min. Thus, some changes probably did not influence the actual protein equipment but were a kind of transcriptional overreaction. Genes belonging to the group two and three are to a large extent located on the 153 kb chromid indicating the essential role of chromid in osmoregulation.

4.2.3 Influence of salinity on the metabolome of long-term adapted cells

Several parameters influence the composition of the oceans leading to partly extreme regional diversity. One of these parameters is the salinity which differs, for example, between the open sea and estuary areas or is influenced by the seasons (Reul *et al.*, 2014). With respect to this, the metabolome of *D. shibae* was investigated under various salinities in its exponential growth phase and at OD_{max} to unravel the impact of the ambient salt concentration. The salt concentrations investigated ranged from 0.3 % to 5 % salinity simulating conditions from brackish water to strongly increased salt concentrations. The average salinity of 3.5 % of the oceans was used as reference. Again, glutamate, α-glucosylglycerol and α-glucosylglycerate were examined more closely, because of their putative strong impact on the metabolism of *D. shibae*.

The growth behaviour of *D. shibae* was clearly affected by the salinity but had little impact on the OD_{max} values (Figure 24). Best growth occurred in medium with 2.3 % salinity while 3.5 % salinity led to a comparable growth rate with an extended lag-phase. Slowest growth (lag phase and growth rate) occurred at 0.3 % salinity. The low salt concentration enabled growth, but apparently a higher salt concentration promotes growth. Contrarily, Biebl *et al.* (2005) determined 1 % salinity as lower limit for *D. shibae*, but in this study cultivation occurred in complex medium. At a salinity exceeding natural concentrations, the growth rate was reduced and the lag-phase was prolonged because of the required longer adaptation. Concerning the unchanged OD_{max}, according results were obtained for the marine *R. sulfidophilum* P5 tested in a salt concentration range from 0 to 7 % (Cai *et al.*, 2012). Soil bacteria of the genus *Streptomyces* showed a decreased growth rate and OD_{max} with rising NaCl concentration (Killham and Firestone, 1984), suggesting a

more efficient response to a saline environment of the marine organisms *D. shibae* and *R. sulfidophilum* P5.

Focussing on the metabolic adaptation to various salinities, the biomass concentration of the sum of the three substances glutamate, α-glucosylglycerol and α-glucosylglycerate was remarkable. In maximum 7.6 % of CDW were observed in the exponential phase at 5 % salinity (Figure 25). Otherwise, several soil bacteria also have extreme high concentrations of amino acids in particular glutamate and proline. *Streptomycetes*, indigenous to saline soil, have been reported to accumulate amino acids up to a biomass concentration of 22 % (total amount computed as share of glutamate) by initiating salt stress (Killham and Firestone, 1984), salt stressed *Corynebacterium glutamicum* accumulated proline, glutamate and trehalose to a biomass concentration of 25 % (Guillouet and Engasser, 1995) and salt stressed *Aerobacter aerogenes* contained about 8 % glutamate (Tempest *et al.*, 1970). The α-glucosylglycerate forming organism, *Erwinia chrysanthemi* has been shown to contain 19.9 % of glutamate, glutamine and α-glucosylglycerate (Goude *et al.*, 2004). With respect to this, the accumulation of glutamate, α-glucosylglycerol and α-glucosylglycerate by *D. shibae* seems rather moderate.

4.2.3.1 Glutamate, α-glucosylglycerol and α-glucosylglycerate

In the exponential growth phase of *D. shibae*, glutamate was detected exclusively at conditions comparable with brackish water (0.3-2.3 % salinity). From salt concentrations equating natural conditions, additionally α-glucosylglycerol and α-glucosylglycerate were detected (Figure 25). This indicate that glutamate is used as the first choice counter-ion by *D. shibae*, providing that a surplus of nutrients is available. When a certain threshold value of salt is reached, additional compatible solutes other than glutamate are needed. Hence, α-glucosylglycerol is formed by *D. shibae*. The accessory osmolyte α-glucosylglycerol leads to an improved salt tolerance as has been shown before, for example, for *Synechocystis* sp. PCC 6803 and its Δ*ggpS* (glucosylglycerol-phosphate synthase) mutant. The loss of *ggpS* led to a reduced salt tolerance of around 40 % (Ferjani *et al.*, 2003). Even the salt tolerance of the plant *Arabidopsis thaliana* can be improved by transferring a *ggpPS* gene into its genome (Klähn *et al.*, 2009) and two organisms of the bacterial genus *Stenotrophomonas* showed different salt tolerances depending on their ability to form α-glucosylglycerol (Roder *et al.*, 2005).

As protein biosynthesis is strongly reduced at OD_{max}, the requirement of the usually indispensable glutamate as the nitrogen donor for amino acid biosynthesis and as a protein component is much smaller. Nevertheless, a sufficient turgor pressure must be maintained. Therefore, *D. shibae* is compelled to replace glutamate. This is done mainly by α-glucosylglycerate (Figure 25). The α-glucosylglycerol concentration was hardly affected by the growth phase. Thus, no correlation between α-glucosylglycerol and the growth phase is assumed. Contrarily, α-glucosylglycerate formation is obviously affected by the growth phase in combination with the α-glucosylglycerol concentration. In general, α-glucosylglycerate occurs with the entry into stationary phase but the present concentration of α-glucosylglycerol influences its accumulation (Figure 25). Hence, α-glucosylglycerate accumulation is strongest under moderate salt conditions when exclusively glutamate is used as compatible solute in the exponential phase (Figure 25). To maintain the necessary turgor pressure in the stationary phase, α-glucosylglycerol and α-glucosylglycerate are used. This indicates that glutamate can partly be replaced by the uncharged α-glucosylglycerol.

An increased concentration of α-glucosylglycerate in the stationary phase was also reported for *Halomonas elongata* (Cánovas *et al.*, 1999). In *E. chrysanthemi* 3937, α-glucosylglycerate becomes the most abundant osmolyte in stationary phase but unlike observations made in *D. shibae*, its concentration continuously increases throughout growth (Goude *et al.*, 2004). Such an accumulation of osmotically active substances during the transition into stationary growth has also been reported for trehalose in *E. coli* (Hengge-Aronis *et al.*, 1991), which uses the disaccharid as an osmolyte (Giæver *et al.*, 1988b). However, in the case of trehalose not only the potential function as compatible solute but also the function as a storage compound has to be considered. The trehalose reservoir can be used to maintain essential cell functions in times of starvation.

4.2.3.2 Influence of salinity on the metabolome

0.3 % salinity compared with 3.5 % reference: An unexpected and interesting result of this study was the strongly increased level of putrescine in *D.* shibae cells cultivated in low-salt medium (0.3 % salts, Table 12). Polyamines such as putrescine, spermidine or spermine are known to be used to stabilise negatively charged macromolecules such as DNA, tRNA and ribosomes, partly as a replacement for the cation Mg^{2+} (Ohtaka and

Uchida, 1963; Tabor and Tabor, 1976; Bachrach, 2005), and to influence interactions between proteins and nucleic acids (Record Jr *et al.*, 1998). Under low osmolarity conditions, *E. coli* also exhibits an increased putrescine concentration (Munro and Bell, 1973). In *Pasteurella tularensis*, polyamine content has been reported to be reduced with increasing medium osmolarity (Mager, 1955). Additionally, for *E. coli* the essential role of putrescine^{2+} in protein-nucleic acid interaction has been shown under low osmolarity (Capp *et al.*, 1996). The low osmopressure at 0.3 % salinity leads to a lower intracellular salt concentration and probably, putrescine partly takes the role of K^+ and Mg^{2+}. Thus, putrescine is accumulated to guarantee the functionality of macromolecules and their interactions. In accordance, the putrescine concentration of *D. shibae* cells decreased almost proportional with increase of the salinity of the medium in the exponential phase of cells (Table 12). This context suggests that the intracellular putrescine concentration is probably influenced by the medium salinity, at least to a certain extent. The data suggest that putrescine is a further compatible solute for *D. shibae* only to compensate low instead of high osmolarity.

In addition, putrescine can potentially be used as a nitrogen-store. *D. shibae* has several enzymes with an aminotransferase class III domain and is therefore probably able to regenerate glutamate quickly by the transfer of an amino group to 2-oxoglutarate. In the case of a rapid change of salinity, glutamate would immediately be available as osmoprotectant and as a nitrogen donor.

Beside putrescine, the high concentration of the fatty acid vaccenic acid in combination with 3-phosphoglycerol is notable (Table 12). Possibly, adaptations of the cell membrane are necessary under these conditions, achieved by changes in lipid or phospholipid composition. Further analyses of cell wall or lipid composition are needed, which were beyond the scope of this study.

In general, all amino acids showed a clearly decreased abundance compared with the reference (Table 12). As discussed previously, the entire amino acid pool seems to be affected by the osmolarity of the medium as has been shown for several bacteria (Tempest *et al.*, 1970; Killham and Firestone, 1984). Accordingly, the reduced amino acid pool of *D. shibae* supports these studies. At OD_{max} this effect was more extreme. Here the cell proliferation is strongly reduced and thus the protein biosynthesis indicated by the low

abundance of amino acids. In accordance, low concentrations of most metabolites in the stationary phase has been shown for *P. inhibens* (Hensler, 2015).

2.3 % and 5 % salinity compared with 3.5 % reference: Few changes were observed between exponentially growing cells at 2.3 %, 5 % and 3.5 % salinity (Table 12). Contrary to 0.3 % salinity, this indicates that only slight metabolic adaptations between the saline conditions are needed apart from the observed changes in the glutamate, α-glucosylglycerol and α-glucosylglycerate concentrations. Hence, these are the essential substances for coping with various salinities.

However, great differences were observed at OD_{max} of cells cultivated at 5 % salinity. Some amino acids and putrescine are strongly increased in abundance. Probably, the high osmolarity of the medium hampers a decrease of amino acids as discussed. In particular, the amount of charged amino acids aspartate and lysine as well as the charged putrescine are increased, indicating a potential function of balancing present ions.

4.2.4 Nitrogen-limitation

As shown in the experiments discussed previously, glutamate plays an essential role for the osmoregulation of *D. shibae*. Glutamate and many widespread osmolytes are nitrogen-containing substances, such as other amino acids or betaines. Because of this, *D. shibae* was exposed to nitrogen limitation simulating nitrogen poor regions or seasons. Thereby, it was tested if the organism has a suitable answer to the high salt concentration (3.5 % salinity) together with nitrogen-limitation.

The nitrogen-limitation of *D. shibae* resulted in changed growth behaviour (Figure 26). In the first 10 h of cultivation, growth was similar to the reference culture, but afterwards the limitation got obvious. The otherwise observed exponential growth of *D. shibae* was not true for the limited culture and OD_{max} was clearly reduced and the time needed to reach it was prolonged. Such impact on growth was expected as nitrogen is important for protein formation which is essential for replication and biomass production.

The concentrations of glutamate and α-glucosylglycerate showed remarkable changes compared with unlimited cultures, whereas α-glucosylglycerol is obviously unaffected by the nitrogen supply. Glutamate decreased 25-fold and contrarily α-glucosylglycerate increased 259-fold compared with reference conditions (Figure 27A). This suggest that

α-glucosylglycerate is an essential and adequate substituent for the nitrogen-containing glutamate under these conditions. As mentioned previously, the osmoregulation by glutamate is based on its negative charge and thus cations can be balanced. The same is probably true for α-glucosylglycerate which is therefore formed when the glutamate concentration is not sufficient for balancing intracellular cations. The nitrogen dependence of α-glucosylglycerate formation has also been shown for the soil bacterium *Erwinia chrysanthemi*, which accumulated α-glucosylglycerate up to a biomass concentration of 26.8 % (Goude *et al.*, 2004) unlike *D.* shibae whose α-glucosylglycerate level was 1.7 %. Furthermore, several cyanobacteria increase their α-glucosylglycerate concentration under nitrogen-limited conditions (Kollman *et al.*, 1979; Klähn *et al.*, 2010b), whereas other organisms are not known to use α-glucosylglycerate as a compatible solute at all (Robertson *et al.*, 1992; Cánovas *et al.*, 1999). In the latter cases, the function of α-glucosylglycerate is not clarified, yet. By using α-glucosylglycerate, *D. shibae* maintains a cellular turgor pressure, which guarantees not only survival but growth, although to a lesser extent (Figure 26). The marine environment is a nitrogen-poor environment for non N_2-fixing bacteria (Vitousek and Howarth, 1991; Rivkin and Anderson, 1997). To a certain extent, the algae-associated *D. shibae* is certainly relying on organic nitrogen sources that are released during a collapse of algal blooms (Baines and Pace, 1991) or on direct exchange during its symbiosis with algae (Wagner-Döbler *et al.*, 2010; Wang *et al.*, 2014). Nevertheless, a nitrogen-independent strategy for osmoregulation is a strong advantage for survival.

Generally, the metabolome of *D. shibae* under nitrogen-limitation agreed with expectations. Striking was the at least 7.7-fold reduced concentrations of nitrogen-containing substances, except for tyrosine (Table 13). The decrease of nitrogen-containing substances is a result of the limited nitrogen supply. Under these conditions, *D. shibae* uses probably the energy demanding glutamine synthetase glutamine:2-oxoglutarate amidotransferase system due to the limitation as has been reported for *C. glutamicum* (Beckers *et al.*, 2001). In accordance, 2-oxoglutarate concentration was slightly increased (1.7-fold, appendix A4). 2-oxoglutarate is used by *D. shibae* for ammonia assimilation by the glutamate synthase. Consequently, the limited nitrogen supply led to an accumulation of 2-oxoglutarate. The concentration of succinate (provided as carbon source) was unaffected, in contrast to the remaining TCA cycle intermediates, which were strongly

decreased (Table 13). The downregulated TCA cycle is most likely a consequence of the strongly slowed growth (Figure 26), hence the metabolism is slowed down and the requirement of reducing equivalents is reduced. An increase of 2-oxoglutarate and the reduction of nitrogen-containing substances due to nitrogen-limitation has also been shown for the Roseobacter *Phaeobacter inhibens* and the yeast S*chizosaccharomyces pombe* (Sajiki *et al.*, 2013; Hensler, 2015).

The enzymes are the basic tools for the efficiency and productivity of cells. Due to the decreased nitrogen supply, the organism is compelled to work with a reduced number of tools. This circumstance is mirrored by the changes in the metabolism and the strongly affected growth (Figure 26). Without the capability to form α-glucosylglycerate, *D. shibae* probably would not be able to replicate or even to survive in its natural saline environment concomitantly with nitrogen limitation. Consequently, the salt tolerance would be strongly affected. This shows the complexity of the interplay of several parameters as nutrient and stress tolerance. Only a few studies investigated such interactions, thus, for instance a reduced temperature sensitivity of the marine bacterium *Halomonas hydrothermalis* has been shown during iron starvation (Harrison *et al.*, 2015) and a certain salinity promoted the growth rate under low temperatures and high hydrostatic-pressures of further *Halomonas* strains (Kaye and Baross, 2004).

4.2.5 Influence of salinity and C/N ratio on the PHB formation

PHB is a widespread storage compound in bacteria. The influence of carbon sources, energy metabolism and various nutrient limitations on PHB formation has been shown for several bacteria (Wang and Lee, 1997; Shi *et al.*, 2006; Xiao and Jiao, 2011; Cai *et al.*, 2012). The data presented here, give insight how PHB formation is influenced by extracellular salt concentrations, growth phase and the C/N ratio of the medium.

PHB formation of *D. shibae* is hardly affected by the salt concentration of the medium, although a slight increasing tendency with increasing salinity could be assumed (Figure 27). The PHB biomass concentration ranges between 20 and 30 % in the exponential growth phase of the organism. Only at 0.3 % salinity the PHB content is clearly reduced to 8.6 %. The determined values are in good accordance with the previously published PHB biomass concentration of 24.7 % in *D. shibae* under succinate feeding conditions (salinity

2.3 %) in its exponential growth phase (Rex *et al.*, 2013). *R. sulfidophilum* P5 and *Paracoccus denitrificans* were investigated regarding their PHB biomass concentration at various NaCl concentrations. Both organisms belong to the family of *Rhodobacteraceae*. *R. sulfidophilum* was analysed in a salt range from 0 to 7 % NaCl and the PHB concentration increased slightly from 0 to 2 % NaCl and decreased again reaching a minimum at 7 % NaCl (Chien *et al.*, 2007; Mothes *et al.*, 2007; Cai *et al.*, 2012). The PHB concentration of *P. denitrificans*, during the exposure to nitrogen limitation, was constant in a NaCl range from 0 of 5 % and decreased with higher NaCl concentrations (Mothes *et al.*, 2007). Furthermore, marine bacteria of the genus *Vibrio* were analysed in a salt concentration range from 0 to 4 %, but the impact of salt concentration differed between the organisms tested (Chien *et al.*, 2007). On the basis of these information, the influence of the NaCl concentration on PHB seems to be arbitrarily. This suggests, that NaCl has rather a direct impact on the organism and its metabolism, but not on PHB formation.

By trend, the PHB biomass concentration of *D. shibae* was increased at OD_{max} (Figure 27). This is in accordance with a continuous PHB formation throughout the active growth of the both *Rhodobacteraceae*, *Dinoroseobacter* sp. JL 1447 and *R. sulfidophilum* P5. In both cases PHB consumption started during entry into stationary phase (Cai *et al.*, 2012; Xiao *et al.*, 2015). By recycling of PHB, cell functionality during stationary phase can be maintained. Probably this is happening *D. shibae*, too.

Under standard cultivation conditions, the initial C/N ratio of cells grown in SWM was 14.4, which was increased to 67.7 in the nitrogen-limitation experiment. Thus, the PHB biomass concentration increased 2.4-fold to a total amount of 57.4 % (Figure 27). For *Dinoroseobacter* sp. JL1447 even a maximal PHB yield of 72.3 % was determined, but under different conditions (Xiao and Jiao, 2011). In general, nitrogen-limitation is used for the induction of an increased PHB for some biotechnological relevant organisms as the *Rhodobacteraceae P. denitrificans* and *Roseobacter denitrificans* OCh 114, but also *e.g. Pseudomonas putida* KT2442 (Wang and Lee, 1997; Mothes *et al.*, 2007; Xiao and Jiao, 2011; Poblete-Castro *et al.*, 2012). Due to the nitrogen-limitation, the biomass production of *D. shibae* is strongly restricted (Figure 26). Instead, formation of the nitrogen-free PHB as store of carbon is induced, a beneficial mechanism for *D. shibae* in times of famine.

4.2.6 Conclusion

D. shibae is ideally prepared to deal with salinity changes and nitrogen limitation. However, as revealed by the phenotypic microarray experiment, it is in particular optimised to NaCl. Overall, the organism uses glutamate, α-glucosylglycerol, α-glucosylglycerate and putrescine to confront osmotic stress. Putrescine is assumed to be used under hypo-osmotic conditions to protect macromolecules and guarantee their functionality as the putrescine concentration was strongly increased at 0.3 % salinity. Otherwise, glutamate is the first choice compatible solute for osmoregulation. Under more challenging salt concentrations, additionally α-glucosylglycerol is used, which has been shown clearly with the salt shock experiment and with the metabolome analysis of long-term adapted cells. Besides, these results suggest that the adjustment of glutamate and α-glucosylglycerol is sufficient for the salt regulation of *D. shibae*. Additionally, the immediate formation of α-glucosylglycerol after the salt shock revealed that the organism is well prepared to react to rapid changing salinity. Hence, the transition to the new salinity was completed within 30 min as indicated by the growth observations (Figure 20). Similar to the transition to anoxic conditions (section 4.1) the adaptation process was very fast and specific which was supported by the transcriptional analysis. Additionally, this analysis revealed the essential role of the 153 kb chromid in adaptation to changing salinity. This chromid carries genes for the α-glucosylglycerol formation and several exchange systems and thus is essential for the regulation of the ion balance in cell.

The formation of α-glucosylglycerate, which was found here for the first time within the α-proteobacteria class, is linked to special conditions. During nitrogen limitation, α-glucosylglycerate replaced the nitrogen-containing glutamate as counter-ion for cations and guarantees an adequate turgor pressure of the cells. Carbon source not used for cell proliferation under nitrogen limitation was stored as PHB to avoid the waste of carbon. Since *D. shibae* is probably relying on nitrogen sources supplied by its algal host, the formation of α-glucosylglycerate represents a survival strategy independent of algal blooms.

The strategy of *D. shibae* of using α-glucosylglycerol and α-glucosylglycerate to deal with changing salinity and nitrogen limitation is probably transferable to some further marine *Rhodobacteraceae*, as has been shown in the cooperative study with Marcus

Ulbrich (Kleist *et al.*, 2016). Other marine *Rhodobacteraceae* might developed alternative strategies. This result highlights again the diversity of the marine *Rhodobacteraceae*.

References

Adams, M. (1999) Simultaneous determination by capillary gas chromatography of organic acids, sugars, and sugar alcohols in plant tissue extracts as their trimethylsilyl derivatives. *Anal. Biochem.* **266**: 77–84.

Alavi, M.R. (2003) Predator/prey interaction between *Pfiesteria piscicida* and *Rhodomonas* mediated by a marine alpha proteobacterium. *Microb. Ecol.* **47**: 48–58.

Allgaier, M., Uphoff, H., Felske, A., and Wagner-Döbler, I. (2003) Aerobic anoxygenic photosynthesis in *Roseobacter* clade bacteria from diverse marine habitats. *Appl. Environ. Microbiol.* **69**: 5051–5059.

Appeltans, W., Ahyong, S.T., Anderson, G., Angel, M.V., Artois, T., Bailly, N., et al. (2012) The magnitude of global marine species diversity. *Curr. Biol.* **22**: 2189–2202.

Bachrach, U. (2005) Naturally occurring polyamines: interaction with macromolecules. *Curr. Protein Pept. Sci.* **6**: 559–566.

Baines, S.B. and Pace, M.L. (1991) The production of dissolved organic matter by phytoplankton and its importance to bacteria: Patterns across marine and freshwater systems. *Limnol. Oceanogr.* **36**: 1078–1090.

Barbour, R.G.H. and Vincent, J.M. (1950) The bacteriostatic action of phenol, benzoic acid and related compounds on *Bacterium aerogenes*. *Microbiology* **4**: 110–121.

Becker, G. (1998) Der Salzgehalt im Wattenmeer. In, *Umweltatlas Wattenmeer*. Ulmer, pp. 60–61.

Beckers, G., Nolden, L., and Burkovski, A. (2001) Glutamate synthase of *Corynebacterium glutamicum* is not essential for glutamate synthesis and is regulated by the nitrogen status. *Microbiology* **147**: 2961–2970.

Benjamini, Y. and Hochberg, Y. (1995) Controlling the false discovery rate: A practical and powerful approach to multiple testing. *J. R. Stat. Soc. Ser. B Methodol.* **57**: 289–300.

Bianchi, G., Gamba, A., Limiroli, R., Pozzi, N., Elster, R., Salamini, F., and Bartels, D. (1993) The unusual sugar composition in leaves of the resurrection plant *Myrothamnus flabellifolia*. *Physiol. Plant.* **87**: 223–226.

Biebl, H., Allgaier, M., Tindall, B.J., Koblizek, M., Lünsdorf, H., Pukall, R., and Wagner-Döbler, I. (2005) *Dinoroseobacter shibae* gen. nov., sp. nov., a new aerobic phototrophic bacterium isolated from dinoflagellates. *Int. J. Syst. Evol. Microbiol.* **55**: 1089–1096.

Biebl, H. and Wagner-Döbler, I. (2006) Growth and bacteriochlorophyll *a* formation in taxonomically diverse aerobic anoxygenic phototrophic bacteria in chemostat culture: Influence of light regimen and starvation. *Process Biochem.* **41**: 2153–2159.

Blatt, J.M., Pledger, W.J., and Umbarger, H.E. (1972) Isoleucine and valine metabolism in *Escherichia coli*. XX. Multiple forms of acetohydroxy acid synthetase. *Biochem.*

Biophys. Res. Commun. **48**: 444–450.

Bolten, C.J., Kiefer, P., Letisse, F., Portais, J.-C., and Wittmann, C. (2007) Sampling for metabolome analysis of microorganisms. *Anal. Chem.* **79**: 3843–3849.

Botsford, J.L. (1984) Osmoregulation in *Rhizobium meliloti*: inhibition of growth by salts. *Arch. Microbiol.* **137**: 124–127.

Brinkhoff, T., Giebel, H.-A., and Simon, M. (2008) Diversity, ecology, and genomics of the Roseobacter clade: a short overview. *Arch. Microbiol.* **189**: 531–539.

Brown, A.D. (1976) Microbial water stress. *Bacteriol. Rev.* **40**: 803–846.

Bruhn, J.B., Gram, L., and Belas, R. (2007) Production of antibacterial compounds and biofilm formation by *Roseobacter* species are influenced by culture conditions. *Appl. Environ. Microbiol.* **73**: 442–450.

Buchan, A., González, J.M., and Moran, M.A. (2005) Overview of the marine Roseobacter lineage. *Appl. Environ. Microbiol.* **71**: 5665–5677.

Cai, J., Wei, Y., Zhao, Y., Pan, G., and Wang, G. (2012) Production of polyhydroxybutyrate by the marine photosynthetic bacterium *Rhodovulum sulfidophilum* P5. *Chin. J. Oceanol. Limnol.* **30**: 620–626.

Cannata, J.J.B. and Stoppani, A.O.M. (1963) Phosphopyruvate carboxylase from bakers' yeast I. Isolation, purification, and characterization. *J. Biol. Chem.* **238**: 1196–1207.

Cánovas, D., Borges, N., Vargas, C., Ventosa, A., Nieto, J.J., and Santos, H. (1999) Role of Nγ-acetyldiaminobutyrate as an enzyme stabilizer and an intermediate in the biosynthesis of hydroxyectoine. *Appl. Environ. Microbiol.* **65**: 3774–3779.

Capp, M.W., Cayley, S.D., Zhang, W., Guttman, H.J., Melcher, S.E., Saecker, R.M., et al. (1996) Compensating effects of opposing changes in putrescine (2+) and K^+ concentrations on *lac* repressor-*lac* operator binding: *in vitro* thermodynamic analysis and *in vivo* relevance. *J. Mol. Biol.* **258**: 25–36.

de Carvalho, L.P.S., Frantom, P.A., Argyrou, A., and Blanchard, J.S. (2009) Kinetic evidence for interdomain communication in the allosteric regulation of α-isopropylmalate synthase from *Mycobacterium tuberculosis*. *Biochemistry (Mosc.)* **48**: 1996–2004.

Chambers, S.T., Peddie, B.A., Randall, K., and Lever, M. (1999) Inhibitors of bacterial growth in urine: what is the role of betaines? *Int. J. Antimicrob. Agents* **11**: 293–296.

Charette, M.A. and Smith, W.H.F. (2010) The volume of earth's ocean.

Chien, C.-C., Chen, C.-C., Choi, M.-H., Kung, S.-S., and Wei, Y.-H. (2007) Production of poly-β-hydroxybutyrate (PHB) by *Vibrio* spp. isolated from marine environment. *J. Biotechnol.* **132**: 259–263.

Cho, J.-C. and Giovannoni, S.J. (2004) *Oceanicola granulosus* gen. nov., sp. nov. and *Oceanicola batsensis* sp. nov., poly-β-hydroxybutyrate-producing marine bacteria in the order "*Rhodobacterales*." *Int. J. Syst. Evol. Microbiol.* **54**: 1129–1136.

Cooper, R.A. and Kornberg, H.L. (1965) Net formation of phosphoenolpyruvate from pyruvate by *Escherichia coli*. *Biochim. Biophys. Acta BBA - Gen. Subj.* **104**: 618–

620.

Costa, J., Empadinhas, N., and da Costa, M.S. (2007) Glucosylglycerate biosynthesis in the deepest lineage of the bacteria: characterization of the thermophilic proteins GpgS and GpgP from *Persephonella marina*. *J. Bacteriol.* **189**: 1648–1654.

Costa, J., Empadinhas, N., Gonçalves, L., Lamosa, P., Santos, H., and Costa, M.S. da (2006) Characterization of the biosynthetic pathway of glucosylglycerate in the archaeon *Methanococcoides burtonii*. *J. Bacteriol.* **188**: 1022–1030.

Costa, M.S. da, Santos, H., and Galinski, E.A. (1998) An overview of the role and diversity of compatible solutes in Bacteria and Archaea. In, Antranikian,G. (ed), *Biotechnology of Extremophiles*, Advances in Biochemical Engineering/Biotechnology. Springer Berlin Heidelberg, pp. 117–153.

Cox, J. and Mann, M. (2011) Quantitative, High-Resolution Proteomics for Data-Driven Systems Biology. *Annu. Rev. Biochem.* **80**: 273–299.

Csonka, L.N. (1989) Physiological and genetic responses of bacteria to osmotic stress. *Microbiol. Rev.* **53**: 121–147.

Curson, A.R.J., Todd, J.D., Sullivan, M.J., and Johnston, A.W.B. (2011) Catabolism of dimethylsulphoniopropionate: microorganisms, enzymes and genes. *Nat. Rev. Microbiol.* **9**: 849–859.

D'Alvise, P.W., Phippen, C.B.W., Nielsen, K.F., and Gram, L. (2016) Influence of iron on production of the antibacterial compound tropodithietic acid and its noninhibitory analog in *Phaeobacter inhibens*. *Appl. Environ. Microbiol.* **82**: 502–509.

Dettmer, K., Aronov, P.A., and Hammock, B.D. (2007) Mass spectrometry-based metabolomics. *Mass Spectrom. Rev.* **26**: 51–78.

Diaz, R.J. and Rosenberg, R. (2008) Spreading Dead Zones and Consequences for Marine Ecosystems. *Science* **321**: 926–929.

Dickschat, J.S., Zell, C., and Brock, N.L. (2010) Pathways and substrate specificity of DMSP catabolism in marine bacteria of the *Roseobacter* clade. *ChemBioChem* **11**: 417–425.

Drüppel, K., Hensler, M., Trautwein, K., Koßmehl, S., Wöhlbrand, L., Schmidt-Hohagen, K., et al. (2013) Pathways and substrate-specific regulation of amino acid degradation in *Phaeobacter inhibens* DSM 17395 (archetype of the marine Roseobacter clade). *Environ. Microbiol.* n/a–n/a.

Dybas, C.L. (2005) Dead zones spreading in world oceans. *BioScience* **55**: 552–557.

Ebert, M., Laaß, S., Burghartz, M., Petersen, J., Koßmehl, S., Wöhlbrand, L., et al. (2013) Transposon mutagenesis identified chromosomal and plasmid genes essential for adaptation of the marine bacterium *Dinoroseobacter shibae* to anaerobic conditions. *J. Bacteriol.* **195**: 4769–4777.

Edgar, R., Domrachev, M., and Lash, A.E. (2002) Gene Expression Omnibus: NCBI gene expression and hybridization array data repository. *Nucleic Acids Res.* **30**: 207–210.

Empadinhas, N. and da Costa, M.S. (2008) To be or not to be a compatible solute: Bioversatility of mannosylglycerate and glucosylglycerate. *Syst. Appl. Microbiol.* **31**: 159–168.

Ferjani, A., Mustardy, L., Sulpice, R., Marin, K., Suzuki, I., Hagemann, M., and Murata, N. (2003) Glucosylglycerol, a compatible solute, sustains cell division under salt stress. *Plant Physiol.* **131**: 1628–1637.

Fiehn, O. (2002) Metabolomics--the link between genotypes and phenotypes. *Plant Mol. Biol.* **48**: 155–171.

Fuhrman, J.A., Steele, J.A., Hewson, I., Schwalbach, M.S., Brown, M.V., Green, J.L., and Brown, J.H. (2008) A latitudinal diversity gradient in planktonic marine bacteria. *Proc. Natl. Acad. Sci.* **105**: 7774–7778.

Fukuyo, Y. (1981) Taxonomical study on benthic dinoflagellates collected in coral reefs. *Nippon Suisan Gakkaishi* **47**: 967–978.

Fulda, S., Mikkat, S., Huang, F., Huckauf, J., Marin, K., Norling, B., and Hagemann, M. (2006) Proteome analysis of salt stress response in the cyanobacterium *Synechocystis* sp. strain PCC 6803. *PROTEOMICS* **6**: 2733–2745.

Fürch, T., Preusse, M., Tomasch, J., Zech, H., Wagner-Döbler, I., Rabus, R., and Wittmann, C. (2009) Metabolic fluxes in the central carbon metabolism of *Dinoroseobacter shibae* and *Phaeobacter gallaeciensis*, two members of the marine *Roseobacter* clade. *BMC Microbiol.* **9**: 1–11.

Ge, Y.-D., Cao, Z.-Y., Wang, Z.-D., Chen, L.-L., Zhu, Y.-M., and Zhu, G.-P. (2010) Identification and biochemical characterization of a thermostable malate dehydrogenase from the mesophile *Streptomyces coelicolor* A3(2). *Biosci. Biotechnol. Biochem.* **74**: 2194–2201.

Giebel, H.-A., Kalhoefer, D., Gahl-Janssen, R., Choo, Y.-J., Lee, K., Cho, J.-C., et al. (2013) *Planktomarina temperata* gen. nov., sp. nov., belonging to the globally distributed RCA cluster of the marine Roseobacter clade, isolated from the German Wadden Sea. *Int. J. Syst. Evol. Microbiol.* **63**: 4207–4217.

Gilbert, J.A., Steele, J.A., Caporaso, J.G., Steinbrück, L., Reeder, J., Temperton, B., et al. (2012) Defining seasonal marine microbial community dynamics. *ISME J.* **6**: 298–308.

Giovannoni, S.J. and Stingl, U. (2005) Molecular diversity and ecology of microbial plankton. *Nature* **437**: 343–348.

Giæver, H.M., Styrvold, O.B., Kaasen, I., and Strøm, A.R. (1988a) Biochemical and genetic characterization of osmoregulatory trehalose synthesis in *Escherichia coli*. *J. Bacteriol.* **170**: 2841–2849.

Giæver, H.M., Styrvold, O.B., Kaasen, I., and Strøm, A.R. (1988b) Biochemical and genetic characterization of osmoregulatory trehalose synthesis in *Escherichia coli*. *J. Bacteriol.* **170**: 2841–2849.

Gonzalez, B., de Graaf, A., Renaud, M., and Sahm, H. (2000) Dynamic *in vivo* ^{31}P nuclear magnetic resonance study of *Saccharomyces cerevisiae* in glucose-limited chemostat culture during the aerobic–anaerobic shift. *Yeast* **16**: 483–497.

González, J.M., Covert, J.S., Whitman, W.B., Henriksen, J.R., Mayer, F., Scharf, B., et al. (2003) *Silicibacter pomeroyi* sp. nov. and *Roseovarius nubinhibens* sp. nov., dimethylsulfoniopropionate-demethylating bacteria from marine environments. *Int. J. Syst. Evol. Microbiol.* **53**: 1261–1269.

González, J.M., Simó, R., Massana, R., Covert, J.S., Casamayor, E.O., Pedrós-Alió, C., and Moran, M.A. (2000) Bacterial community structure associated with a dimethylsulfoniopropionate-producing North Atlantic algal bloom. *Appl. Environ. Microbiol.* **66**: 4237–4246.

Goude, R., Renaud, S., Bonnassie, S., Bernard, T., and Blanco, C. (2004) Glutamine, glutamate, and α-glucosylglycerate are the major osmotic solutes accumulated by *Erwinia chrysanthemi* strain 3937. *Appl. Environ. Microbiol.* **70**: 6535–6541.

Grasshoff, K., Ehrhardt, M., and Kremling, K. (1983) Methods of seawater analysis Second Edition. Verlag Chemie.

Guillouet, S. and Engasser, J.M. (1995) Sodium and proline accumulation in *Corynebacterium glutamicum* as a response to an osmotic saline upshock. *Appl. Microbiol. Biotechnol.* **43**: 315–320.

Hagemann, M. (2011) Molecular biology of cyanobacterial salt acclimation. *FEMS Microbiol. Rev.* **35**: 87–123.

Hagemann, M. and Erdmann, N. (1994) Activation and pathway of glucosylglycerol synthesis in the cyanobacterium *Synechocystis* sp. PCC 6803. *Microbiology* **140**: 1427–1431.

Hagemann, M., Ribbeck-Busch, K., Klähn, S., Hasse, D., Steinbruch, R., and Berg, G. (2008) The plant-associated bacterium *Stenotrophomonas rhizophila* expresses a new enzyme for the synthesis of the compatible solute glucosylglycerol. *J. Bacteriol.* **190**: 5898–5906.

Hagemann, M., Schoor, A., Jeanjean, R., Zuther, E., and Joset, F. (1997) The *stpA* gene from *Synechocystis* sp. strain PCC 6803 encodes the glucosylglycerol-phosphate phosphatase involved in cyanobacterial osmotic response to salt shock. *J. Bacteriol.* **179**: 1727–1733.

Hahne, H., Mäder, U., Otto, A., Bonn, F., Steil, L., Bremer, E., et al. (2010) A comprehensive proteomics and transcriptomics analysis of *Bacillus subtilis* salt stress adaptation. *J. Bacteriol.* **192**: 870–882.

Hansen, T., Schlichting, B., and Schönheit, P. (2002) Glucose-6-phosphate dehydrogenase from the hyperthermophilic bacterium *Thermotoga maritima*: expression of the g6pd gene and characterization of an extremely thermophilic enzyme. *FEMS Microbiol. Lett.* **216**: 249–253.

Harrison, J.P., Hallsworth, J.E., and Cockell, C.S. (2015) Reduction of the temperature sensitivity of *Halomonas hydrothermalis* by iron starvation combined with microaerobic conditions. *Appl. Environ. Microbiol.* **81**: 2156–2162.

Harrison, P.W., Lower, R.P.J., Kim, N.K.D., and Young, J.P.W. (2010) Introducing the bacterial "chromid": not a chromosome, not a plasmid. *Trends Microbiol.* **18**: 141–148.

Hartwig, A. (2001) Role of magnesium in genomic stability. *Mutat. Res. Mol. Mech. Mutagen.* **475**: 113–121.

Hengge-Aronis, R., Klein, W., Lange, R., Rimmele, M., and Boos, W. (1991) Trehalose synthesis genes are controlled by the putative sigma factor encoded by *rpoS* and are involved in stationary-phase thermotolerance in *Escherichia coli*. *J. Bacteriol.* **173**:

7918–7924.

Hensler, M. (2015) Metabolic characterisation of the nutritional versatile marine bacterium *Phaeobacter inhibens* DSM 17395 via gas chromatography – mass spectrometry.

Hiller, K., Hangebrauk, J., Jäger, C., Spura, J., Schreiber, K., and Schomburg, D. (2009) MetaboliteDetector: Comprehensive analysis tool for targeted and nontargeted GC/MS based metabolome analysis. *Anal. Chem.* **81**: 3429–3439.

Hove-Jensen, B., Harlow, K.W., King, C.J., and Switzer, R.L. (1986) Phosphoribosylpyrophosphate synthetase of *Escherichia coli*. Properties of the purified enzyme and primary structure of the prs gene. *J. Biol. Chem.* **261**: 6765–6771.

Hummel, J., Strehmel, N., Selbig, J., Walther, D., and Kopka, J. (2010) Decision tree supported substructure prediction of metabolites from GC-MS profiles. *Metabolomics Off. J. Metabolomic Soc.* **6**: 322–333.

Jäger, C. (2011) Metabolomanalyse von *Pseudomonas putida* und Entwicklung eines Verfahrens zur Strukturanalyse unbekannter Verbindungen in bakteriellen Zellextrakten.

Kanani, H.H. and Klapa, M.I. (2007) Data correction strategy for metabolomics analysis using gas chromatography–mass spectrometry. *Metab. Eng.* **9**: 39–51.

Karsten, U., Barrow, K.D., and King, R.J. (1993) Floridoside, L-isofloridoside, and D-isofloridoside in the red alga *Porphyra columbina* (seasonal and osmotic effects). *Plant Physiol.* **103**: 485–491.

Kashutina, M.V., Ioffe, S.L., and Tartakovskii, V.A. (1975) Silylation of organic compounds. *Russ. Chem. Rev.* **44**: 733–747.

Kaye, D. (1968) Antibacterial activity of human urine. *J. Clin. Invest.* **47**: 2374–2390.

Kaye, J.Z. and Baross, J.A. (2004) Synchronous effects of temperature, hydrostatic pressure, and salinity on growth, phospholipid profiles, and protein patterns of four *Halomonas* species isolated from deep-sea hydrothermal-vent and sea surface environments. *Appl. Environ. Microbiol.* **70**: 6220–6229.

Kell, D.B. (2004) Metabolomics and systems biology: making sense of the soup. *Curr. Opin. Microbiol.* **7**: 296–307.

Killham, K. and Firestone, M.K. (1984) Salt stress control of intracellular solutes in *Streptomycetes* indigenous to saline soils. *Appl. Environ. Microbiol.* **47**: 301–306.

Kilstrup, M., Jacobsen, S., Hammer, K., and Vogensen, F.K. (1997) Induction of heat shock proteins DnaK, GroEL, and GroES by salt stress in *Lactococcus lactis*. *Appl. Environ. Microbiol.* **63**: 1826–1837.

Kind, T. and Fiehn, O. (2006) Metabolomic database annotations via query of elemental compositions: mass accuracy is insufficient even at less than 1 ppm. *BMC Bioinformatics* **7**: 234.

Klähn, S., Marquardt, D.M., Rollwitz, I., and Hagemann, M. (2009) Expression of the *ggpPS* gene for glucosylglycerol biosynthesis from *Azotobacter vinelandii* improves the salt tolerance of *Arabidopsis thaliana*. *J. Exp. Bot.* **60**: 1679–1689.

Klähn, S., Steglich, C., Hess, W.R., and Hagemann, M. (2010) Glucosylglycerate: a secondary compatible solute common to marine cyanobacteria from nitrogen-poor environments. *Environ. Microbiol.* **12**: 83–94.

Kleist, S., Ulbrich, M., Bill, N., Schmidt-Hohagen, K., Geffers, R., and Schomburg, D. (2016) Dealing with salinity extremes and nitrogen limitation – an unexpected strategy of the marine bacterium *Dinoroseobacter shibae*. *Environ. Microbiol.* n/a–n/a.

Kohlhaw, G., Leary, T.R., and Umbarger, H.E. (1969) α-Isopropylmalate Synthase from Salmonella typhimurium PURIFICATION AND PROPERTIES. *J. Biol. Chem.* **244**: 2218–2225.

Kollman, V.H., Hanners, J.L., London, R.E., Adame, E.G., and Walker, T.E. (1979) Photosynthetic preparation and characterization of 13C-labeled carbohydrates in *Agmenellum quadruplicatum*. *Carbohydr. Res.* **73**: 193–202.

Kováts, E. (1958) Gas-chromatographische Charakterisierung organischer Verbindungen. Teil 1: Retentionsindices aliphatischer Halogenide, Alkohole, Aldehyde und Ketone. *Helv. Chim. Acta* **41**: 1915–1932.

Laass, S., Kleist, S., Bill, N., Drüppel, K., Kossmehl, S., Wöhlbrand, L., et al. (2014) Gene regulatory and metabolic adaptation processes of *Dinoroseobacter shibae* DFL12^{T} during oxygen depletion. *J. Biol. Chem.* **289**: 13219–13231.

Labrenz, M., Collins, M.D., Lawson, P.A., Tindall, B.J., Braker, G., and Hirsch, P. (1998) *Antarctobacter heliothermus* gen. nov., sp. nov., a budding bacterium from hypersaline and heliothermal Ekho Lake. *Int. J. Syst. Evol. Microbiol.* **48**: 1363–1372.

Ladau, J., Sharpton, T.J., Finucane, M.M., Jospin, G., Kembel, S.W., O'Dwyer, J., et al. (2013) Global marine bacterial diversity peaks at high latitudes in winter. *ISME J.* **7**: 1669–1677.

Lebedeva, N.V., Malinina, N.V., and Ivanovsky, R.N. (2002) A comparative study of the isocitrate dehydrogenases of *Chlorobium limicola* forma *thiosulfatophilum* and *Rhodopseudomonas palustris*. *Microbiology* **71**: 657–662.

Lessmann, D., Schimz, K.L., and Kurz, G. (1975) D-glucose-6-phosphate dehydrogenase (Entner-Doudoroff enzyme) from *Pseudomonas fluorescens*. Purification, properties and regulation. *Eur. J. Biochem. FEBS* **59**: 545–559.

Librando, V., Tringali, G., Hjorth, J., and Coluccia, S. (2004) OH-initiated oxidation of DMS/DMSO: reaction products at high NOx levels. *Environ. Pollut.* **127**: 403–410.

Lovelock, J.E., Maggs, R.J., and Rasmussen, R.A. (1972) Atmospheric dimethyl sulphide and the natural sulphur cycle. *Nature* **237**: 452–453.

Luley-Goedl, C. and Nidetzky, B. (2011) Glycosides as compatible solutes: biosynthesis and applications. *Nat. Prod. Rep.* **28**: 875–896.

Mackay, M.A., Norton, R.S., and Borowitzka, L.J. (1984) Organic osmoregulatory solutes in Cyanobacteria. *Microbiology* **130**: 2177–2191.

Mager, J. (1955) Influence of osmotic pressure on the polymaine requirement of *Neisseria perflava* and *Pasteurella tularensis* for growth in defined medium. *Nature* **176**:

933–934.

Makemson, J.C. and Hastings, J.W. (1979) Glutamate functions in osmoregulation in a marine bacterium. *Appl. Environ. Microbiol.* **38**: 178–180.

Mann, H.B. and Whitney, D.R. (1947) On a test of whether one of two random variables is stochastically larger than the other. *Ann. Math. Stat.* **18**: 50–60.

Marin, K., Huckauf, J., Fulda, S., and Hagemann, M. (2002) Salt-dependent expression of glucosylglycerol-phosphate synthase, involved in osmolyte synthesis in the cyanobacterium *Synechocystis* sp. strain PCC 6803. *J. Bacteriol.* **184**: 2870–2877.

Marin, K., Kanesaki, Y., Los, D.A., Murata, N., Suzuki, I., and Hagemann, M. (2004) Gene expression profiling reflects physiological processes in salt acclimation of *Synechocystis* sp. Strain PCC 6803. *Plant Physiol.* **136**: 3290–3300.

Marin, K., Suzuki, I., Yamaguchi, K., Ribbeck, K., Yamamoto, H., Kanesaki, Y., et al. (2003) Identification of histidine kinases that act as sensors in the perception of salt stress in *Synechocystis* sp. PCC 6803. *Proc. Natl. Acad. Sci.* **100**: 9061–9066.

Martens, T., Heidorn, T., Pukall, R., Simon, M., Tindall, B.J., and Brinkhoff, T. (2006) Reclassification of *Roseobacter gallaeciensis* Ruiz-Ponte et al. 1998 as *Phaeobacter gallaeciensis* gen. nov., comb. nov., description of *Phaeobacter inhibens* sp. nov., reclassification of *Ruegeria algicola* (Lafay et al. 1995) Uchino et al. 1999 as *Marinovum algicola* gen. nov., comb. nov., and emended descriptions of the genera *Roseobacter*, *Ruegeria* and *Leisingera*. *Int. J. Syst. Evol. Microbiol.* **56**: 1293–1304.

McCarty, P.L. and McKinney, R.E. (1961) Salt toxicity in anaerobic digestion. *J. Water Pollut. Control Fed.* **33**: 399–415.

Measures, J.C. (1975) Role of amino acids in osmoregulation of non-halophilic bacteria. *Nature* **257**: 398–400.

Mikkat, S., Galinski, E.A., Berg, G., Minkwitz, A., and Schoor, A. (2000) Salt adaptation in pseudomonads: Characterization of glucosylglycerol-synthesizing isolates from brackish coastal waters and the rhizosphere. *Syst. Appl. Microbiol.* **23**: 31–40.

Miura, Y., Akano, T., Fukatsu, K., Miyasaka, H., Mizoguchi, T., Yagi, K., et al. (1997) Stably sustained hydrogen production by biophotolysis in natural day/night cycle. *Energy Convers. Manag.* **38**: S533–S537.

Moran, M.A., Belas, R., Schell, M.A., González, J.M., Sun, F., Sun, S., et al. (2007) Ecological Genomics of Marine Roseobacters. *Appl. Environ. Microbiol.* **73**: 4559–4569.

Moran, M.A., Buchan, A., González, J.M., Heidelberg, J.F., Whitman, W.B., Kiene, R.P., et al. (2004) Genome sequence of *Silicibacter pomeroyi* reveals adaptations to the marine environment. *Nature* **432**: 910–913.

Mothes, G., Schnorpfeil, C., and Ackermann, J.-U. (2007) Production of PHB from crude glycerol. *Eng. Life Sci.* **7**: 475–479.

Munro, G.F. and Bell, C.A. (1973) Polyamine requirements of a conditional polyamine auxotroph of *Escherichia coli*. *J. Bacteriol.* **115**: 469–475.

Murphy, S. (2007) General Information on Dissolved Oxygen.

Newton, R.J., Griffin, L.E., Bowles, K.M., Meile, C., Gifford, S., Givens, C.E., et al. (2010) Genome characteristics of a generalist marine bacterial lineage. *ISME J.* **4**: 784–798.

Nicholson, J.K. and Lindon, J.C. (2008) Systems biology: Metabonomics. *Nature* **455**: 1054–1056.

NOAA National Centers for Environmental Information (2009) World Ocean Atlas 2009.

Nobre, A., Empadinhas, N., Nobre, M.F., Lourenço, E.C., Maycock, C., Ventura, M.R., et al. (2012) The plant *Selaginella moellendorffii* possesses enzymes for synthesis and hydrolysis of the compatible solutes mannosylglycerate and glucosylglycerate. *Planta* **237**: 891–901.

Obi-Tabot, E.T., Hanrahan, L.M., Cachecho, R., Beer, E.R., Hopkins, S.R., Chan, J.C.K., et al. (1993) Changes in hepatocyte NADH fluorescence during prolonged hypoxia. *J. Surg. Res.* **55**: 575–580.

Ohtaka, Y. and Uchida, K. (1963) The chemical structure and stability of yeast ribosomes. *Biochem. Biophys. Acta* **76**: 94–104.

Ollivier, B., Caumette, P., Garcia, J.L., and Mah, R.A. (1994) Anaerobic bacteria from hypersaline environments. *Microbiol. Rev.* **58**: 27–38.

Pardo, M.A., Llama, M.J., and Serra, J.L. (1999) Purification, properties and enhanced expression under nitrogen starvation of the $NADP^+$-isocitrate dehydrogenase from the cyanobacterium *Phormidium laminosum*. *Biochim. Biophys. Acta BBA - Protein Struct. Mol. Enzymol.* **1431**: 87–96.

Parsell, D.A., Kowal, A.S., Singer, M.A., and Lindquist, S. (1994) Protein disaggregation mediated by heat-shock protein Hspl04. *Nature* **372**: 475–478.

Patzelt, D., Wang, H., Buchholz, I., Rohde, M., Gröbe, L., Pradella, S., et al. (2013) You are what you talk: quorum sensing induces individual morphologies and cell division modes in *Dinoroseobacter shibae*. *ISME J.* **7**: 2274–2286.

Paul, C., Mausz, M.A., and Pohnert, G. (2013) A co-culturing/metabolomics approach to investigate chemically mediated interactions of planktonic organisms reveals influence of bacteria on diatom metabolism. *Metabolomics* **9**: 349–359.

Pawlowicz, R. (2013) Key physical variables in the ocean: Temperature, salinity, and density. *Nat. Educ.* **4.**:

Penninckx, M. (2000) A short review on the role of glutathione in the response of yeasts to nutritional, environmental, and oxidative stresses. *Enzyme Microb. Technol.* **26**: 737–742.

Petersen, J., Frank, O., Göker, M., and Pradella, S. (2013) Extrachromosomal, extraordinary and essential—the plasmids of the *Roseobacter* clade. *Appl. Microbiol. Biotechnol.* **97**: 2805–2815.

Piekarski, T., Buchholz, I., Drepper, T., Schobert, M., Wagner-Doebler, I., Tielen, P., and Jahn, D. (2009) Genetic tools for the investigation of *Roseobacter* clade bacteria. *BMC Microbiol.* **9**: 265.

Poblete-Castro, I., Escapa, I.F., Jäger, C., Puchalka, J., Lam, C.M.C., Schomburg, D., et al. (2012) The metabolic response of *P. putida* KT2442 producing high levels of

polyhydroxyalkanoate under single- and multiple-nutrient-limited growth: Highlights from a multi-level omics approach. *Microb. Cell Factories* **11**: 34.

Pocard, J.A., Smith, L.T., Smith, G.M., and Rudulier, D.L. (1994) A prominent role for glucosylglycerol in the adaptation of *Pseudomonas mendocina* SKB70 to osmotic stress. *J. Bacteriol.* **176**: 6877–6884.

Pradella, S., Päuker, O., and Petersen, J. (2009) Genome organisation of the marine *Roseobacter* clade member *Marinovum algicola*. *Arch. Microbiol.* **192**: 115–126.

Prágai, Z. and Harwood, C.R. (2002) Regulatory interactions between the Pho and σ^B-dependent general stress regulons of *Bacillus subtilis*. *Microbiol. Read. Engl.* **148**: 1593–1602.

Pukall, R., Buntefuß, D., Frühling, A., Rohde, M., Kroppenstedt, R.M., Burghardt, J., et al. (1999) *Sulfitobacter mediterraneus* sp. nov., a new sulfite-oxidizing member of the α-Proteobacteria. *Int. J. Syst. Evol. Microbiol.* **49**: 513–519.

Randall, K., Lever, M., Peddie, B.A., and Chambers, S.T. (1996) Natural and synthetic betaines counter the effects of high NaCl and urea concentrations. *Biochim. Biophys. Acta BBA - Gen. Subj.* **1291**: 189–194.

Rao, D.R. and Oesper, P. (1961) Purification and properties of muscle phosphoglycerate kinase.

Record Jr, M.T., Courtenay, E.S., Cayley, S., and Guttman, H.J. (1998) Biophysical compensation mechanisms buffering *E. coli* protein–nucleic acid interactions against changing environments. *Trends Biochem. Sci.* **23**: 190–194.

Reul, N., Fournier, S., Boutin, J., Hernandez, O., Maes, C., Chapron, B., et al. (2014) Sea surface salinity observations from space with the SMOS satellite: A new means to monitor the marine branch of the water cycle. *Surv. Geophys.* **35**: 681–722.

Rex, R., Bill, N., Schmidt-Hohagen, K., and Schomburg, D. (2013) Swimming in light: A large-scale computational analysis of the metabolism of *Dinoroseobacter shibae*. *PLoS Comp Biol*.

Riemann, L. and Winding, A. (2001) Community dynamics of free-living and particle-associated bacterial assemblages during a freshwater phytoplankton bloom. *Microb. Ecol.* **42**: 274–285.

Ritchie, G.A.F., Senior, P.J., and Dawes, E.A. (1971) The purification and characterization of acetoacetyl-coenzyme A reductase from *Azotobacter beijerinckii*. *Biochem. J.* **121**: 309–316.

Rivkin, R.B. and Anderson, M.R. (1997) Inorganic nutrient limitation of oceanic bacterioplankton. *Limnol. Oceanogr.* **42**: 730–740.

Robertson, D.E., Lai, M.C., Gunsalus, R.P., and Roberts, M.F. (1992) Composition, variation, and dynamics of major osmotic solutes in *Methanohalophilus* strain FDF1. *Appl. Environ. Microbiol.* **58**: 2438–2443.

Roberts, T.A. (1975) The microbiological role of nitrite and nitrate. *J. Sci. Food Agric.* **26**: 1755–1760.

Roder, A., Hoffmann, E., Hagemann, M., and Berg, G. (2005) Synthesis of the compatible solutes glucosylglycerol and trehalose by salt-stressed cells of *Stenotrophomonas*

strains. *FEMS Microbiol. Lett.* **243**: 219–226.

Roeßler, M. and Müller, V. (2001) Osmoadaptation in bacteria and archaea: common principles and differences. *Environ. Microbiol.* **3**: 743–754.

Saeed, A.I., Sharov, V., White, J., Li, J., Liang, W., Bhagabati, N., et al. (2003) TM4: a free, open-source system for microarray data management and analysis. *BioTechniques* **34**: 374–378.

Sajiki, K., Pluskal, T., Shimanuki, M., and Yanagida, M. (2013) Metabolomic analysis of fission yeast at the onset of nitrogen starvation. *Metabolites* **3**: 1118–1129.

Schaeffer, F. and Stanier, R.Y. (1978) Glucose-6-phosphate dehydrogenase of *Anabaena* sp. kinetic and molecular properties. *Arch. Microbiol.* **116**: 9–19.

Schoor, A., Hagemann, M., and Erdmann, N. (1999) Glucosylglycerol-phosphate synthase: target for ion-mediated regulation of osmolyte synthesis in the cyanobacterium *Synechocystis* sp. strain PCC 6803. *Arch. Microbiol.* **171**: 101–106.

Selje, N., Simon, M., and Brinkhoff, T. (2004) A newly discovered *Roseobacter* cluster in temperate and polar oceans. *Nature* **427**: 445–448.

Senior, P.J. and Dawes, E.A. (1971) Poly-β-hydroxybutyrate biosynthesis and the regulation of glucose metabolism in *Azotobacter beijerinckii*. *Biochem. J.* **125**: 55–66.

Severin, J., Wohlfarth, A., and Galinski, E.A. (1992) The predominant role of recently discovered tetrahydropyrimidines for the osmoadaptation of halophilic eubacteria. *Microbiology* **138**: 1629–1638.

Seyedsayamdost, M.R., Case, R.J., Kolter, R., and Clardy, J. (2011) The Jekyll-and-Hyde chemistry of *Phaeobacter gallaeciensis*. *Nat. Chem.* **3**: 331–335.

Shapiro, S.S. and Wilk, M.B. (1965) An analysis of variance test for normality (complete samples). *Biometrika* **52**: 591–611.

Shelp, B.J., Bown, A.W., and McLean, M.D. (1999) Metabolism and functions of gamma-aminobutyric acid. *Trends Plant Sci.* **4**: 446–452.

Shiba, T. (1991) *Roseobacter litoralis* gen. nov., sp. nov., and *Roseobacter denitrificans* sp. nov., aerobic pink-pigmented bacteria which contain bacteriochlorophyll a. *Syst. Appl. Microbiol.* **14**: 140–145.

Shi, H.-P., Lee, C.-M., and Ma, W.-H. (2006) Influence of electron acceptor, carbon, nitrogen, and phosphorus on polyhydroxyalkanoate (PHA) production by *Brachymonas* sp. P12. *World J. Microbiol. Biotechnol.* **23**: 625–632.

Simoneit, B.R.T., Elias, V.O., Kobayashi, M., Kawamura, K., Rushdi, A.I., Medeiros, P.M., et al. (2004) Sugars - Dominant water-soluble organic compounds in soils and characterization as tracers in atmospheric particulate matter. *Environ. Sci. Technol.* **38**: 5939–5949.

Sintes, E., Witte, H., Stodderegger, K., Steiner, P., and Herndl, G.J. (2013) Temporal dynamics in the free-living bacterial community composition in the coastal North Sea. *FEMS Microbiol. Ecol.* **83**: 413–424.

Sommer, U. (2005) Biologische Meereskunde.

Soora, M., Tomasch, J., Wang, H., Michael, V., Petersen, J., Engelen, B., et al. (2015) Oxidative stress and starvation in *Dinoroseobacter shibae*: the role of extrachromosomal elements. *Front. Microbiol.* **6.**:

Sørensen, J. (1978) Capacity for denitrification and reduction of nitrate to ammonia in a coastal marine sediment. *Appl. Environ. Microbiol.* **35**: 301–305.

Spura, J., Christian Reimer, L., Wieloch, P., Schreiber, K., Buchinger, S., and Schomburg, D. (2009) A method for enzyme quenching in microbial metabolome analysis successfully applied to gram-positive and gram-negative bacteria and yeast. *Anal. Biochem.* **394**: 192–201.

Stan, H.-J. and Linkerhägner, M. (1996) Large-volume injection in residue analysis with capillary gas chromatography using a conventional autosampler and injection by programmed-temperature vaporization with solvent venting. *J. Chromatogr. A* **727**: 275–289.

Stirnberg, M., Fulda, S., Huckauf, J., Hagemann, M., Krämer, R., and Marin, K. (2007) A membrane-bound FtsH protease is involved in osmoregulation in *Synechocystis* sp. PCC 6803: the compatible solute synthesizing enzyme GgpS is one of the targets for proteolysis. *Mol. Microbiol.* **63**: 86–102.

Strehmel, N., Hummel, J., Erban, A., Strassburg, K., and Kopka, J. (2008) Retention index thresholds for compound matching in GC–MS metabolite profiling. *J. Chromatogr. B* **871**: 182–190.

Strehmel, N., Kopka, J., Scheel, D., and Böttcher, C. (2014) Annotating unknown components from GC/EI-MS-based metabolite profiling experiments using GC/APCI(+)-QTOFMS. *Metabolomics* **10**: 324–336.

Sunda, W., Kieber, D.J., Kiene, R.P., and Huntsman, S. (2002) An antioxidant function for DMSP and DMS in marine algae. *Nature* **418**: 317–320.

Tabor, C.W. and Tabor, H. (1976) 1,4-Diaminobutane (putrescine), spermidine, and spermine. *Annu. Rev. Biochem.* **45**: 285–306.

Tachibana, C. (2015) Transcriptomics today: Microarrays, RNA-seq, and more. *Science*.

Takenaka, F. and Uchiyama, H. (2000) Synthesis of α-D-glucosylglycerol by α-glucosidase and some of its characteristics. *Biosci. Biotechnol. Biochem.* **64**: 1821–1826.

Tempest, D.W., Meers, J.L., and Brown, C.M. (1970) Influence of environment on the content and composition of microbial free amino acid pools. *Microbiology* **64**: 171–185.

Tomasch, J., Gohl, R., Bunk, B., Diez, M.S., and Wagner-Döbler, I. (2011) Transcriptional response of the photoheterotrophic marine bacterium *Dinoroseobacter shibae* to changing light regimes. *ISME J.* **5**: 1957–1968.

Trautwein, K., Kühner, S., Wöhlbrand, L., Halder, T., Kuchta, K., Steinbüchel, A., and Rabus, R. (2008) Solvent stress response of the denitrifying bacterium "*Aromatoleum aromaticum*" strain EbN1. *Appl. Environ. Microbiol.* **74**: 2267–2274.

Vandecandelaere, I., Segaert, E., Mollica, A., Faimali, M., and Vandamme, P. (2008) *Leisingera aquimarina* sp. nov., isolated from a marine electroactive biofilm, and

emended descriptions of *Leisingera methylohalidivorans* Schaefer *et al.* 2002, *Phaeobacter daeponensis* Yoon *et al.* 2007 and *Phaeobacter inhibens* Martens *et al.* 2006. *Int. J. Syst. Evol. Microbiol.* **58**: 2788–2793.

Visscher, P.T. and Gemerden, H. van (1991) Production and consumption of dimethylsulfoniopropionate in marine microbial mats. *Appl. Environ. Microbiol.* **57**: 3237–3242.

Vitousek, P.M. and Howarth, R.W. (1991) Nitrogen limitation on land and in the sea: How can it occur? *Biogeochemistry* **13**: 87–115.

Voget, S., Wemheuer, B., Brinkhoff, T., Vollmers, J., Dietrich, S., Giebel, H.-A., et al. (2015) Adaptation of an abundant *Roseobacter* RCA organism to pelagic systems revealed by genomic and transcriptomic analyses. *ISME J.* **9**: 371–384.

Vuilleumier, S. and Pagni, M. (2002) The elusive roles of bacterial glutathione S-transferases: new lessons from genomes. *Appl. Microbiol. Biotechnol.* **58**: 138–146.

Wagner-Döbler, I., Ballhausen, B., Berger, M., Brinkhoff, T., Buchholz, I., Bunk, B., et al. (2010) The complete genome sequence of the algal symbiont *Dinoroseobacter shibae*: a hitchhiker's guide to life in the sea. *ISME J.* **4**: 61–77.

Wagner-Döbler, I. and Biebl, H. (2006) Environmental biology of the marine *Roseobacter* lineage. *Annu. Rev. Microbiol.* **60**: 255–280.

Wang, F. and Lee, S.Y. (1997) Poly(3-hydroxybutyrate) production with high productivity and high polymer content by a fed-batch culture of *Alcaligenes latus* under nitrogen limitation. *Appl. Environ. Microbiol.* **63**: 3703–3706.

Wang, H., Tomasch, J., Jarek, M., and Wagner-Döbler, I. (2014) A dual-species co-cultivation system to study the interactions between Roseobacters and dinoflagellates. *Front. Microbiol.* **5.**:

Wang, H., Tomasch, J., Michael, V., Bhuju, S., Jarek, M., Petersen, J., and Wagner-Döbler, I. (2015) Identification of genetic modules mediating the Jekyll and Hyde interaction of *Dinoroseobacter shibae* with the dinoflagellate *Prorocentrum minimum*. *Aquat. Microbiol.* 1262.

Wang, Z., Gerstein, M., and Snyder, M. (2009) RNA-Seq: a revolutionary tool for transcriptomics. *Nat. Rev. Genet.* **10**: 57–63.

Warren, C.R. (2011) Use of chemical ionization for GC–MS metabolite profiling. *Metabolomics* **9**: 110–120.

Weber, A., Kögl, S.A., and Jung, K. (2006) Time-dependent proteome alterations under osmotic stress during aerobic and anaerobic growth in *Escherichia coli*. *J. Bacteriol.* **188**: 7165–7175.

Weitzman, P.D.J. (1972) Regulation of α-ketoglutarate dehydrogenase activity in *Acinetobacter. FEBS Lett.* **22**: 323–326.

Welsh, D.T. (2000) Ecological significance of compatible solute accumulation by micro-organisms: from single cells to global climate. *FEMS Microbiol. Rev.* **24**: 263–290.

Wietz, M., Gram, L., Jørgensen, B., and Schramm, A. (2010) Latitudinal patterns in the abundance of major marine bacterioplankton groups. *Aquat. Microb. Ecol.* **61**: 179–189.

Wolf, S.G., Frenkiel, D., Arad, T., Finkel, S.E., Kolter, R., and Minsky, A. (1999) DNA protection by stress-induced biocrystallization. *Nature* **400**: 83–85.

WoRMS (2016) WoRMS - World Register of Marine Species.

Xiao, N. and Jiao, N. (2011) Formation of polyhydroxyalkanoate in aerobic anoxygenic phototrophic bacteria and its relationship to carbon source and light availability. *Appl. Environ. Microbiol.* **77**: 7445–7450.

Xiao, N., Jiao, N., and Liu, Y. (2015) *In vivo* and *in vitro* observations of polyhydroxybutyrate granules formed by *Dinoroseobacter* sp. JL 1447. *Int. J. Biol. Macromol.* **74**: 467–475.

Yancey, P.H., Clark, M.E., Hand, S.C., Bowlus, R.D., and Somero, G.N. (1982) Living with water stress: evolution of osmolyte systems. *Science* **217**: 1214–1222.

Yurkov, V.V. and Beatty, J.T. (1998) Aerobic anoxygenic phototrophic bacteria. *Microbiol. Mol. Biol. Rev.* **62**: 695–724.

Zan, J., Liu, Y., Fuqua, C., and Hill, R.T. (2014) Acyl-Homoserine lactone quorum sensing in the *Roseobacter* clade. *Int. J. Mol. Sci.* **15**: 654–669.

Zeyer, J., Eicher, P., Wakeham, S.G., and Schwarzenbach, R.P. (1987) Oxidation of dimethyl sulfide to dimethyl sulfoxide by phototrophic purple bacteria. *Appl. Environ. Microbiol.* **53**: 2026–2032.

Zhang, Y., Zhang, Y., Zhu, Y., Mao, S., and Li, Y. (2010) Proteomic analyses to reveal the protective role of glutathione in resistance of *Lactococcus lactis* to osmotic stress. *Appl. Environ. Microbiol.* **76**: 3177–3186.

Zumft, W.G. (1997) Cell biology and molecular basis of denitrification. *Microbiol. Mol. Biol. Rev.* **61**: 533–616.

Appendix

A1

SDS-PAGE used to verify the purity of glucosylglycerate-3-phosphate synthase, expressed from *E. coli*, origin of gene: *Synechococcus* sp. PCC7002. Mass of target enzyme plus His-Tag: 52 kDa, marked with white circle. M: marker.

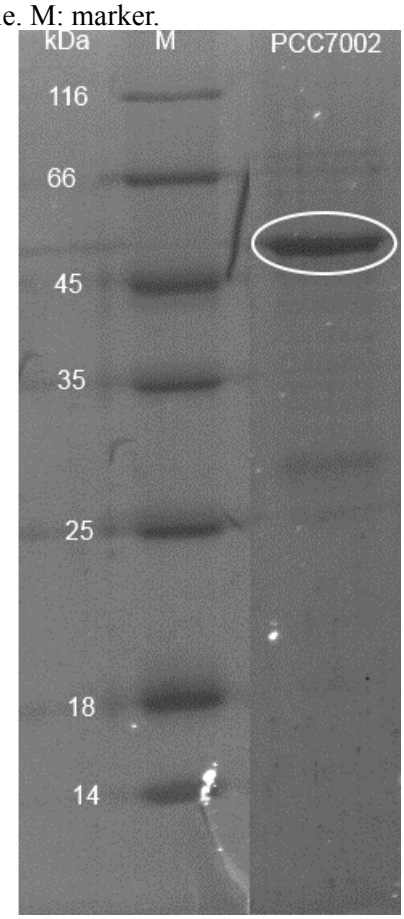

A2

Selected metabolites of *D. shibae* intracellularly regulated after oxygen shut-down. Fold changes were computed by comparison with the aerobic state of cells. ": Not detected under aerobic condition, hence the fold changes were computed by comparison with the first time-point detected. n.d: not detected; KDG: 2-keto-3-deoxy-gluconate. Experiments section 3.1.

Metabolites	time after oxygen shut-down [min]				
	15	30	60	120	240
Amino acids and derivatives					
Alanine	0.77 ± 0.21	2.54 ± 0.45	12.58 ± 1.90	3.50 ± 0.38	2.89 ± 0.28
Glutamate	0.76 ± 0.05	1.03 ± 0.06	0.59 ± 0.05	0.41 ± 0.04	0.52 ± 0.05
Homoserine"			1.00	1.68 ± 0.09	0.68 ± 0.11
Isoleucine	1.43 ± 0.55	8.34 ± 1.64	7.26 ± 2.10	8.31 ± 0.59	4.68 ± 0.97
Leucine	1.08 ± 0.38	11.15 ± 1.96	25.11 ± 6.52	14.41 ± 2.32	5.83 ± 0.98
Lysine	1.07 ± 0.18	1.67 ± 0.11	2.58 ± 0.41	1.99 ± 0.35	1.40 ± 0.13
N-Acetyl-glutamate	0.97 ± 0.17	1.99 ± 0.28	1.76 ± 0.24	2.12 ± 0.15	2.47 ± 0.39
Serine	1.75 ± 0.51	2.07 ± 0.53	5.03 ± 1.29	4.08 ± 0.30	3.66 ± 0.65
Threonine	1.71 ± 0.35	3.78 ± 0.66	5.03 ± 1.01	3.66 ± 0.28	3.41 ± 0.38
Valine	1.51 ± 0.39	24.27 ± 3.85	32.69 ± 6.82	14.88 ± 1.21	6.92 ± 0.93
Amino acid metabolism					
2-Isopropylmalate	0.66 ± 0.19	62.45 ± 45.08	27.71 ± 5.19	12.21 ± 0.93	4.64 ± 1.29
2-Methylmalate	1.91 ± 0.78	13.31 ± 1.99	25.83 ± 6.38	18.45 ± 0.91	3.92 ± 0.67
TCA Cycle					
Aconitate"	1.00	3.34 ± 1.00	4.78 ± 1.41	4.86 ± 0.04	3.20 ± 0.99
Citrate	0.76 ± 0.24	5.61 ± 1.00	10.88 ± 1.96	11.30 ± 1.36	3.80 ± 0.84
Fumarate	1.98 ± 0.64	3.84 ± 0.93	9.87 ± 2.75	7.39 ± 0.74	3.11 ± 0.68
Malate	1.20 ± 0.33	3.71 ± 0.70	17.99 ± 4.06	12.58 ± 0.43	5.08 ± 0.99
2-Oxoglutarate	0.85 ± 0.16	2.26 ± 0.37	1.10 ± 0.22	1.04 ± 0.14	1.09 ± 0.26
Succinate	1.20 ± 0.28	3.21 ± 0.47	14.24 ± 3.02	8.09 ± 3.95	3.91 ± 0.72
Gluconeogenesis and Entner-Doudoroff pathway					
Dihydroxyacetone phosphate	1.03 ± 0.38	1.05 ± 0.29	0.51 ± 0.19	0.96 ± 0.07	1.07 ± 0.31
Fructose-6-phosphate	0.59 ± 0.21	1.88 ± 0.63	3.02 ± 1.13	4.36 ± 0.39	1.85 ± 0.71
Glucose	0.93 ± 0.09	0.58 ± 0.01	0.20 ± 0.01	0.31 ± 0.01	0.32 ± 0.05
Glucose-6-phosphate	1.09 ± 0.24	2.72 ± 0.32	3.23 ± 0.53	4.79 ± 0.77	2.05 ± 0.35
KDG	1.15 ± 0.52	2.08 ± 0.32	2.63 ± 0.47	1.32 ± 0.01	1.87 ± 0.22
Phosphoenolpyruvate	0.75 ± 0.19	4.19 ± 2.33	4.05 ± 1.18	1.74 ± 0.17	1.26 ± 0.39
6-Phosphogluconate	0.97 ± 0.05	0.98 ± 0.13	n.d.	2.52 ± 3.70	1.00 ± 0.16
2-Phosphoglycerate	1.00 ± 0.27	1.83 ± 0.36	2.83 ± 0.59	2.02 ± 0.29	1.03 ± 0.23
3-Phosphoglycerate	1.00 ± 0.26	2.99 ± 0.40	4.18 ± 0.52	2.83 ± 0.27	1.37 ± 0.19
Pyruvate	2.97 ± 2.07	0.69 ± 0.20	3.11 ± 1.00	4.40 ± 0.44	4.21 ± 1.32

Continuation page ii

Metabolites	time after oxygen shut-down [min]				
	15	30	60	120	240
Others					
1,6-Anhydro-glucose	0.64 ± 0.08	0.58 ± 0.18	0.15 ± 0.02	0.28 ± 0.04	0.38 ± 0.05
11-Octadecenoate	0.91 ± 0.48	0.54 ± 0.29	1.34 ± 0.67	0.51 ± 0.14	1.43 ± 0.83
2-Amino-2-methyl-3-hydroxy-propanoate	1.74 ± 0.56	1.97 ± 0.87	2.74 ± 0.77	2.03 ± 0.25	2.09 ± 0.46
3-Aminoisobutanoate	1.72 ± 0.43	1.18 ± 0.49	0.74 ± 0.25	0.49 ± 0.12	0.48 ± 0.13
3-Hydroxybutanoate	0.56 ± 0.1	0.87 ± 0.1	1.42 ± 0.35	2.24 ± 0.23	2.08 ± 0.38
3-Ketoadipate"	n.d.	1	1.9 ± 1.14	2.91 ± 0.13	1.39 ± 1.11
Adenine	n.d.	2.99 ± 1.75	1.25 ± 1.12	n.d.	0.03 ± 0.02
Adenosine	0.04 ± 0.04	0.1 ± 0.13	0.02 ± 0.02	n.d.	n.d.
Cytosine	0.62 ± 0.36	1.42 ± 0.33	1.75 ± 0.77	1.13 ± 0.42	2.69 ± 0.97
Ethanolamine	0.78 ± 0.35	1.63 ± 0.5	0.97 ± 0.43	0.98 ± 0.38	0.79 ± 0.34
Fructose-6-phosphate	0.59 ± 0.21	1.88 ± 0.63	3.02 ± 1.13	4.36 ± 0.39	1.85 ± 0.71
Galacturonate	0.53 ± 0.23	0.72 ± 0.13	0.48 ± 0.05	0.46 ± 0.01	0.2 ± 0.06
Glucoheptonic acid-1,4-lactone	1.32 ± 0.14	1.29 ± 0.17	0.61 ± 0.32	1.15 ± 0.06	1.3 ± 0.16
Glucosylglycerate	1.18 ± 0.35	1.09 ± 0.09	0.31 ± 0.07	0.59 ± 0.37	0.31 ± 0.06
Glucosylglycerol	1.07 ± 0.14	0.8 ± 0.06	0.69 ± 0.14	0.5 ± 0.12	0.74 ± 0.07
Glutarate	0.97 ± 0.48	1.1 ± 0.86	3.79 ± 1.84	2.24 ± 0.12	1.1 ± 0.42
Glycerate	1 ± 0.43	0.65 ± 0.25	0.74 ± 0.41	0.55 ± 0.05	0.4 ± 0.16
Glycerol-3-phosphate	0.85 ± 0.27	0.86 ± 0.22	0.93 ± 0.28	0.61 ± 0.06	1 ± 0.31
Glycolate	0.66 ± 0.21	0.84 ± 0.29	1.27 ± 0.61	1 ± 0.39	1 ± 0.35
Gulose	1.12 ± 0.17	0.87 ± 0.06	0.86 ± 0.16	0.73 ± 0.06	0.58 ± 0.05
Mannose	0.98 ± 0.28	0.88 ± 0.25	2.64 ± 0.99	0.65 ± 0.22	0.63 ± 0.16
N-Acetylglucosamine	1.07 ± 0.16	0.97 ± 0.16	1.18 ± 0.21	1.34 ± 0.11	0.92 ± 0.12
Nicotinamide	0.92 ± 0.2	1.37 ± 0.3	1.22 ± 0.16	1.02 ± 0.03	0.95 ± 0.15
Nicotinate	1.71 ± 0.96	1.96 ± 0.41	1.34 ± 0.42	0.54 ± 0.02	0.39 ± 0.09
Putrescine	0.63 ± 0.06	1.54 ± 0.31	0.61 ± 0.08	1.24 ± 0.03	1.15 ± 0.26
Ribose	0.43 ± 0.22	0.6 ± 0.3	0.33 ± 0.17	0.5 ± 0.03	0.65 ± 0.33
Succinic-acid-methylester	1.22 ± 0.42	0.89 ± 0.17	0.88 ± 0.27	1 ± 0.11	0.96 ± 0.18
Sucrose	0.37 ± 0.13	0.4 ± 0.12	0.21 ± 0.09	0.31 ± 0.08	0.23 ± 0.15
Thymine	1.39 ± 0.31	0.92 ± 0.12	1 ± 0.23	0.86 ± 0.07	0.9 ± 0.17
Trehalose	0.5 ± 0.35	0.06 ± 0.03	0.24 ± 0.22	0.04 ± 0.02	0.61 ± 0.42
Uracil	3.09 ± 1.03	1.9 ± 0.82	1.8 ± 0.67	2.18 ± 0.24	1.74 ± 0.66
Uridine	0.1 ± 0.09	0.14 ± 0.12	0.06 ± 0.04	0.08 ± 0.02	0.05 ± 0.04
Xylose-1-phosphate	0.56 ± 0.14	n.d.	n.d.	n.d.	0.38 ± 0.24
Xylulose-5-phosphate	1 ± 0.15	0.92 ± 0.1	0.82 ± 0.17	0.87 ± 0.06	0.48 ± 0.06

Continuation page iii

Metabolites	time after oxygen shut-down [min]				
	15	30	60	120	240
Unknowns					
NA_2276.5	1.4 ± 0.3	5.93 ± 0.62	4 ± 0.79	3.06 ± 0.97	1.83 ± 0.28
NA261	1.52 ± 0.4	3.00 ± 0.53	3.66 ± 0.72	3.33 ± 2.52	2.77 ± 0.78
Unknown#1145-dsh-skl_001	1.21 ± 0.24	0.85 ± 0.14	0.66 ± 0.18	0.5 ± 0.07	0.53 ± 0.11
Unknown#1171.6-pin-mhe_002	1.45 ± 0.54	0.6 ± 0.33	0.41 ± 0.28	0.52 ± 0.21	0.69 ± 0.14
Unknown#1226.1-pin-mhe_004	1.13 ± 0.51	0.86 ± 0.17	0.48 ± 0.19	0.47 ± 0.14	0.39 ± 0.12
Unknown#1669.1-pin-mhe_033	0.93 ± 0.1	1.2 ± 0.12	0.85 ± 0.2	0.72 ± 0.11	0.96 ± 0.19
Unknown#1830.2-pin-mhe_038	1.22 ± 0.21	0.95 ± 0.08	0.62 ± 0.09	1.07 ± 0.22	1.12 ± 0.09
Unknown#1881.9-pin-mhe_041	1.22 ± 0.18	1.34 ± 0.27	2.24 ± 0.37	2.97 ± 0.33	2.48 ± 0.54
Unknown#1953.9-pin-mhe_025	1.38 ± 0.38	1.07 ± 0.12	1.08 ± 0.31	1.49 ± 0.21	1.15 ± 0.18
Unknown#2018.7-pin-mhe_028	0.94 ± 0.14	0.94 ± 0.14	0.74 ± 0.15	0.55 ± 0.12	0.56 ± 0.1
Unknown#2139.6-pin-mhe_045	1.09 ± 0.23	0.86 ± 0.11	0.81 ± 0.18	0.89 ± 0.03	0.95 ± 0.07
Unknown#2377.8-pin-mhe_054''	1	0.95 ± 0.17	0.87 ± 0.08	0.75 ± 0	0.81 ± 0.17
Unknown#bth-pae-013_1169.9	0.69 ± 0.2	0.53 ± 0.08	0.54 ± 0.14	0.75 ± 0.04	0.7 ± 0.11
Unknown#cja-ppu-001_1953.27	0.87 ± 0.1	1.92 ± 0.19	1.36 ± 0.29	1.1 ± 0.18	0.84 ± 0.09
Unknown#cja-ppu-004_1201.76	1.09 ± 0.35	0.64 ± 0.15	0.78 ± 0.12	0.9 ± 0.23	0.76 ± 0.14
Unknown#cja-ppu-005_1277.11	0.9 ± 0.19	0.95 ± 0.13	0.85 ± 0.25	1.02 ± 0.06	0.74 ± 0.13
Unknown#cja-ppu-010_1366.60	n.d.	1	0.87 ± 0.24	0.46 ± 0.01	0.09 ± 0.04
Unknown#mse-ypy-008_1437.3	3.17 ± 2.18	1.08 ± 0.53	2.68 ± 1.65	3.07 ± 0.4	2.42 ± 1.36
Unknown#mse-ypy-021_2090.5	1.05 ± 0.2	0.73 ± 0.06	0.46 ± 0.12	0.67 ± 0.11	0.6 ± 0.07
Unknown#mse-ypy-025_2215.8	1.26 ± 1.01	5.18 ± 2.83	1.95 ± 1.93	0.61 ± 0.71	0.14 ± 0.08

colour scale for fold changes:

< 0.1	0.1 – 0.2	0.2 – 0.5	0.5 – 2	2 – 5	5 – 10	> 10

A3

log_2 fold-changes of selected gene transcripts of *D. shibae* after oxygen shut-down. Fold changes were computed by comparison with the aerobic state of cells. Experiments section 3.1.

			time after oxygen shut-down [min]						
Locus tag	**Gene**	**Description**	**5**	**10**	**15**	**20**	**30**	**60**	**120**
Genes encoding ribosomal components									
Dshi_0230	*rpmI*	50S ribosomal protein L35	0.26	0.14	-0.14	-0.14	-0.58	-1.54	-0.68
Dshi_0231	*rplT*	50S ribosomal protein L20	0.14	0.14	-0.26	-0.49	-0.68	-1.54	-0.77
Dshi_0246	*rpsU*	30S ribosomal protein S21	0.14	0.14	0.00	-0.26	-1.00	-1.38	-0.49
Dshi_0260	*rplK*	50S ribosomal protein L11	0.00	0.14	-0.26	-0.58	-1.14	-2.17	-1.00
Dshi_0261	*rplA*	50S ribosomal protein L1	0.00	0.00	-0.14	-0.49	-1.26	-2.17	-1.07
Dshi_0265	*rplJ*	50S ribosomal protein L10	0.00	0.00	-0.14	-0.49	-1.68	-2.96	-1.43
Dshi_0266	*rplL*	50S ribosomal protein L7/L12	0.00	0.00	-0.14	-0.38	-1.68	-2.98	-1.58
Dshi_0271	*rpsL*	30S ribosomal protein S12	0.26	0.26	-0.38	-0.85	-1.07	-2.04	-0.49
Dshi_0272	*rpsG*	30S ribosomal protein S7	0.14	0.14	-0.49	-1.07	-1.20	-1.96	-0.68
Dshi_0275	*rpsJ*	30S ribosomal protein S10	0.00	0.00	-0.14	-0.26	-2.14	-2.70	-1.38
Dshi_0276	*rplC*	ribosomal protein L3	0.00	0.00	-0.14	-0.14	-2.00	-2.54	-1.26
Dshi_0277	*rplD*	50S ribosomal protein L4	0.00	0.00	-0.14	-0.14	-1.89	-2.41	-1.26
Dshi_0278	*rplW*	50S ribosomal protein L23	0.00	0.00	0.00	-0.14	-1.89	-2.74	-1.32
Dshi_0285	*rplB*	50S ribosomal protein L2	0.14	0.14	-0.26	-1.00	-1.20	-2.23	-0.85
Dshi_0286	*rpsS*	30S ribosomal protein S19	0.00	0.14	-0.38	-0.68	-1.49	-2.14	-1.32
Dshi_0287	*rplV*	50S ribosomal protein L22	0.00	0.00	-0.38	-0.68	-1.96	-2.54	-1.43
Dshi_0289	*rplP*	50S ribosomal protein L16	0.00	0.00	-0.26	-0.49	-1.68	-2.10	-1.32
Dshi_0293	*rpmC*	50S ribosomal protein L29	0.38	0.38	-0.14	-0.68	-0.49	-1.43	-0.38
Dshi_0294	*rpsQ*	ribosomal protein S17	0.26	0.38	-0.26	-0.77	-0.77	-1.63	-0.58
Dshi_0295	*rplN*	50S ribosomal protein L14	0.14	0.26	-0.38	-1.00	-1.43	-2.29	-1.00
Dshi_0296	*rplX*	50S ribosomal protein L24	0.14	0.14	-0.38	-1.14	-1.49	-2.10	-0.93
Dshi_0297	*rplE*	50S ribosomal protein L5	0.00	0.14	-0.38	-0.85	-2.10	-2.49	-1.38
Dshi_0298	*rpsN*	30S ribosomal protein S14	0.00	0.00	-0.38	-0.85	-1.96	-2.29	-1.00
Dshi_0299	*rpsH*	30S ribosomal protein S8	0.00	0.00	-0.38	-0.49	-1.89	-2.29	-1.14
Dshi_0300	*rplF*	50S ribosomal protein L6	0.00	0.00	-0.26	-0.58	-1.96	-2.29	-1.20
Dshi_0301	*rplR*	50S ribosomal protein L18	0.00	0.00	-0.26	-0.38	-1.77	-1.89	-0.93
Dshi_0302	*rpsE*	30S ribosomal protein S5	0.00	0.00	-0.26	-0.14	-1.43	-2.04	-1.14
Dshi_0303	*rpmD*	50S ribosomal protein L30	0.00	0.00	-0.14	-0.38	-1.68	-2.29	-1.14
Dshi_0304	*rplO*	50S ribosomal protein L15	0.00	0.00	-0.26	-0.26	-1.58	-2.07	-1.07
Dshi_0307	*rpsM*	ribosomal protein S13	0.26	0.26	0.00	-0.14	-0.58	-1.58	-0.58
Dshi_0308	*rpsK*	30S ribosomal protein S11	0.14	0.14	0.00	-0.26	-0.68	-1.49	-0.58
Dshi_0310	*rplQ*	50S ribosomal protein L17	0.00	0.14	-0.38	-0.85	-1.07	-2.04	-0.93
Dshi_0333	*rpmH*	50S ribosomal protein L34	0.38	0.26	-0.14	-0.26	0.00	-0.93	-0.14
Dshi_0340	*rpmE*	50S ribosomal protein L31	0.14	0.14	-0.14	-0.49	-0.49	-1.00	-0.38
Dshi_0341	*rplS*	50S ribosomal protein L19	0.26	0.26	-0.26	-0.58	-0.77	-1.63	-0.49
Dshi_0348	*rpsP*	30S ribosomal protein S16	0.00	0.00	-0.14	-0.38	-2.14	-2.38	-1.54
Dshi_0387	*rpmJ*	50S ribosomal protein L36	0.26	0.26	-0.26	-0.26	-0.26	-1.26	-0.26
Dshi_0950	*rplY*	50S ribosomal protein L25/general stress protein Ctc	0.14	0.14	-0.26	-0.68	-1.32	-1.89	-1.14
Dshi_1025	*rpsA*	30S ribosomal protein S1	0.00	0.00	-0.38	-0.93	-1.68	-1.89	-0.85
Dshi_1460	rplU	50S ribosomal protein L21/unknown domain fusion protein	0.14	0.14	-0.14	-0.38	-0.77	-1.32	-0.38
Dshi_1461	rpmA	50S ribosomal protein L27	0.14	0.14	-0.26	-0.49	-1.00	-1.26	-0.49

Continuation page v

Locus tag	Gene	Description	time after oxygen shut-down [min] 5	10	15	20	30	60	120
Dshi_1548	*rpsB*	30S ribosomal protein S2	0.14	0.14	-0.26	-0.68	-1.00	-1.85	-0.85
Dshi_1601	*rpsI*	30S ribosomal protein S9	0.14	0.14	-0.26	-0.68	-1.07	-2.07	-1.20
Dshi_1602	*rplM*	50S ribosomal protein L13	0.26	0.14	-0.26	-0.68	-1.00	-2.00	-1.07
Dshi_1718	*rpmF*	50S ribosomal protein L32	0.26	0.14	-0.26	-0.49	-0.68	-1.38	-0.58
Dshi_2186	*rpsF*	30S ribosomal protein S6	0.14	0.14	-0.26	-0.49	-1.07	-2.04	-1.00
Dshi_2187	*rpsR*	30S ribosomal protein S18	0.00	0.14	-0.26	-0.68	-1.26	-1.81	-1.00
Dshi_2188	*rplI*	50S ribosomal protein L9	0.00	0.14	-0.26	-0.85	-1.43	-2.23	-1.26
Dshi_2583	*rpmB*	50S ribosomal protein L28	0.26	0.26	-0.14	-0.26	-0.49	-0.93	-0.26
Dshi_2781	*rpmG*	50S ribosomal protein L33	0.26	0.26	-0.14	-0.14	-0.38	-0.93	-0.26
Dshi_2948	*rpsD*	30S ribosomal protein S4	0.14	0.26	-0.26	-0.68	-0.68	-1.77	-0.26
Dshi_2994	*rpsO*	30S ribosomal protein S15	0.26	0.26	-0.14	-0.38	-0.68	-1.43	-0.68
Dshi_3371	*rpsT*	30S ribosomal protein S20	0.38	0.38	-0.14	-0.26	-0.38	-1.32	-0.38
Genes involved in translation processes									
Dshi_0223	*tufA*	elongation factor Tu	0.00	0.14	-0.14	-0.49	-1.89	-2.32	-1.00
Dshi_0237	*pheT*	phenylalanyl-tRNA synthetase subunit beta	0.14	0.14	0.00	-0.26	-0.49	-0.93	-0.26
Dshi_0273	*fusA*	elongation factor G	0.00	0.00	-0.38	-0.93	-1.85	-2.38	-1.07
Dshi_0309	*rpoA*	DNA-directed RNA polymerase subunit alpha	0.14	0.14	-0.14	-0.49	-1.00	-1.58	-0.77
Dshi_0326	*engB*	ribosome biogenesis GTP-binding protein YsxC	0.00	0.00	-0.14	-0.38	-0.85	-0.93	-0.38
Dshi_0344	*rimM*	16S rRNA-processing protein RimM	0.00	0.00	-0.14	0.00	-1.07	-1.32	-1.14
Dshi_0954	*engD*	GTP-dependent nucleic acid-binding protein EngD	0.26	0.14	-0.14	-0.26	-0.58	-1.14	-0.38
Dshi_0990		putative DNA helicase related protein	0.00	0.00	0.00	0.14	1.07	1.20	0.93
Dshi_1019		RNA modification protein	0.26	0.26	-0.14	0.00	-0.26	-0.85	0.00
Dshi_1207	*gatB*	aspartyl/glutamyl-tRNA amidotransferase subunit B	0.14	0.14	-0.14	-0.14	-0.38	-0.85	-0.49
Dshi_1549	*tsf*	elongation factor Ts	0.00	0.14	-0.26	-0.68	-1.77	-2.35	-1.43
Dshi_1642	*alaS*	alanyl-tRNA synthetase	0.14	0.14	0.00	-0.26	-0.26	-0.93	-0.26
Dshi_1728	*argS*	arginyl-tRNA synthetase	0.14	0.14	-0.26	-0.49	-0.58	-1.14	-0.49
Dshi_1933	*ileS*	isoleucyl-tRNA synthetase	0.14	0.14	-0.26	-0.58	-0.68	-0.85	-0.49
Dshi_2094	*efp*	elongation factor P	0.38	0.26	-0.26	-0.38	-0.68	-1.32	-0.49
Dshi_2151	*tyrS*	tyrosyl-tRNA synthetase	0.26	0.26	-0.14	-0.58	-0.26	-0.93	0.00
Dshi_2206	*lysK*	lysyl-tRNA synthetase	0.26	0.26	-0.14	-0.49	-0.49	-1.00	-0.49
Dshi_2402	*glyS*	glycyl-tRNA synthetase, beta subunit	0.00	0.00	0.00	-0.58	-0.85	-1.07	-0.49
Dshi_2618		MiaB-like tRNA modifying enzyme YliG	0.14	0.14	-0.14	-0.49	-0.38	-0.85	-0.14
Dshi_2633	*aspS*	aspartyl-tRNA synthetase	0.14	0.14	-0.38	-0.68	-0.85	-1.38	-0.68
Dshi_2785	*gatA*	aspartyl/glutamyl-tRNA amidotransferase subunit A	0.26	0.14	-0.26	-0.58	-0.77	-1.32	-0.38
Dshi_2786	*gatC*	aspartyl/glutamyl-tRNA amidotransferase subunit C	0.26	0.14	-0.14	-0.77	-0.49	-1.14	-0.26
Dshi_2836	*trpS*	tryptophanyl-tRNA synthetase	0.26	0.14	-0.14	-0.26	-0.49	-0.93	-0.38
Dshi_2955	*hisS*	histidyl-tRNA synthetase	0.14	0.14	-0.38	-0.93	-0.77	-1.26	-0.26

Continuation page vi

Locus tag	Gene	Description	time after oxygen shut-down [min] 5	10	15	20	30	60	120
Dshi_3076	*greA*	transcription elongation factor GreA	0.00	0.00	-0.14	0.00	-0.14	-0.49	-0.77
Dshi_3453	*rho*	transcription termination factor Rho	0.26	0.14	-0.38	-0.58	-0.38	-1.14	0.26
Dshi_3454	*trmE*	tRNA modification GTPase TrmE	0.00	0.00	-0.26	-0.49	-0.93	-1.14	-0.38
Dshi_3455	*gidA*	tRNA uridine 5-carboxymethylaminomethyl modification enzyme GidA	0.14	0.00	-0.14	-0.26	-0.85	-1.07	-0.26
Dshi_3456	*gidB*	methyltransferase GidB	-0.14	0.00	0.00	0.00	-0.77	-0.93	-0.38
Dshi_3461		endoribonuclease L-PSP	0.00	-0.14	-0.26	-0.49	-1.00	-1.20	-0.68
Dshi_3463	*rph*	ribonuclease PH	0.14	0.00	-0.14	-0.26	-0.58	-1.07	-0.49
Dshi_3561	*nusA*	transcription elongation factor NusA	0.00	0.14	-0.26	-0.93	-0.77	-1.43	-0.77
Dshi_3563	*infB*	translation initiation factor IF-2	0.14	0.14	-0.14	-0.38	-0.85	-1.20	-0.58
Genes involved in denitrification									
Dshi_0660	*fixK/fnrL*	Crp/FNR family transcriptional regulator	-0.14	-0.26	-0.68	-0.93	-1.26	-0.68	0.00
Dshi_1450		NnrS family protein	0.00	0.00	0.14	0.38	2.26	2.29	1.81
Dshi_2303		NnrS family protein	0.00	0.00	0.14	0.14	2.00	3.66	3.43
Dshi_2304		hemerythrin HHE cation binding domain-containing protein	0.00	0.00	0.14	0.26	2.63	4.03	4.07
Dshi_3161	*napC*	NapC/NirT cytochrome c domain-containing protein	0.14	0.77	1.20	1.68	1.54	1.32	0.58
Dshi_3162	*napB*	nitrate reductase cytochrome c-type subunit (NapB)	0.14	0.58	1.14	1.43	1.32	0.85	0.49
Dshi_3163	*napH*	quinol dehydrogenase membrane component	0.26	0.93	1.38	1.85	1.68	1.26	0.68
Dshi_3164	*napG*	MauM/NapG family ferredoxin-type protein	0.26	0.93	1.38	1.26	1.58	1.14	0.58
Dshi_3165	*napA*	nitrate reductase catalytic subunit	0.38	1.38	1.77	1.77	2.14	1.20	0.77
Dshi_3166	*napD*	NapD family protein	0.38	1.20	1.54	1.63	1.85	1.07	0.38
Dshi_3167	*napF*	ferredoxin-type protein NapF	0.00	0.49	0.93	1.38	0.49	0.14	0.14
Dshi_3168	*apbE*	ApbE family lipoprotein	0.38	0.00	0.85	2.83	4.55	4.10	3.84
Dshi_3169	*cycA*	cytochrome c class I	0.49	-0.14	0.68	1.77	5.17	4.40	4.78
Dshi_3170		hypothetical protein	0.00	0.00	0.00	0.26	2.58	2.74	2.79
Dshi_3171	*cbiX*	cobalamin (vitamin B12) biosynthesis CbiX protein	0.00	0.00	0.00	-0.14	3.22	3.23	3.17
Dshi_3172	*nirN*	cytochrome d1 heme region	0.14	0.00	0.38	0.58	3.85	3.55	3.52
Dshi_3173	*nirJ*	radical SAM domain-containing protein	0.14	0.00	0.38	1.26	2.72	2.49	2.66
Dshi_3174	*nirH*	AsnC family transcriptional regulator	0.38	-0.14	0.85	2.77	4.02	3.54	3.85

Continuation page vii

			time after oxygen shut-down [min]						
Locus tag	**Gene**	**Description**	**5**	**10**	**15**	**20**	**30**	**60**	**120**
Dshi_3187		cytochrome c oxidase subunit III	0.14	0.00	0.00	0.00	2.54	3.00	2.85
Dshi_3188		nitric oxide reductase F protein, putative	0.00	0.00	0.00	0.00	3.07	3.74	3.25
Dshi_3189		cyclic nucleotide-binding protein	0.14	0.26	0.58	1.00	2.17	1.72	1.38
Dshi_3190	*hemA*	5-aminolevulinate synthase	0.49	0.00	0.93	2.43	3.55	3.07	3.25
Dshi_3191	*dnr*	Crp/FNR family transcriptional regulator	0.26	0.00	0.68	2.38	3.68	3.31	3.15
Dshi_3192		hypothetical protein	0.38	0.00	1.00	2.51	3.83	3.52	3.67
Dshi_3193	*nosR*	FMN-binding domain-containing protein	0.26	0.14	0.77	1.96	3.51	2.61	2.41
Dshi_3194	*nosZ*	nitrous-oxide reductase	0.14	0.00	0.58	1.07	4.20	3.50	2.81
Dshi_3195	*nosD*	periplasmic copper-binding	0.00	0.00	0.26	0.14	3.68	2.68	1.63
Dshi_3196	*nosF*	ABC transporter related	0.14	0.00	0.14	0.49	3.07	2.56	1.81
Dshi_3197	*nosY*	nitrous oxide maturation protein NosY	0.00	-0.14	0.00	0.38	3.63	3.00	1.63
Dshi_3198	*nosL*	NosL family protein	0.00	0.00	0.00	0.26	2.56	2.43	1.54
Dshi_3199	*nosX*	ApbE family lipoprotein	0.00	0.00	-0.14	0.26	2.20	2.14	1.00
Dshi_3270		CRP/FNR family transcriptional regulator	0.68	1.32	2.20	3.20	3.58	2.51	2.04
RDRS03175	*nosR*	nitrous oxide reductase regulatory protein NosR IMG_id: 2500133228	0.26	0.00	0.58	2.38	3.70	3.17	3.19
Genes involved TCA cycle									
Dshi_0213	*pckA*	phosphoenolpyruvate carboxykinase	0.38	0.38	0.14	0.00	0.85	0.26	1.20
Dshi_1045		HpcH/HpaI aldolase	0.00	0.00	0.26	0.14	0.58	0.85	0.77
Dshi_1966	*lpdA*	dihydrolipoamide dehydrogenase	0.00	0.14	0.14	0.26	0.38	0.49	1.00
Dshi_1967	*aceF*	dehydrogenase catalytic domain-containing protein	0.00	0.14	0.14	0.26	0.38	0.26	0.85
Dshi_1968	*aceE*	pyruvate dehydrogenase subunit E1	0.14	0.14	0.14	0.49	1.58	0.68	1.26
Dshi_1986	*icd*	isocitrate dehydrogenase, NADP-dependent	-0.14	0.14	-0.14	-0.58	-1.32	-0.68	-0.49
Dshi_2060	*acnB*	bifunctional aconitate hydratase 2/2-methylisocitrate dehydratase	-0.26	0.14	0.00	-0.77	-0.85	-0.14	-0.49
Dshi_2159	*pdhB*	pyruvate dehydrogenase subunit beta	0.00	0.00	-0.14	-0.58	-0.93	-1.07	-1.20
Dshi_2160	*pdhC*	branched-chain alpha-keto acid dehydrogenase subunit E2	0.00	0.00	-0.14	-0.26	-1.26	-1.26	-1.32
Dshi_2861	*sdhB*	succinate dehydrogenase iron-sulfur subunit	0.00	0.14	0.14	0.38	0.49	0.38	0.85
Dshi_2865	*sdhA*	succinate dehydrogenase flavoprotein subunit	0.00	0.14	0.38	0.68	1.07	0.68	1.07
Dshi_2866		succinate dehydrogenase hydrophobic membrane anchor	0.00	0.14	0.49	0.85	1.26	0.77	1.20

Continuation page viii

Locus tag	Gene	Description	time after oxygen shut-down [min] 5	10	15	20	30	60	120
Genes involved in glycolysis/gluconeogenesis									
Dshi_0213	*pckA*	phosphoenolpyruvate carboxykinase	0.38	0.38	0.14	0.00	0.85	0.26	1.20
Dshi_0228	*pykA*	pyruvate kinase	-0.58	-0.26	0.00	0.00	-1.89	-1.26	-1.68
Dshi_1399	*acsA*	acetate--CoA ligase	0.00	0.14	0.14	0.26	0.85	0.26	0.85
Dshi_1655	*glk*	glucokinase	-0.38	-0.14	-0.14	-0.26	-0.85	-0.49	-0.77
Dshi_1740	*gap*	glyceraldehyde-3-phosphate dehydrogenase, type I	0.77	0.77	0.38	-0.26	0.77	0.68	1.38
Dshi_1742	*gap*	glyceraldehyde-3-phosphate dehydrogenase, type I	-0.77	-0.38	-0.26	0.00	-1.63	-1.26	-1.58
Dshi_2145	*eno*	phosphopyruvate hydratase	-0.26	-0.14	-0.38	-0.49	-1.00	-1.32	-0.68
Dshi_2155	*pgk*	phosphoglycerate kinase	0.14	0.00	-0.14	-0.49	-0.49	-0.85	-0.26
Dshi_2673		Pyrrolo-quinoline quinone	-0.14	-0.14	-0.14	-0.38	-0.49	-0.58	-0.77
Dshi_3553	*acs*	acetate--CoA ligase	0.00	0.14	0.14	0.26	0.85	0.26	1.20
Genes involved in oxidative phosphorylation									
Dshi_0216	*etfA*	electron transfer flavoprotein alpha subunit	-0.14	-0.14	-0.14	-0.38	-1.00	-1.38	-0.49
Dshi_0217	*etfB*	electron transfer flavoprotein alpha/beta-subunit	-0.14	0.00	-0.14	-0.38	-1.00	-1.26	-0.58
Dshi_0450	*pqqA*	coenzyme PQQ biosynthesis protein A	-0.14	-0.14	-0.58	-1.07	-2.54	-1.63	-2.10
Dshi_0452	*pqqC*	pyrroloquinoline quinone biosynthesis protein PqqC	-0.14	-0.26	-0.14	-0.26	-0.68	-0.26	-0.77
Dshi_0476	*gcd*	Pyrrolo-quinoline quinone	0.00	-0.14	-0.26	-0.26	-1.07	-0.49	-1.07
Dshi_0654	*cycM*	cytochrome c class I	0.26	0.38	0.49	0.77	1.00	0.26	1.26
Dshi_0661	*fixN*	cytochrome c oxidase, cbb3-type, subunit I	0.93	2.10	2.46	2.63	3.12	2.51	2.10
Dshi_0662	*fixO*	cytochrome c oxidase, cbb3-type, subunit II	0.77	1.93	2.41	2.20	2.96	2.58	2.17
Dshi_0663	*fixQ*	Cbb3-type cytochrome oxidase component	0.49	1.43	1.77	1.93	2.10	1.96	1.77
Dshi_0664	*fixP*	cytochrome c oxidase, cbb3-type, subunit III	0.49	1.72	2.10	2.29	2.51	2.32	2.17
Dshi_0665	*fixG*	cytochrome c oxidase cbb3 type accessory protein FixG	0.77	1.77	2.41	2.68	3.43	2.85	2.43
Dshi_0666	*fixH*	FixH family protein	0.49	1.49	1.96	2.29	2.79	2.29	2.23
Dshi_0667	*fixI*	heavy metal translocating P-type ATPase	0.26	1.00	1.49	1.96	2.10	2.04	1.85
Dshi_0668	*fixS*	cytochrome oxidase maturation protein, cbb3-type	0.14	0.26	0.58	0.93	1.07	1.26	0.93
Dshi_1140	*ctaC*	cytochrome c oxidase subunit II	-0.14	-0.49	-1.00	-1.20	-2.07	-1.93	-1.20
Dshi_1141	*ctaB*	protoheme IX farnesyltransferase	-0.14	-0.49	-0.85	-0.85	-1.20	-1.32	-0.77
Dshi_1143	*ctaG*	cytochrome C oxidase assembly protein	-0.14	-0.38	-0.68	-1.00	-1.58	-1.68	-1.00
Dshi_1144	*ctaE*	cytochrome c oxidase subunit III	-0.14	-0.26	-0.49	-0.68	-1.54	-1.43	-0.77
Dshi_1321	*nuoH*	NADH dehydrogenase subunit H	0.00	0.26	0.38	0.58	0.58	0.49	0.85
Dshi_1322	*nuoI*	NADH dehydrogenase subunit I	0.00	0.14	0.14	0.26	0.68	0.26	0.85
Dshi_1326	*nuoK*	NADH dehydrogenase subunit K	0.00	0.14	0.14	0.49	0.49	0.49	0.77
Dshi_1390		NADH dehydrogenase	0.00	0.14	0.49	0.49	0.85	0.49	0.68
Dshi_2081		cytochrome c class I	0.00	-0.14	-0.38	-0.58	-1.32	-0.85	-1.26

Continuation page ix

			time after oxygen shut-down [min]						
Locus tag	**Gene**	**Description**	**5**	**10**	**15**	**20**	**30**	**60**	**120**
Dshi_2383	*ctaD*	cytochrome c oxidase subunit I type	0.00	0.00	-0.26	-0.68	-1.20	-1.14	0.14
Dshi_2655	*ccpA*	cytochrome-c peroxidase	0.26	1.00	1.85	2.14	3.22	2.96	3.22
Dshi_2672		cytochrome c class I	0.58	1.26	2.23	2.77	3.67	2.79	2.23
Dshi_2694		cytochrome c family protein, putative	0.38	0.58	1.68	2.54	3.32	2.54	1.81
Dshi_2799	*fccB*	flavocytochrome c sulphide dehydrogenase flavin-binding	-0.14	-0.14	-0.14	-0.26	-0.77	-0.58	-1.00
Dshi_2800		cytochrome c class I	-0.14	-0.14	0.00	-0.68	-0.58	-0.38	-0.85
Dshi_2804	*soxA*	diheme cytochrome c SoxA	-0.14	-0.14	-0.14	-0.26	-0.77	-0.77	-1.00
Dshi_2805		sulphur oxidation protein SoxZ	0.00	-0.14	-0.14	-0.26	-0.85	-0.38	-0.77
Dshi_2807		monoheme cytochrome c SoxX	-0.14	-0.14	-0.14	-0.26	-0.93	-0.58	-1.07
Dshi_2861	*sdhB*	succinate dehydrogenase iron-sulfur subunit	0.00	0.14	0.14	0.38	0.49	0.38	0.85
Dshi_2865	*sdhA*	succinate dehydrogenase flavoprotein subunit	0.00	0.14	0.38	0.68	1.07	0.68	1.07
Dshi_2866		succinate dehydrogenase hydrophobic membrane anchor	0.00	0.14	0.49	0.85	1.26	0.77	1.20
Dshi_2867		succinate dehydrogenase cytochrome b556 subunit	0.00	0.26	0.49	0.68	1.32	0.85	1.20
Dshi_2933	*atpC*	ATP synthase F1, epsilon subunit	0.00	0.00	0.00	0.14	-1.49	-1.32	-0.38
Dshi_2934	*atpD*	F0F1 ATP synthase subunit beta	0.00	0.00	0.00	-0.14	-1.58	-1.20	-0.26
Dshi_2935	*atpG*	F0F1 ATP synthase subunit gamma	0.00	0.14	-0.14	-0.38	-1.32	-1.14	-0.26
Dshi_2936	*atpA*	F0F1 ATP synthase subunit alpha	0.14	0.14	0.00	-0.77	-0.85	-1.07	0.00
Dshi_2937	*atpH*	ATP synthase F1, delta subunit	0.26	0.38	0.00	-0.26	-0.38	-1.00	0.00
Dshi_2982		hypothetical protein	0.00	-0.14	-0.49	-0.85	-1.49	-1.38	-1.63
Dshi_3027	*atpF*	F0F1 ATP synthase subunit B	0.00	0.14	0.14	0.14	-1.43	-1.63	-0.14
Dshi_3028	*atpX*	F0F1 ATP synthase subunit B'	0.00	0.14	0.00	0.14	-1.43	-1.43	-0.26
Dshi_3029	*atpE*	F0F1 ATP synthase subunit C	0.00	0.14	0.14	0.00	-1.38	-1.49	-0.26
Dshi_3030	*atpB*	F0F1 ATP synthase subunit A	0.14	0.38	0.26	0.26	-0.68	-1.07	0.00
Dshi_3075	*ydiS*	electron-transferring-flavoprotein dehydrogenase	-0.26	-0.14	-0.58	-1.00	-0.85	-0.68	-0.58
Dshi_3276	*petC*	cytochrome c1	0.00	0.14	0.14	0.00	0.26	0.00	0.85
Dshi_3277	*petB*	cytochrome b/b6 domain-containing protein	0.14	0.26	0.26	0.26	0.58	0.14	1.00
Dshi_3278		ubiquinol-cytochrome c reductase, iron-sulfur subunit	0.14	0.26	0.26	0.38	0.49	0.00	0.93
Dshi_3408	*cycH*	TPR repeat-containing protein	0.00	0.14	0.38	0.26	1.14	0.68	0.38
Dshi_3409	*cycL*	cytochrome C biogenesis protein	0.00	0.14	0.38	0.38	1.20	0.93	0.38
Dshi_3410	*dsbE*	periplasmic protein thiol--disulphide oxidoreductase DsbE	0.00	0.26	0.58	0.68	1.49	1.20	0.49

Continuation page x

			time after oxygen shut-down [min]						
Locus tag	**Gene**	**Description**	**5**	**10**	**15**	**20**	**30**	**60**	**120**
Genes involved in stress response									
Dshi_0009	*csp*	cold-shock DNA-binding domain-containing protein	0.00	-0.14	-0.26	-0.38	-0.68	-0.93	-0.14
Dshi_0737		heat shock protein DnaJ domain-containing protein	0.00	0.14	0.38	0.49	0.77	0.93	0.49
Dshi_1338	*uspA*	UspA domain-containing protein	0.68	1.32	2.63	3.36	3.77	3.19	2.35
Dshi_2213		UspA domain-containing protein	0.26	0.68	1.72	2.87	3.67	2.83	1.96
Dshi_2219		cold-shock DNA-binding domain-containing protein	0.00	-0.14	-0.26	-0.38	-0.93	-0.49	-0.14
Dshi_2686		UspA domain-containing protein	0.26	0.58	1.72	2.77	3.29	2.54	1.32
Dshi_2796		heat shock protein Hsp20	0.49	1.32	2.26	2.93	3.81	3.32	2.77
Dshi_2892		heat shock protein Hsp20	0.00	0.00	0.14	0.14	0.38	1.26	1.00
Dshi_2919	*groEL*	chaperonin GroEL	-0.14	0.00	-0.14	-0.26	-1.77	-1.93	-0.85
Dshi_2920		chaperonin Cpn10	0.00	0.00	-0.14	-0.14	-1.58	-1.63	-0.68
Genes involved in PHB synthesis									
Dshi_2231		phasin, PhaP	0.26	0.38	0.38	0.58	1.72	0.85	1.89
Dshi_2232		phasin, PhaP	0.26	0.38	0.14	0.49	1.26	0.26	1.54
Dshi_2233	*phbC*	poly(R)-hydroxyalkanoic acid synthase, class I	0.14	0.26	0.58	1.20	1.63	1.07	1.20

A4

Intracellular metabolites in *D. shibae* DFL12^T grown under different salinities (0.3 – 5 %), after a salt shock (2.3 to 5 % salinity) and nitrogen limited (salinity 3.5 %). Long-term adapted cells were sampled in the exponential growth phase and at a maximal optical density (OD_{max}). Nitrogen limited culture was exclusively sampled during active growth. These data were compared to the according growth situation in a culture grown in medium with a salinity of 3.5 %. Salt shocked cells were harvested 10 and 90 min after the shock and were compared to an untreated reference culture (continuous 2.3 % salinity) at the same time points. Experiments section 3.3.

Metabolites	Fold change								
	log phase			ODmax			osmotic up-shock		
	salinity [%]			salinity [%]			time past after osmotic shock		
	0.3	2.3	5	0.3	2.3	5	10 min	90 min	-N
Amino acids & Dipeptides									
Alanine	0.15 ± 0.03	0.71 ± 0.19	1.03 ± 0.21	0.56 ± 0.07	1.93 ± 0.27	10.53 ± 1.36	8.40 ± 2.06	2.48 ± 1.04	
Asparagine		0.73 ± 0.07	1.73 ± 0.23			d		x	
Aspartate	0.04 ± 0.00	0.84 ± 0.05	1.03 ± 0.05		0.27 ± 0.10	11.24 ± 2.85	0.41 ± 0.03	0.73 ± 0.11	
gamma-Glutamylleucine						d			
gamma-Glutamylvaline						1.42 ± 0.63			
Glycine	0.30 ± 0.03	1.13 ± 0.08	1.56 ± 0.16	1.39 ± 0.28	1.52 ± 0.27	2.00 ± 0.45	0.92 ± 0.25	0.99 ± 0.37	0.31 ± 0.07
Isoleucine	0.28 ± 0.05	0.75 ± 0.19	0.78 ± 0.13	0.64 ± 0.19	3.08 ± 2.02	1.28 ± 0.28	7.54 ± 3.60	1.69 ± 0.86	0.11 ± 0.02
Leucine	0.22 ± 0.04	0.95 ± 0.24	0.93 ± 0.17	0.11 ± 0.02	1.41 ± 0.14	0.23 ± 0.04	6.58 ± 1.66	1.84 ± 0.91	
Lysine	0.56 ± 0.03	1.08 ± 0.07	2.45 ± 0.39		0.10 ± 0.10	22.96 ± 2.56	0.30 ± 0.18	0.94 ± 0.48	0.06 ± 0.01
Methionine	0.35 ± 0.03	1.18 ± 0.21	0.79 ± 0.03			0.94 ± 0.26	1.34 ± 0.30	1.71 ± 0.21	
Ornithine	0.24 ± 0.03	2.51 ± 0.22	0.61 ± 0.04			1.51 ± 0.36		0.13 ± 0.08	
Phenylalanine	0.17 ± 0.01	1.25 ± 0.21	1.19 ± 0.10	0.01 ± 0.00	0.65 ± 0.33	0.12 ± 0.02	1.11 ± 0.25	0.66 ± 0.07	0.46 ± 0.03
Proline	0.89 ± 0.07	1.01 ± 0.10	0.86 ± 0.04	0.60 ± 0.15	0.70 ± 0.11	1.14 ± 0.18	0.96 ± 0.23	1.40 ± 0.22	0.61 ± 0.08
Serine	0.38 ± 0.03	0.81 ± 0.09	2.47 ± 0.33	1.14 ± 0.25	1.23 ± 0.23	5.16 ± 1.56	4.14 ± 0.52	3.15 ± 0.25	0.45 ± 0.07
Threonine	0.50 ± 0.03	1.27 ± 0.11	1.26 ± 0.13	0.32 ± 0.05	0.70 ± 0.11	1.87 ± 0.27	2.10 ± 0.18	0.98 ± 0.15	0.13 ± 0.02
Tyrosine		0.94 ± 0.23	0.85 ± 0.08		1.66 ± 0.30	0.74 ± 0.06	0.27 ± 0.16	0.91 ± 0.54	2.73 ± 0.27

Continuation page xii

Metabolites	Fold change								
	log phase			ODmax			osmotic up-shock		
	salinity [%]			salinity [%]			time past after osmotic shock		
	0.3	2.3	5	0.3	2.3	5	10 min	90 min	-N
Amino acid metabolism									
2-Aminoadipate						d			
2-Isopropylmalate	0.85 ± 0.07	1.13 ± 0.26	0.67 ± 0.03		0.80 ± 0.07	0.61 ± 0.07	1.11 ± 0.39	0.95 ± 0.12	
2-Methylmalate	0.50 ± 0.05	0.45 ± 0.13	0.39 ± 0.04	0.43 ± 0.16	1.04 ± 0.10	0.85 ± 0.10	0.82 ± 0.31	0.31 ± 0.04	0.30 ± 0.04
3-Aminoisobutanoate		1.32 ± 0.29	0.85 ± 0.10	0.61 ± 0.08	0.64 ± 0.08	0.63 ± 0.07	0.96 ± 0.37	1.05 ± 0.20	0.57 ± 0.12
Phenylpyruvate				0.55 ± 0.05	3.72 ± 0.33				d
Polyamines									
Putrescine	7.36 ± 0.71	3.75 ± 0.22	0.43 ± 0.02	17.91 ± 9.55	4.81 ± 1.73	3.29 ± 1.21	0.58 ± 0.20	2.70 ± 0.96	0.03 ± 0.00
Butanoates									
3-Hydroxybutanoate		1.46 ± 0.31	0.58 ± 0.02		1.04 ± 0.06	0.91 ± 0.06	1.79 ± 0.70	0.71 ± 0.07	1.84 ± 0.44
Fatty acids & Lipids									
Ethanolamine	1.20 ± 0.26	2.39 ± 0.92	0.34 ± 0.10	1.33 ± 0.57	3.90 ± 1.52	0.74 ± 0.26	1.39 ± 0.55	0.95 ± 0.36	0.10 ± 0.02
Glycerol	0.93 ± 0.07	0.90 ± 0.13	1.28 ± 0.08	1.25 ± 0.20	0.62 ± 0.10	0.68 ± 0.10	1.30 ± 0.37	1.25 ± 0.20	1.04 ± 0.17
Glycerol-3-phosphate	8.07 ± 1.29	1.64 ± 0.19	0.94 ± 0.08	2.78 ± 0.34	0.87 ± 0.11	0.69 ± 0.09	1.40 ± 0.53	2.14 ± 0.80	0.44 ± 0.06
11-(Z)-Octadecenoate	3.21 ± 0.58	1.30 ± 0.47		3.53 ± 0.76	0.75 ± 0.14				0.50 ± 0.28
TCA cycle									
Citrate	0.30 ± 0.04	0.99 ± 0.06	0.70 ± 0.11		0.86 ± 0.19	0.40 ± 0.09	0.64 ± 0.22	0.58 ± 0.25	0.30 ± 0.04
Fumarate	0.47 ± 0.04	1.23 ± 0.29	1.06 ± 0.08	0.69 ± 0.09	0.85 ± 0.14	1.20 ± 0.21	1.05 ± 0.30	1.20 ± 0.16	0.78 ± 0.08
2-Oxoglutarate	0.33 ± 0.05	1.10 ± 0.11	0.85 ± 0.10	0.08 ± 0.02	2.10 ± 0.44	0.15 ± 0.03	0.78 ± 0.13	0.62 ± 0.08	1.66 ± 0.20
Malate	0.60 ± 0.07	1.00 ± 0.16	0.98 ± 0.12	0.36 ± 0.07	0.80 ± 0.11	1.35 ± 0.28	1.01 ± 0.16	1.08 ± 0.10	0.39 ± 0.05
Succinate	1.25 ± 0.09	1.10 ± 0.16	0.62 ± 0.06	1.39 ± 0.27	1.14 ± 0.17	1.01 ± 0.17	0.86 ± 0.16	0.99 ± 0.22	0.81 ± 0.07

Continuation page xiii

Metabolites	Fold change								
	log phase			ODmax			osmotic up-shock		
	salinity [%]			salinity [%]			time past after osmotic shock		
	0.3	2.3	5	0.3	2.3	5	10 min	90 min	-N
Gluconeogenesis and Entner-Doudoroff pathway									
Glucono-1,5-lactone					d	d	d		
Glucose	0.10 ± 0.11	0.73 ± 0.16	0.98 ± 0.09	0.57 ± 0.16	0.71 ± 0.06	1.13 ± 0.09	2.40 ± 0.69	5.22 ± 0.66	0.93 ± 0.14
Glucose-6-phosphate	0.74 ± 0.15		0.77 ± 0.15		1.54 ± 0.14	0.37 ± 0.03			0.18 ± 0.10
Phosphoenolpyruvate	d				1.17 ± 0.19	0.48 ± 0.16			
Pyruvate	0.78 ± 0.16	1.09 ± 0.18	0.81 ± 0.11	0.81 ± 0.10	2.01 ± 0.21	1.30 ± 0.08	1.51 ± 0.37	1.62 ± 0.60	0.76 ± 0.09
Ribose	0.88 ± 0.10	1.06 ± 0.27	0.71 ± 0.06	0.92 ± 0.08	0.78 ± 0.04	0.77 ± 0.07	1.07 ± 0.29	0.79 ± 0.11	1.14 ± 0.11
Xylulose-5-phosphate	d				1.00 ± 0.11	0.64 ± 0.26			
Sugars									
Hexose 1	0.64 ± 0.04	0.97 ± 0.16	1.10 ± 0.07	1.01 ± 0.04	0.91 ± 0.02	1.15 ± 0.06	1.17 ± 0.35	1.00 ± 0.12	1.32 ± 0.06
Hexose 2	2.17 ± 0.17	1.96 ± 0.28	0.69 ± 0.04	2.34 ± 0.20	0.93 ± 0.10	0.60 ± 0.07	1.43 ± 0.34	0.57 ± 0.11	0.83 ± 0.06
1,6-Anhydroglucose	0.27 ± 0.08	0.34 ± 0.11		d	d	d	1.35 ± 0.36	0.80 ± 0.15	
Disaccharid						d			
Others									
3-Aminoisobutanoate		1.32 ± 0.29	0.85 ± 0.10	0.61 ± 0.08	0.64 ± 0.08	0.63 ± 0.07	0.96 ± 0.37	1.05 ± 0.20	0.57 ± 0.12
3-Hydroxy-3-methylglutarate					1.03 ± 0.08				
4-Aminobutanoate	d			d	d		d	d	
4-hydroxybenzoate	0.74 ± 0.10	1.46 ± 0.40	0.82 ± 0.07	0.52 ± 0.05	1.00 ± 0.12	0.33 ± 0.04	1.15 ± 0.52	0.93 ± 0.12	1.33 ± 0.16
Levulinate	0.63 ± 0.04	1.16 ± 0.19	1.04 ± 0.07	0.88 ± 0.14	0.95 ± 0.10	1.02 ± 0.11	1.22 ± 0.35	1.13 ± 0.15	0.98 ± 0.14
Malonate				x	x	x			d
Unknown#2224-dsh-skl_003_GG_associat		0.11 ± 0.03	1.47 ± 0.37		0.06 ± 0.01	0.17 ± 0.03	1.76 ± 0.75	63.06 ± 21.98	
Threonate		1.20 ± 0.42			d		0.96 ± 0.43	x	

Continuation page xiv

Metabolites	Fold change								
	log phase			ODmax			salt shock		
	salinity [%]			salinity [%]			time past after osmotic shock		
	0.3	2.3	5	0.3	2.3	5	10 min	90 min	-N
Unknowns									
D215058_2156.02_gg_associated		0.12 ± 0.03	2.08 ± 0.23		0.05 ± 0.01	0.29 ± 0.05	1.78 ± 0.71	45.40 ± 4.26	0.13 ± 0.01
NA135011_(classified_unknown]_1366.02	0.66 ± 0.09	1.34 ± 0.10	0.57 ± 0.05	0.77 ± 0.10	0.93 ± 0.15	0.67 ± 0.09	0.78 ± 0.13	0.53 ± 0.18	0.30 ± 0.04
Unknown#2066-dsh-skl_002	1.31 ± 0.12	1.34 ± 0.23	1.00 ± 0.06	1.17 ± 0.14	0.80 ± 0.17	0.75 ± 0.11	0.99 ± 0.26	1.55 ± 0.38	0.55 ± 0.05
pentose-5-phosphate	1.53 ± 0.20		0.87 ± 0.10		0.78 ± 0.06	0.54 ± 0.08	d		
Unknown#1226.1-pin-mhe_004	4.58 ± 0.61	2.47 ± 0.45	0.71 ± 0.09	3.81 ± 0.96	2.68 ± 0.63	1.37 ± 0.26	1.30 ± 0.23	1.22 ± 0.17	0.31 ± 0.06
Unknown#1385.3-pae-bth_025	0.55 ± 0.12	0.86 ± 0.18	1.37 ± 0.33	0.76 ± 0.17	0.99 ± 0.30	1.32 ± 0.39	1.17 ± 0.23	0.83 ± 0.19	0.41 ± 0.06
Unknown#1830.2-pin-mhe_039	1.73 ± 0.35	1.09 ± 0.35	0.99 ± 0.34	1.06 ± 0.20	0.70 ± 0.17	0.84 ± 0.18	1.18 ± 0.37	1.34 ± 0.46	0.95 ± 0.20
Unknown#1953.9-pin-mhe_026	1.32 ± 0.13	1.32 ± 0.25	0.99 ± 0.09	1.24 ± 0.10	0.75 ± 0.18	0.96 ± 0.11	0.98 ± 0.26	1.66 ± 0.57	0.58 ± 0.08
Unknown#2195.6-dsh-nbi_002					2.47 ± 0.32	0.00			d
Unknown#1145-dsh-skl_001	1.11 ± 0.25	1.52 ± 0.36	1.25 ± 0.20	0.71 ± 0.11	2.56 ± 0.34	2.96 ± 0.37	1.22 ± 0.25	1.40 ± 0.18	0.43 ± 0.07

colour scale for fold changes: < 0.1 | 0.1 – 0.2 | 0.2 – 0.5 | 0.5 – 2 | 2 – 5 | 5 – 10 | > 10

Danksagung

Zunächst bedanke ich mich bei meinem Mentor Prof. Dietmar Schomburg, für die Bereitstellung dieses Themas und für die hilfreichen Diskussionen. Außerdem danke ich Prof. Irene Wagner-Döbler für die Übernahme des Zweitgutachtens sowie Prof. Michael Hust für die Übernahme des Vorsitzes der Prüfungskommission.

Ein großer Dank gebührt meinen Kooperationspartnern aus der Arbeitsgruppe von Prof. Jahn, insbesondere Sebastian Laaß und der Arbeitsgruppe von Prof. Rabus sowie Dr. Geffers.

Dr. Meine Neumann-Schaal danke ich für das Korrekturlesen großer Teile meiner Arbeit und weiterer Unterstützung. Auch Dr. Michael Hensler möchte ich danken für das Korrekturlesen meiner Arbeit und für die vielen Roseobacter und MetaboliteDetector Diskussionen, aus denen ich viel gelernt habe. Unseren beiden guten Feen Sabine Kaltenhäuser und Sabine Noppenberger möchte ich insbesondere danken, da ohne sie das Labor still stehen würde. Nelli Bill möchte ich besonders danken für ihre Geduld bei der Einführung eines Mikrobiologie- und MS-Neulings und für ihre Freundschaft. Zudem danke ich Dr. Kerstin Schmidt-Hohagen von der ich einiges lernte und mit der die Zusammenarbeit immer Spaß machte.

Allen ehemaligen und aktuellen Laborratten möchte ich danken für die immer gute Atmosphäre, die das Arbeiten enorm erleichtert hat und die bedingungslose Unterstützung jeglicher Art wenn ich sie brauchte.

Zum Schluss möchte ich meiner Familie und Freunden danken, die mir privat den Rückhalt gegeben haben, um immer wieder mit Motivation an die Arbeit zu gehen.